

KEY ISSUES REVIEW

## The challenge of spin-orbit-tuned ground states in iridates: a key issues review

To cite this article: Gang Cao and Pedro Schlottmann 2018 *Rep. Prog. Phys.* **81** 042502

View the [article online](#) for updates and enhancements.

### Related content

- [Models and materials for generalized Kitaev magnetism](#)

Stephen M Winter, Alexander A Tsirlin, Maria Daghofer et al.

- [Decoupling of magnetism and electric transport in single-crystal  \$\(\text{Sr}\_{1-x}\text{A}\_x\)\_2\text{IrO}\_4\$  \( \$\text{A} = \text{Ca or Ba}\$ \)](#)

H D Zhao, J Terzic, H Zheng et al.

- [Recent progress on correlated electron systems with strong spin-orbit coupling](#)

Robert Schaffer, Eric Kin-Ho Lee, Bohm-Jung Yang et al.

### Recent citations

- [Decoupling of magnetism and electric transport in single-crystal  \$\(\text{Sr}\_{1-x}\text{A}\_x\)\_2\text{IrO}\_4\$  \( \$\text{A} = \text{Ca or Ba}\$ \)](#)

H D Zhao et al

## Key Issues Review

# The challenge of spin–orbit-tuned ground states in iridates: a key issues review

Gang Cao<sup>1</sup>  and Pedro Schlottmann<sup>2</sup>

<sup>1</sup> Department of Physics, University of Colorado at Boulder, Boulder, CO 80309, United States of America

<sup>2</sup> Department of Physics, Florida State University, Tallahassee, FL 32306, United States of America

E-mail: [gang.cao@colorado.edu](mailto:gang.cao@colorado.edu)

Received 20 April 2017, revised 14 December 2017

Accepted for publication 22 January 2018

Published 23 February 2018



Corresponding Editor Professor Piers Coleman

### Abstract

Effects of spin–orbit interactions in condensed matter are an important and rapidly evolving topic. Strong competition between spin–orbit, on-site Coulomb and crystalline electric field interactions in iridates drives exotic quantum states that are unique to this group of materials. In particular, the ' $J_{\text{eff}} = \frac{1}{2}$ ' Mott state served as an early signal that the combined effect of strong spin–orbit and Coulomb interactions in iridates has unique, intriguing consequences. In this *Key Issues Review*, we survey some current experimental studies of iridates. In essence, these materials tend to defy conventional wisdom: absence of conventional correlations between magnetic and insulating states, avoidance of metallization at high pressures, ‘S-shaped’  $I$ – $V$  characteristic, emergence of an odd-parity hidden order, etc. It is particularly intriguing that there exist conspicuous discrepancies between current experimental results and theoretical proposals that address superconducting, topological and quantum spin liquid phases. This class of materials, in which the lattice degrees of freedom play a critical role seldom seen in other materials, evidently presents some profound intellectual challenges that call for more investigations both experimentally and theoretically. Physical properties unique to these materials may help unlock a world of possibilities for functional materials and devices. We emphasize that, given the rapidly developing nature of this field, this *Key Issues Review* is by no means an exhaustive report of the current state of experimental studies of iridates.

**Keywords:** spin–orbit interaction, electron correlations, metal-insulator transitions,  $J_{\text{eff}} = \frac{1}{2}$  state, superconductivity, spin liquids, iridates

(Some figures may appear in colour only in the online journal)

---

### Contents

1. Introduction.....	<a href="#">2</a>	2.1.3. Transport properties.....	<a href="#">7</a>
2. Survey of physical properties of Ruddlesden–Popper iridates, $\text{Sr}_{n+1}\text{Ir}_n\text{O}_{3n+1}$ ( $n = 1, 2$ , and $\infty$ ) .....	<a href="#">4</a>	2.1.3.1. Magnetoresistance.....	<a href="#">8</a>
2.1. $\text{Sr}_2\text{IrO}_4$ ( $n = 1$ ).....	<a href="#">4</a>	2.1.3.2. The ‘S’-shaped $I$ – $V$ characteristic and switching effect.....	<a href="#">8</a>
2.1.1. Critical structural features.....	<a href="#">4</a>	2.1.3.3. Thermal conductivity—pseudospin trans- port.....	<a href="#">9</a>
2.1.2. Magnetic properties.....	<a href="#">6</a>	2.1.4. Effects of high pressure.....	<a href="#">9</a>

2.1.5. Effects of chemical substitution.....	10
2.1.6. Elusive superconductivity and odd-parity hidden order.....	11
2.2. Sr <sub>3</sub> Ir <sub>2</sub> O <sub>7</sub> ( $n = 2$ ) .....	12
2.2.1. Critical structural features.....	13
2.2.2. Magnetic properties.....	13
2.2.3. Transport properties.....	14
2.2.4. Effects of chemical substitution.....	14
2.2.5. Effects of high pressure.....	14
2.3. SrIrO <sub>3</sub> and its derivative ( $n = \infty$ ) .....	15
3. Magnetism of Honeycomb lattices and other geometrically frustrated iridates.....	16
3.1. Two-dimensional honeycomb lattices.....	16
3.1.1. Na <sub>2</sub> IrO <sub>3</sub> and Li <sub>2</sub> IrO <sub>3</sub> .....	16
3.1.2. Ru-based Honeycomb lattices Na <sub>2</sub> RuO <sub>3</sub> , Li <sub>2</sub> RuO <sub>3</sub> , and $\alpha$ -RuCl <sub>3</sub> .....	17
3.2. $\beta$ -Li <sub>2</sub> IrO <sub>3</sub> and $\gamma$ -Li <sub>2</sub> IrO <sub>3</sub> .....	18
3.3. Hyperkagome Na <sub>4</sub> Ir <sub>3</sub> O <sub>8</sub> and pyrochlore iridates.....	19
4. Double-perovskite iridates with Ir <sup>5+</sup> (5d <sup>4</sup> ) ions: nonmagnetic singlet $J_{\text{eff}} = 0$ state? .....	20
5. Future challenges and outlook .....	21
Acknowledgments.....	22
References.....	23

## 1. Introduction

It is now apparent that novel materials, which often exhibit surprising or even revolutionary physical properties, are necessary for critical advances in technologies that affect the everyday lives of people. For example, a number of discoveries involving superconducting and magnetic materials, polymers and thin-film processing have underpinned the development of novel medical diagnostic tools, personal electronic devices, advanced computers, and powerful motors and actuators for automobiles. Transition metal oxides have recently been the subject of enormous activity within both the applied and basic science communities. However, the overwhelming balance of interest was devoted to 3d-elements and their compounds for many decades. Scientists, confronted with ever-increasing pace and competition in research, are beginning to examine the remaining ‘unknown territories’ located in the lower rows of the periodic table of the elements. Although the rare earth and light actinide elements have been aggressively studied for many decades, the heavier 4d- and 5d-elements and their oxides have largely been ignored until recently. The reduced abundance and increased production costs for many of these elements have certainly discouraged basic and applied research into their properties. What has not been widely appreciated, however, is that 4d- and 5d-elements and their compounds exhibit unique competitions between fundamental interactions that result in physical behaviors and empirical trends that markedly differ from their 3d counterparts.

Recently, iridium oxides or iridates have attracted growing attention, due to the influence of strong spin-orbit interactions (SOI) on their physical properties; these effects were justifiably ignored in theoretical treatments of 3d and other materials

of interest (except for the rare earth and actinide classes). Traditional arguments suggest that iridates should be more metallic and less magnetic than materials based upon 3d and 4f-elements, because 5d-electron orbitals are more extended in space, which increases their electronic bandwidth (figure 1(a)). This conventional wisdom conflicts with early observations of two empirical trends inherent in iridates such as the Ruddlesden-Popper phases, Sr <sub>$n+1$</sub> Ir <sub>$n$</sub> O <sub>$3n+1$</sub>  ( $n = 1$  and 2;  $n$  defines the number of Ir-O layers in a unit cell) [1–5] and hexagonal BaIrO<sub>3</sub> [6]. First, complex magnetic states occur with high critical temperatures but unusually low ordered moments. Second, ‘exotic’ insulating states, rather than metallic states, are commonly observed [1–6] (see table 1).

The early observations during the 1990s and early 2000s [1–6], for example, signaled physics unique to the 5d-based materials and motivated extensive investigations in recent years, which eventually led to the recognition that a rare interplay of on-site Coulomb repulsion,  $U$ , crystalline fields and strong SOI has unique, intriguing consequences in iridates. The most profound manifestation of such an interplay is characterized by the  $J_{\text{eff}} = 1/2$  Mott state in Sr<sub>2</sub>IrO<sub>4</sub>, which was first identified in 2008 [7–9]. This quantum state represents novel physics and has since generated a surge of interest in this class of materials.

It is now recognized that the strong SOI along with  $U$  can drive novel narrow-gap Mott states in iridates. *The SOI is a relativistic effect that is proportional to Z<sup>2</sup>* ( $Z$  is the atomic number; e.g.  $Z = 29$  and 77 for Cu and Ir, respectively) [10, 11]. It needs to be pointed out that for the outer electrons, the strength of SOI scales with  $Z^2$ , rather than  $Z^4$  although the  $Z^4$ -dependence is more often cited in the literature [11]. This is because the screening of the nuclear charge by the core electrons renders the effective  $Z^2$ -dependence of SOI for the large  $Z$  outer electrons; the  $Z^4$ -dependence of SOI is for the unscreened hydrogenic wavefunctions. *The SOI is approximately 0.4 eV in iridates (compared to ~20 meV in 3d materials), and splits the t<sub>2g</sub> bands into states with  $J_{\text{eff}} = 1/2$  and  $J_{\text{eff}} = 3/2$ , the latter having lower energy* [7] (figure 1(b) and table 2). Since Ir<sup>4+</sup>(5d<sup>5</sup>) ions provide five 5d-electrons to bonding states, four of them fill the lower  $J_{\text{eff}} = 3/2$  bands, and one electron partially fills the  $J_{\text{eff}} = 1/2$  band, where the Fermi level  $E_F$  resides (figure 1(c)). A combined effect of the strong SOI and  $U$  opens an energy gap  $\Delta$  of the Mott type in the  $J_{\text{eff}} = 1/2$  band supporting the insulating state in the iridates (figure 1(b)) [7]. The splitting between the  $J_{\text{eff}} = 1/2$  and  $J_{\text{eff}} = 3/2$  bands narrows as the dimensionality (i.e.  $n$ ) increases in Sr <sub>$n+1$</sub> Ir <sub>$n$</sub> O <sub>$3n+1$</sub> , and the two bands progressively broaden and contribute to the density of states (DOS) near the Fermi surface. In particular, the bandwidth,  $W$ , of the  $J_{\text{eff}} = 1/2$  band increases from 0.48 eV for  $n = 1$  to 0.56 eV for  $n = 2$  and 1.01 eV for  $n = \infty$  [8]. The ground state evolves with decreasing charge gap  $\Delta$ , from a robust insulating state for Sr<sub>2</sub>IrO<sub>4</sub> ( $n = 1$ ) to a metallic state for SrIrO<sub>3</sub> ( $n = \infty$ ) as  $n$  increases. While the electron hopping occurs via direct d-d overlap and/or through the intermediate oxygen atoms between Ir ions, it is emphasized that the lattice plays a critical role that is seldom seen in other materials in determining the ground state, as discussed below.

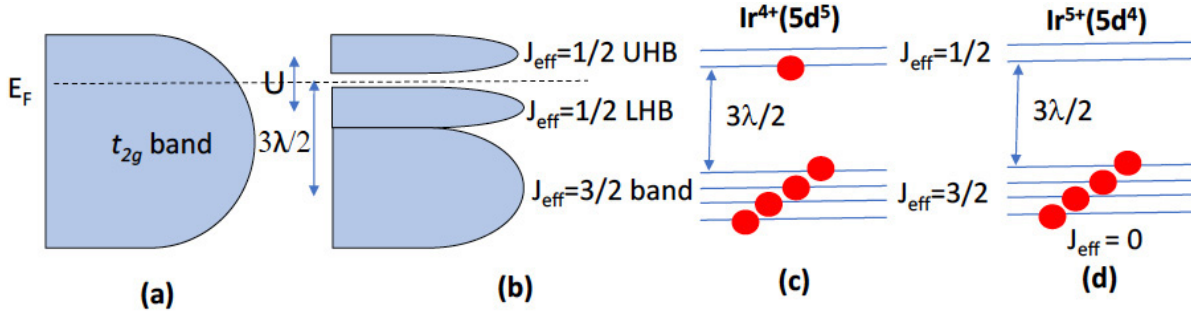


**Figure 1.** Band schematic: (a) the traditionally anticipated broad  $t_{2g}$  band for  $5d$ -electrons; (b) the splitting of the  $t_{2g}$  band into  $J_{\text{eff}} = 1/2$  and  $J_{\text{eff}} = 3/2$  bands due to SOI; (c)  $\text{Ir}^{4+}(5d^5)$  ions provide five  $5d$ -electrons, four of them fill the lower  $J_{\text{eff}} = 3/2$  bands, and one electron partially fills the  $J_{\text{eff}} = 1/2$  band where the Fermi level  $E_F$  resides; and (d) for  $\text{Ir}^{5+}(5d^4)$  ions, four  $5d$ -electrons fill the  $J_{\text{eff}} = 3/2$  bands, leading to a singlet  $J_{\text{eff}} = 0$  state for the strong SOI limit.  $\lambda$  is the strength of SOI.

**Table 1.** Examples of layered iridates.

System	Néel temperature (K)	Ground state
$\text{Sr}_2\text{IrO}_4$ ( $n = 1$ )	240	Canted AFM insulator
$\text{Sr}_3\text{Ir}_2\text{O}_7$ ( $n = 2$ )	285	AFM insulator
$\text{BaIrO}_3$	183	Canted AFM insulator

The SOI-driven  $J_{\text{eff}} = 1/2$  model captures the essence of physics of many iridates with tetravalent  $\text{Ir}^{4+}(5d^5)$  ions (see figure 1(c)). The  $J_{\text{eff}} = 3/2$  states can accommodate four  $5d$  electrons, leaving the fifth electron and one hole in the  $J_{\text{eff}} = 1/2$  band because there are six states (figure 1(c)). This can lead to the opening of a Mott gap. For  $\text{Ir}^{5+}(5d^4)$  ions, on the other hand, the  $J_{\text{eff}} = 3/2$  band exhausts the available electrons and the  $J_{\text{eff}} = 1/2$  states remain empty (see figure 1(d)). However, it is a single-particle approach that is limited to situations where Hund's rule interactions among the electrons can be neglected and it may break down when non-cubic crystal fields, which are not taken into account in this model, become comparable to the SOI. This may result in a mixing of  $J_{\text{eff}} = 1/2$  and  $J_{\text{eff}} = 3/2$  states, altering isotropic wavefunctions that the model is based upon. Indeed, the Hund's rule interactions are more critical for iridates with  $\text{Ir}^{5+}(5d^4)$  ions, and can mix  $J_{\text{eff}} = 1/2$  and  $J_{\text{eff}} = 3/2$  states, resulting in a qualitatively different picture (more discussion in section 4). One such breakdown occurs in  $\text{Sr}_3\text{CuIrO}_6$  due to strong non-octahedral crystal fields [12].

Nevertheless, a wide array of novel phenomena in iridates has been revealed in recent years (e.g. [13–25], and references therein). It has become apparent that materials with such a delicate interplay between SOI,  $U$  and other competing interactions offer wide-ranging opportunities for the discovery of new physics and development of new devices, and it is not surprising that the physics of iridates is one of the most important topics in contemporary condensed matter physics. A great deal of recent theoretical work has appeared in response to early experiments on iridates, such as spin liquids in hyper-kagome structures [20, 21], superconductivity [22–28], Weyl semimetals with Fermi arcs, axion insulators [29], topological insulators, correlated topological insulators [17], Kitaev modes, 3D spin liquids with Fermionic spinons, topological semimetals [13, 17, 30–38], etc. These and many

other theoretical studies have advanced our understanding of  $5d$ -based materials and motivated enormous activity in search of novel states in iridates. It is particularly intriguing that many proposals have met limited experimental confirmation thus far, which makes iridates even more unique and challenging. We note that the SOI is a strong competitor with  $U$  and other interactions, which creates an entirely new hierarchy of energy scales (table 2); the lack of experimental confirmation underscores a critical role of subtle structural distortions that may dictate the low-energy Hamiltonian [13] and need to be more thoroughly addressed both experimentally and theoretically.

In this *Review*, we will discuss some underlying properties of certain representative iridates, namely, layered perovskite or Ruddlesden–Popper iridates (section 2), honeycomb and other geometrically frustrated lattices, all of which feature  $\text{Ir}^{4+}(5d^5)$  ions (figure 1(c)) (section 3), and double perovskite iridates with  $\text{Ir}^{5+}(5d^4)$  ions (see figure 1(d)) (section 4). We review the current status of experimental studies of these materials and challenges that this class of materials presents. We conclude the *Review* with a list of outstanding issues and our outlook of the field, which hopefully could help stimulate more discussions (section 5). It is emphasized that this *Review* is intended to offer only a brief (thus incomplete) survey of some exemplary *experimental observations* and challenges, and it is by no means an exhaustive one. Given the nature of the broad and rapidly evolving field, it is inevitable that we may miss some important results in this field. In addition, this *Review* primarily focuses on properties of bulk single crystals, as a result, a large number of excellent studies of thin films and heterostructures of iridates, for example [39–46], are not included in this article. Since lattice properties are so critical to ground states of iridates, epitaxial thin films with varied strain and/or heterostructures offer a unique, powerful tool for tuning ground states of iridates. This is evidenced in [39–46] and many other recent publications. There are also excellent review articles emphasizing theoretical aspects of iridates [17, 18].

We tabulate a number of existing iridates in table 3. These iridates are grouped according to their underlying crystal structures. Exemplary phenomena along with valence states of the iridates are also listed. There are a few general remarks on these iridates: With a few exceptions (e.g.  $\text{SrIrO}_3$ ,  $\text{Bi}_2\text{Ir}_2\text{O}_7$ ,

**Table 2.** Comparison between  $3d$  and  $4d/5d$  electrons.

Electron type	$U$ (eV)	$\lambda$ (eV)	Spin state	Interactions	Phenomena
$3d$	5–7	0.01–0.1	High	$U > CF > \lambda$	Magnetism/HTSC
$4d$	0.5–3	0.1–0.3	Low/intermediate	$U \sim CF > \lambda$	p-wave SC
$5d$	0.4–2	0.1–1	Low	$U \sim CF \sim \lambda$	$J_{\text{eff}} = 1/2$ Mott State

Note: SC = superconductivity; Hund's rule coupling is significant for  $4d$ - and  $5d$ -electrons.

and  $\text{Pr}_2\text{Ir}_2\text{O}_7$ ), most iridates feature insulating and magnetic ground states; while the insulating states of these materials may vary in detail, they are due largely to the combined effect of SOI and  $U$ . Magnetic moments are in general weak, often a fraction of one Bohr magneton per Ir ion (The local moment for  $J_{\text{eff}} = 1/2$  state has  $1 \mu_B$  but covalency of Ir–O bonding reduces the moment). Furthermore, no first-order transitions are discerned thus far, and insulator-metal transitions tend to be gradual and continuous in this class of materials. A rotation of the  $\text{IrO}_6$ -octahedra about the  $c$ -axis is commonplace but tilting of the  $\text{IrO}_6$ -octahedra is rare in layered perovskite iridates.

## 2. Survey of physical properties of Ruddlesden–Popper iridates, $\text{Sr}_{n+1}\text{Ir}_n\text{O}_{3n+1}$ ( $n = 1, 2$ , and $\infty$ )

### 2.1. $\text{Sr}_2\text{IrO}_4$ ( $n = 1$ )

$\text{Sr}_2\text{IrO}_4$  is the archetype  $J_{\text{eff}} = 1/2$  Mott insulator with a Néel temperature  $T_N = 240\text{ K}$  [1–4, 7, 9], an energy gap  $\Delta \leqslant 0.62\text{ eV}$  (see figure 2) [84–86] and a relatively small magnetic coupling energy of 60–100 meV [24, 85]. It is perhaps the most extensively studied iridate thus far. The distinct energy hierarchy featuring a strong SOI and its structural, electronic and magnetic similarities to those of the celebrated  $\text{La}_2\text{CuO}_4$  (i.e.  $\text{K}_2\text{NiF}_4$  type, one hole per Ir or Cu ion, pseudospin- or spin-1/2 AFM, etc) have motivated a large number of experimental and theoretical investigations on  $\text{Sr}_2\text{IrO}_4$  in recent years.

**2.1.1. Critical structural features.** A unique and important structural feature of  $\text{Sr}_2\text{IrO}_4$ , which has critical implications for the ground state, is a rotation of the  $\text{IrO}_6$ -octahedra about the  $c$ -axis by  $\sim 11^\circ$ , which results in a larger unit cell volume by a factor  $\sqrt{2} \times \sqrt{2} \times 2$ . It is commonly thought that  $\text{Sr}_2\text{IrO}_4$  crystallizes in a tetragonal structure with space-group  $I4_1/acd$  (No. 142) with  $a = b = 5.4846\text{ \AA}$  and  $c = 25.804\text{ \AA}$  at 13 K [1–3], as shown in figure 3. More recently, studies of neutron diffraction and second-harmonic generation (SHG) of single-crystal  $\text{Sr}_2\text{IrO}_4$  [87, 88] reveal structural distortions and forbidden reflections such as  $(1, 0, 2n + 1)$  for the space group  $I4_1/acd$  over a wide temperature interval,  $4\text{ K} < T < 600\text{ K}$ . These results indicate the absence of the  $c$ - and  $d$ -glide planes, leading to a further reduced structural symmetry with a space group  $I4_1/a$  (No. 88). One defining characteristic of  $\text{Sr}_2\text{IrO}_4$  and other iridates is that the strong SOI strongly couples physical properties to the lattice degrees of freedom [13, 50, 87, 89], which is seldom seen in other materials [90, 91].

The relationship between the rotation of the  $\text{IrO}_6$  octahedra and magnetic moment canting in the iridates was first discussed in [13] in which a theoretical model proposed a strong magnetoelastic coupling in  $\text{Sr}_2\text{IrO}_4$ , and a close association

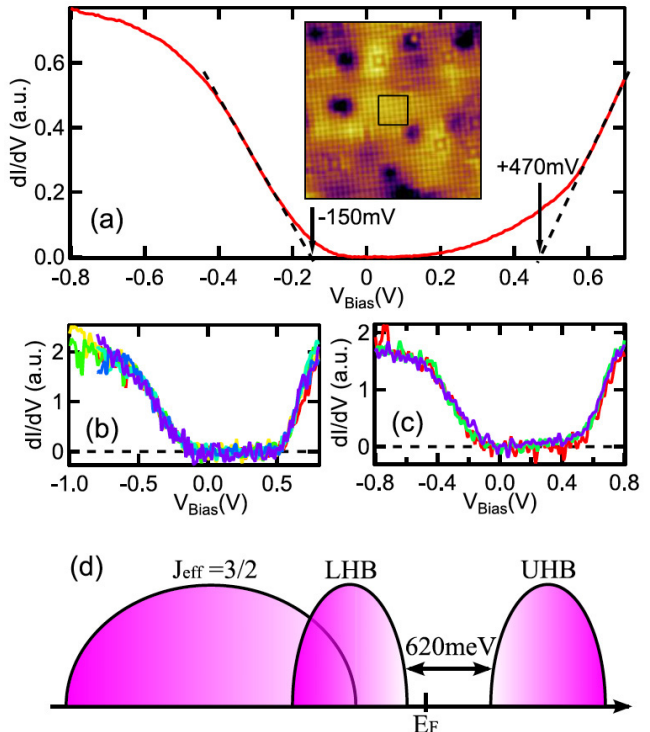


**Figure 2.**  $\text{Sr}_2\text{IrO}_4$ : the 620 meV energy gap. (a) The local density of states (LDOS) measured over the  $2 \times 2\text{ nm}^2$  area indicated by the square in the image (inset). The dashed lines are drawn to indicate the band edges at  $-150\text{ mV}$  and  $+470\text{ mV}$ . (b) and (c) LDOS taken at locations away from defects, (b) without and (c) with the gradual increase. (d) Diagram showing energy bands with two important features: the 620 meV insulating gap and the overlap between the lower Hubbard band (LHB) and the  $J_{\text{eff}} = 3/2$  band [86]. Reprinted figure with permission from [86], Copyright (2014) by the American Physical Society.

between the magnetic moment canting and the ratio of the lattice parameter of the  $c$ -axis to the  $a$ -axis [13], as a consequence of the strong SOI. Indeed, the strong locking of the moment canting to the  $\text{IrO}_6$ -rotation (by  $11.8(1)^\circ$ ) is experimentally manifest in studies of x-ray resonant scattering [92] and SHG [93]. In particular, the SHG study indicates that the  $I4_1/a$  space group requires a staggering of the sign of the tetragonal distortion ( $\Delta_1$  and  $\Delta_2$ ), which helps explain the magnetoelastic locking, as illustrated in figure 4 [93].

As discussed below, the rotation of  $\text{IrO}_6$  octahedra, which corresponds to a distorted in-plane  $\text{Ir1}-\text{O2}-\text{Ir1}$  bond angle, plays an extremely important role in determining the electronic and magnetic structures. The  $\text{Ir1}-\text{O2}-\text{Ir1}$  bond angle can be tuned via magnetic field [50], high pressure [94], electric field [89] and epitaxial strain [39]. The lattice properties not only make the ground state readily tunable but also provide a new paradigm for development of functional materials and devices.

**Table 3.** Some existing iridates and exemplary phenomena.

Structure	Compound	Ir ion	Exemplary phenomena
Layered perovskite	1. Sr <sub>2</sub> IrO <sub>4</sub> <sup>a</sup>	Ir <sup>4+</sup> (5d <sup>5</sup> )	1. $J_{\text{eff}} = 1/2$ insulator; $T_N = 240\text{ K}$ [1–4], S-shaped IV curves [4] <sup>b</sup>
	2. Sr <sub>3</sub> Ir <sub>2</sub> O <sub>7</sub> <sup>a</sup>		2. $J_{\text{eff}} = 1/2$ or band insulator; $T_N = 285\text{ K}$ [5], confined metal at 60 GPa [47] <sup>b</sup>
	3. SrIrO <sub>3</sub>		3. Paramagnetic (semi-)metal (high pressure phase) [8, 48]
	4. Ba <sub>2</sub> IrO <sub>4</sub>		4. $J_{\text{eff}} = 1/2$ insulator; $T_N \sim 240\text{ K}$ (high pressure phase) [49]
Hexagonal perovskite	1. BaIrO <sub>3</sub> ,	Ir <sup>4+</sup> (5d <sup>5</sup> )	1. $J_{\text{eff}} = 1/2$ Mott insulator; $T_N = 183\text{ K}$ ; CDW, S-shaped IV curves [6]
	2. SrIrO <sub>3</sub>		2. Nearly ferromagnetic metal [58]
	3. Ca <sub>5</sub> Ir <sub>3</sub> O <sub>12</sub>		3. Insulator; $T_N = 12\text{ K}$ [59]
	4. Ca <sub>4</sub> IrO <sub>6</sub>		4. Insulator; $T_N = 6\text{ K}$ [59]
	5. Ba <sub>3</sub> IrTi <sub>2</sub> O <sub>9</sub>		5. Insulator; no long-range order [60]
	6. Ba <sub>3</sub> NdIr <sub>2</sub> O <sub>9</sub>		6. Magnetic insulator; $T_N = 20\text{ K}$ [61]
	7. Ba <sub>3</sub> LiIr <sub>2</sub> O <sub>8</sub>		7. AFM order at $T_N = 75\text{ K}$ [62]
	8. Ba <sub>3</sub> NaIr <sub>2</sub> O <sub>8</sub>		8. AFM order at $T_N = 50\text{ K}$ [62]
	1. Na <sub>2</sub> IrO <sub>3</sub>		1. Zig-Zag Magnetic order; $T_N = 18\text{ K}$ [32, 33]
Honeycomb	2. $\alpha$ -Li <sub>2</sub> IrO <sub>3</sub>	Ir <sup>4+</sup> (5d <sup>5</sup> )	2. Incommensurate order [63]
	3. $\beta$ -Li <sub>2</sub> IrO <sub>3</sub>		3. Incommensurate order [64, 65]
	4. $\gamma$ -Li <sub>2</sub> IrO <sub>3</sub>		4. Incommensurate order [66, 67]
	5. Na <sub>4</sub> Ir <sub>3</sub> O <sub>8</sub>		5. Spin liquid state [20]
	1. Bi <sub>2</sub> Ir <sub>2</sub> O <sub>7</sub>		1 and 2: Metallic states; strong magnetic instability, etc [68–70]
Pyrochlore	2. Pb <sub>2</sub> Ir <sub>2</sub> O <sub>7</sub>	Ir <sup>4+</sup> (5d <sup>5</sup> )	3. Metal-insulator transition, insulating states, spin liquid, RE ionic size dependence [71, 72]
	3. RE <sub>2</sub> Ir <sub>2</sub> O <sub>7</sub> RE = rare earth ion		
	M = Mg, Ni		
Double Perovskite	1. Sr <sub>2</sub> YIrO <sub>6</sub>	Ir <sup>5+</sup> (5d <sup>4</sup> )	1. Weak AFM state, correlated insulator [73]
	2. Ba <sub>2</sub> YIrO <sub>6</sub>		2. Insulator [74, 75], AFM insulator [194]
	3. Sr <sub>2</sub> REIrO <sub>6</sub>		3. Magnetic insulator [73]
	4. Sr <sub>2</sub> CoIrO <sub>6</sub>		4. Magnetic metal, $T_{N1} = 60\text{ K}$ , $T_{N2} = 120\text{ K}$ [76]
	5. Sr <sub>2</sub> FeIrO <sub>6</sub>		5. Magnetic insulator, $T_N = 60\text{ K}$ [76]
	6. La <sub>2</sub> ZnIrO <sub>6</sub>		6. Weak ferromagnetic insulator, $T_N = 7.5\text{ K}$ [77]
	7. La <sub>2</sub> MgIrO <sub>6</sub>		7. Weak ferromagnetic insulator, $T_N = 12\text{ K}$ [77]
	8. RE <sub>2</sub> MIrO <sub>6</sub>		8. Weak AFM ground state with canted spin [78]
	M = Mg, Ni		
Post-perovskite	NaIrO <sub>3</sub>	Ir <sup>5+</sup> (5d <sup>4</sup> )	Paramagnetic insulator [79]
	CaIrO <sub>3</sub>		Quasi-one-dimensional antiferromagnet [80, 81]
Others	Ba <sub>5</sub> AlIr <sub>2</sub> O <sub>11</sub>	Ir <sup>4.5+</sup>	1. Spin-1/2/dimer chain, charge and magnetic orders [82]
	Sr <sub>3</sub> NiIrO <sub>6</sub>		2. One-dimensional chains and large coercivity [83]

<sup>a</sup> Dopants.<sup>b</sup> Dopants: K [50], Ca [51], Mn [52], Ru [53, 54], Rh [55], La [50], Eu [56], Tb [57].

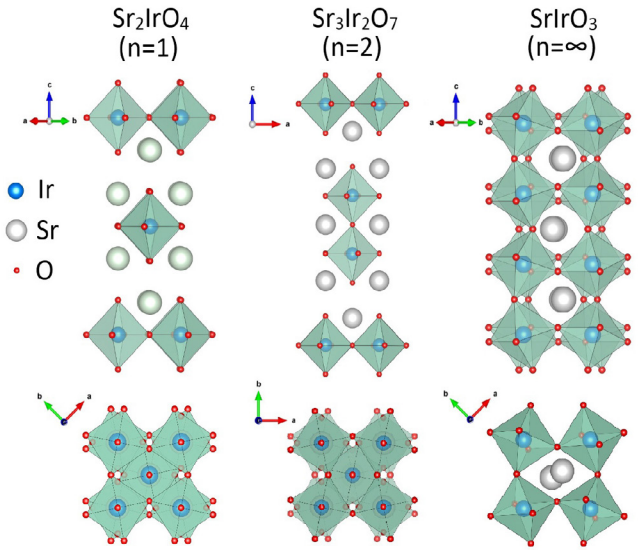


**Figure 3.** The crystal structure of layered perovskites  $\text{Sr}_{n+1}\text{Ir}_n\text{O}_{3n+1}$  for  $n = 1, 2$  and  $\infty$ . Note that the lower three panels illustrate the rotation of  $\text{IrO}_6$  octahedra about the  $c$ -axis for  $\text{Sr}_2\text{IrO}_4$  ( $n = 1$ ),  $\text{Sr}_3\text{Ir}_2\text{O}_7$  ( $n = 2$ ) and  $\text{SrIrO}_3$  ( $n = \infty$ ), respectively.

Remarkably, that the  $13(1)^\circ$  canting of the moments away from the  $a$ -axis closely tracks the staggered rotation of the  $\text{IrO}_6$  octahedra [92, 93] sharply contrasts the behavior of  $3d$  oxides [95], in which structural distortions are noticeably decoupled with magnetic moment canting.

**2.1.2. Magnetic properties.** Early experimental studies suggested that  $\text{Sr}_2\text{IrO}_4$  was a weak ferromagnet with a Curie temperature at  $240\text{K}$  primarily because the temperature dependence of magnetization, along with a positive Curie–Weiss temperature,  $\theta_{\text{CW}} = +236\text{K}$ , appeared to be consistent with that of a weak ferromagnet (see figure 5(a)) [2–5].

It is now understood that the observed weak ferromagnetic behavior arises from an underlying canted antiferromagnetic (AFM) order [87]. This also raises a question as to why  $\theta_{\text{CW}}$  ( $= +236\text{K}$ ), which is extrapolated from the inverse susceptibility  $\Delta\chi^{-1}$  ( $\Delta\chi = \chi(T) - \chi_0$ , where  $\chi_0$  is a  $T$ -independent contribution), is positive in the presence of the AFM ground state (figure 5(a)) [4, 50, 96]. Results of more recent x-ray scattering and neutron diffraction investigations of single-crystal  $\text{Sr}_2\text{IrO}_4$  confirm that the system indeed undergoes a long-range AFM transition at  $224(2)\text{ K}$  with an ordered moment of  $0.208(3)\text{ }\mu_{\text{B}}/\text{Ir}$  and a canted magnetic configuration within the basal plane [87]. The magnetic configuration illustrated in figures 6(b)–(d) shows that magnetic moments are projected along the  $b$ -axis with a staggered  $\downarrow\uparrow\downarrow$  pattern along the  $c$ -axis. Remarkably, these moments deviate  $13(1)^\circ$  away from the  $a$ -axis (figure 6(c)), indicating that the magnetic moment canting rigidly tracks the staggered rotation of the  $\text{Ir}_6$  octahedra discussed above. This strong coupling is a signature feature of the iridates in general and sharply contrasts to the situation in  $3d$  oxides, such as  $\text{Ca}_3\text{Mn}_2\text{O}_7$ , where a collinear magnetic structure exists in a strongly distorted crystal structure [95]. Nevertheless, the magnetic canting results in  $0.202(3)$  and  $0.049(2)\text{ }\mu_{\text{B}}/\text{Ir-site}$  for the  $a$ -axis and the  $b$ -axis, respectively

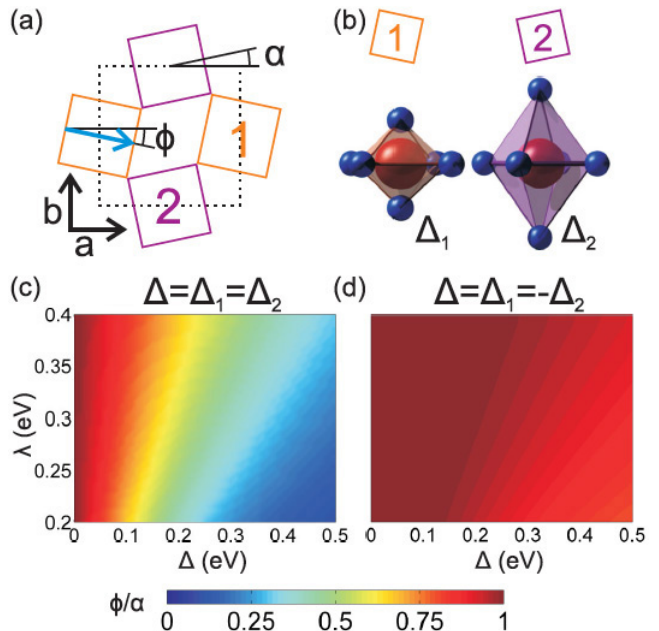


**Figure 4.**  $\text{Sr}_2\text{IrO}_4$ : (a) illustration of an  $\text{IrO}_2$  plane. The oxygen octahedra rotate about the  $c$ -axis by  $\alpha$  creating a two-sublattice structure. The magnetic moments couple to the lattice and exhibit canting angles  $\phi$ . (b) An unequal tetragonal distortion ( $\Delta_1$  and  $\Delta_2$ ) on the two sublattices as required by the  $I4_1/a$  space group. (c) The ratio  $\phi/\alpha$  as a function of both SOI  $\lambda$  and  $\Delta$  calculated for the case of uniform and (d) staggered ( $\Delta_1 = -\Delta_2$ ) tetragonal distortion assuming  $U = 2.4\text{ eV}$ , Hund's coupling  $J_{\text{H}} = 0.3\text{ eV}$ , hopping  $t = 0.13\text{ eV}$ , and  $\alpha = 11.5^\circ$  [93]. Reprinted figure with permission from [93], Copyright (2015) by the American Physical Society.

(figure 6) [87]. For comparison, the ordered moment extrapolated from the magnetization, which measures net magnetic moment, is less than  $0.08\text{ }\mu_{\text{B}}/\text{Ir}$  within the basal plane [96].

Indeed, a muon-spin rotation ( $\mu\text{SR}$ ) study reports a low frequency mode that corresponds to the precession of weak ferromagnetic moments arising from a spin canting and a high frequency mode resulting from the precession of the antiferromagnetic sublattices [97]. Another study indicates a small energy gap for the AFM excitations,  $0.83\text{ meV}$ , suggesting an isotropic Heisenberg dynamics [98]. Remarkably, a high-resolution inelastic light (Raman) scattering study of the low-energy magnetic excitation spectrum of  $\text{Sr}_2\text{IrO}_4$  shows that the high-field ( $>1.5\text{ T}$ ) in-plane spin dynamics is isotropic and governed by the interplay between the applied field and the small in-plane ferromagnetic spin components induced by the Dzyaloshinskii–Moriya interaction. However, the spin dynamics of  $\text{Sr}_2\text{IrO}_4$  at lower fields ( $H < 1.5\text{ T}$ ) exhibits important effects associated with interlayer coupling and in-plane anisotropy, including a spin-flop transition in  $\text{Sr}_2\text{IrO}_4$  that occurs either discontinuously or via a continuous rotation of the spins, depending on the in-plane orientation of the applied field. These results show that in-plane anisotropy and interlayer coupling effects play important roles in the low-field magnetic and dynamical properties of  $\text{Sr}_2\text{IrO}_4$  [56]. It is also found that  $\text{Sr}_2\text{IrO}_4$  (as well as  $\text{Sr}_3\text{Ir}_2\text{O}_7$ ) exhibits pronounced two-magnon Raman scattering features and that the SOI might not be strong enough to quench the orbital dynamics in the paramagnetic state [99].

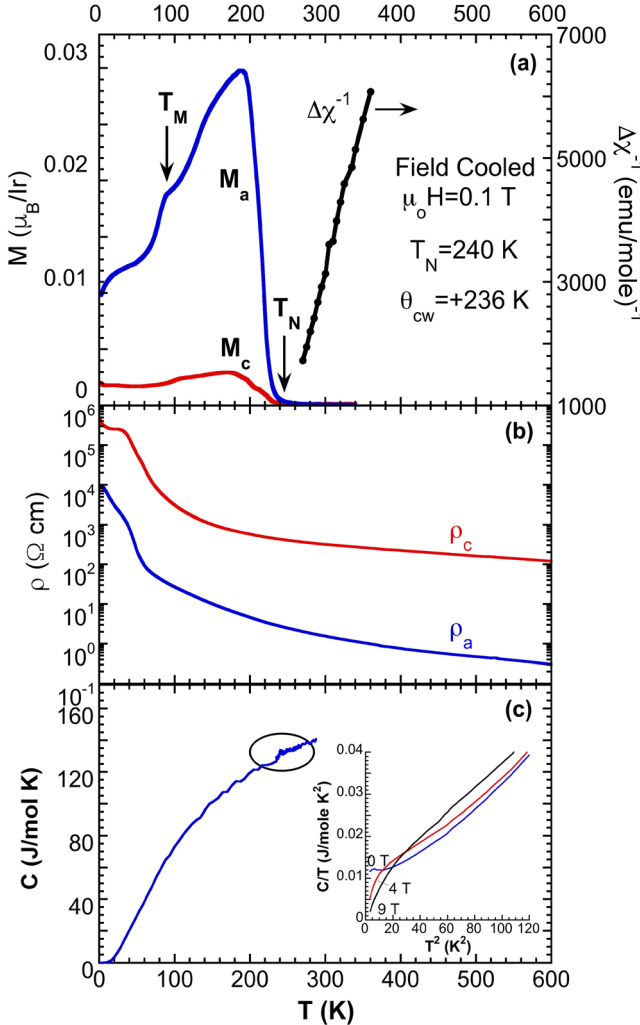


**Figure 5.**  $\text{Sr}_2\text{IrO}_4$ : (a) the temperature dependence of magnetization for the  $a$ - and  $c$ -axis,  $M_a$  and  $M_c$ , at 0.1 T and the inverse magnetic susceptibility  $\Delta\chi^{-1}$  (the right scale), (b) the electrical resistivity for the  $a$ - and  $c$ -axis,  $\rho_a$  and  $\rho_c$ , and (c) the specific heat,  $C$ . The inset:  $C/T$  versus  $T^2$  at a few magnetic fields.  $T_M$  marks a magnetic anomaly near 100 K [50]. Reprinted figure with permission from [50], Copyright (2011) by the American Physical Society.

A close examination of the low-field magnetization,  $M(T)$ , reveals two additional anomalies at  $T_M \approx 100$  K and 25 K (not marked) in  $M_a(T)$  and  $M_c(T)$  (see figure 5(a)), suggesting a moment reorientation below 100 K. The existence of the reorientation is further corroborated by the  $\mu\text{SR}$  study of  $\text{Sr}_2\text{IrO}_4$  in which two structurally equivalent muon sites experience distinct local magnetic fields below 100 K characterized by the development of a second precession signal that is fully established below 20 K [97]. This behavior, which is likely a result of the balance of competing energies that changes with temperature, correlates with a change in the Ir1–O2–Ir1 bond angle that leads to the gradual reorientation near 100 K. This reorientation of the moments may be at the root of the unusual magnetoresistivity [50] and giant magnetoelectric behavior [96] that does not depend on the magnitude and spatial dependence of the magnetization, as conventionally anticipated.

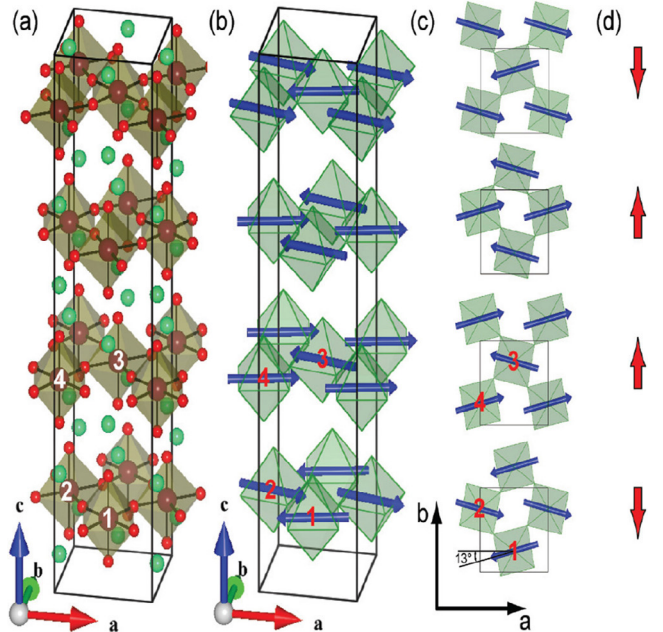


**Figure 6.**  $\text{Sr}_2\text{IrO}_4$ : (a) the crystal structure of  $\text{Sr}_2\text{IrO}_4$ . Each  $\text{IrO}_6$  octahedron rotates 11.8° about the  $c$ -axis. The Ir atoms of the non-primitive basis are labeled 1, 2, 3, and 4 plus the body centering translation (1/2, 1/2, 1/2). (b) The refined magnetic structure from single-crystal neutron diffraction measurements. (c) The same magnetic moment configuration projected on the basal planes. (d) The net moment projected along the  $b$ -axis for individual layers [87]. Note that this figure illustrates that magnetic canting closely tracks the  $\text{IrO}_6$  rotation. Reprinted figure with permission from [87], Copyright (2013) by the American Physical Society.

**2.1.3. Transport properties.** The electrical resistivity of  $\text{Sr}_2\text{IrO}_4$  for the  $a$ - and  $c$ -axis,  $\rho_a$  and  $\rho_c$ , exhibits insulating behavior throughout the entire temperature range measured up to 600 K, as shown in figure 5(b). The anisotropy,  $\rho_c/\rho_a$ , is significant, ranging from  $10^2$  to  $10^3$  although it is much smaller than  $10^4$ – $10^5$  for  $\text{La}_2\text{CuO}_4$  because of the extended nature of the  $5d$ -electrons.

Both  $\rho_a$  and  $\rho_c$  exhibit anomalies at  $T_M (\approx 100 \text{ K})$  and 25 K, but conspicuously not at  $T_N (= 240 \text{ K})$ , as shown in figures 5(a) and (b). It has now become clear that this is a signature behavior of  $\text{Sr}_2\text{IrO}_4$  in which transport properties exhibit no discernable anomaly corresponding to the AFM transition at  $T_N = 240 \text{ K}$  [4, 50, 96]. In addition, the observed specific heat anomaly  $|\Delta C|$  is tiny,  $\sim 4 \text{ mJ mole}^{-1} \text{ K}^{-1}$  for  $\text{Sr}_2\text{IrO}_4$  (figure 5(c)), in spite of its robust, long-range magnetic order at  $T_N = 240 \text{ K}$ . It is worth mentioning that  $C(T)$  below 10 K is predominantly proportional to  $T^3$  at  $\mu_0 H = 0$  and 9 T (figure 5(c) inset), due to a Debye-phonon and/or magnon contributions from the AFM ground state. The field-shift  $[C(T,H) - C(T,0)]/C(T,0) \sim 16\%$  at 9 T indicates a significant magnetic contribution to  $C(T)$ , which is absent near  $T_N$ . The weak phase transition signatures suggest that thermal and transport properties may not be driven by the same mechanisms that dictate the magnetic behavior. Indeed, the energy gap for the AFM excitations, 0.83 meV, is almost negligible compared to the charge gap, 0.62 eV (figure 2). The effect of the magnetic state on the transport properties is thus inconsequential near  $T_N$  but more

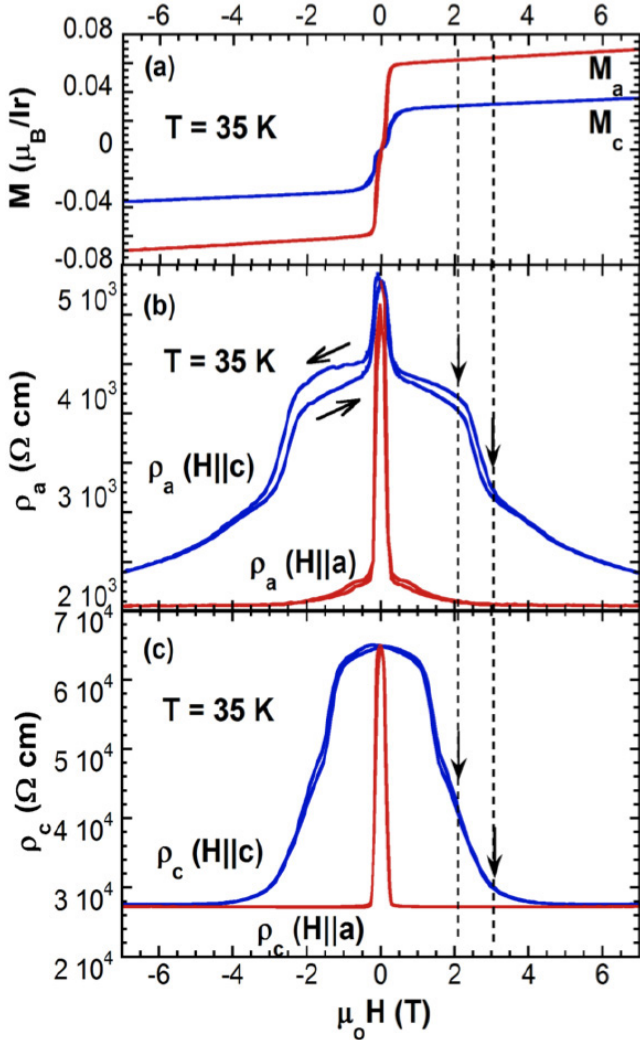


**Figure 7.**  $\text{Sr}_2\text{IrO}_4$ : the field dependences at  $T = 35$  K of: (a) the magnetizations  $M_a$  and  $M_c$ . (b) The  $a$ -axis resistivity  $\rho_a$  for  $\mathbf{H} \parallel \mathbf{a}$  and  $\mathbf{H} \parallel \mathbf{c}$ . (c) The  $c$ -axis resistivity  $\rho_c$  for  $\mathbf{H} \parallel \mathbf{a}$  and  $\mathbf{H} \parallel \mathbf{c}$  [50]. Note that the finite  $M_c$  is induced by a small magnetic field along the  $c$ -axis that tilts the vectors out of the plane, consequently, the DM product is nonzero for  $M_c$ . Reprinted figure with permission from [50], Copyright (2011) by the American Physical Society.

significant at low temperatures. This sharply contrasts with the behavior driven by strong couplings between the magnetic and charge gaps commonly observed in other correlated electron systems, particularly in  $3d$ -transition metal oxides [90, 91].

In addition, the saturating resistivity at low temperatures (figure 5(b)) is interesting, and is commonly seen in  $\text{Sr}_2\text{IrO}_4$ . This behavior, whose origin is still unclear, raises a question as to whether it is due to impurity scattering or profound mechanism(s) such as surface Dirac cones in  $\text{SmB}_6$  [100].

In the following, we examine a few outstanding features of electrical and thermal transport properties that emphasize the importance of lattice degrees of freedom.

**2.1.3.1. Magnetoresistance.** The electrical resistivity is coupled to the magnetic field in a peculiar fashion and so far no available model can describe the observed magnetoresistivity shown in figure 7 [50]. We focus on a representative

temperature  $T = 35$  K. Both  $\rho_a(\mathbf{H} \parallel \mathbf{a})$  (figure 7(b)) and  $\rho_c(\mathbf{H} \parallel \mathbf{a})$  (figure 7(c)) exhibit an abrupt drop by  $\sim 60\%$  near  $\mu_0 H = 0.3$  T applied along the  $a$ -axis, where a metamagnetic transition occurs [4, 50, 96, 101]. These data partially track the field dependences of  $M_a(H)$  and  $M_c(H)$  shown in figure 7(a), and suggest a reduction of spin scattering. However, given the small ordered moment  $< 0.08 \mu_B/\text{Ir}$ , a reduction of spin scattering alone certainly cannot account for such a drastic reduction in  $\rho(H)$ . Even more strikingly, for  $\mathbf{H} \parallel \mathbf{c}$ -axis, both  $\rho_a(\mathbf{H} \parallel \mathbf{c})$  and  $\rho_c(\mathbf{H} \parallel \mathbf{c})$  exhibit anomalies at  $\mu_0 H = 2$  T and 3 T, respectively, which lead to a large overall reduction of resistivity by more than 50%. However, no anomalies corresponding to these transitions in  $M_a(H)$  and  $M_c(H)$  are discerned! In addition,  $dM/dH$  shows no slope change near  $\mu_0 H = 2$  and 3 T. Such behavior is clearly not due to the Lorenz force because  $\rho_c(\mathbf{H} \parallel \mathbf{c})$  exhibits the same behavior in a configuration where both the current and  $\mathbf{H}$  are parallel to the  $c$ -axis (figure 7(c)). Note that a small magnetic field along the  $c$ -axis can readily tilt the vectors out of the plane, as a result, the Dzyaloshinsky–Moriya (DM) product is nonzero for  $M_c$ .  $M_c$  would be zero without the applied magnetic field.

An essential contributor to conventional magnetoresistivity is spin-dependent scattering; negative magnetoresistance is often a result of the reduction of spin scattering due to spin alignment with increasing magnetic field. The data in figure 7 therefore raise a fundamental question: Why does the resistivity sensitively depend on the orientation of magnetic field  $H$ , but show no direct relevance to the measured magnetization when  $H \parallel c$ -axis? While no conclusive answers to the question are yet available, such varied magneto-transport behavior with temperature underscores the temperature-dependent Ir1–O2–Ir1 bond angle [4, 19, 50, 87, 97].

Moreover, such magnetotransport properties on the nanoscale are also examined using a point-contact technique [101]. Negative magnetoresistances up to 28% are discerned at modest magnetic fields (250 mT) applied within the basal plane and electric currents flowing perpendicular to the plane. The angular dependence of the magnetoresistance shows a crossover from fourfold to twofold symmetry in response to an increasing magnetic field with angular variations in resistance from 1% to 14%, which is attributed to the crystalline component of anisotropic magnetoresistance and canted moments in the basal plane. The observed anisotropic magnetoresistance is large compared to that in  $3d$  transition metal alloys or oxides (0.1%–0.5%) and is believed to be associated with the SOI [101].

**2.1.3.2. The ‘S-shaped’ I–V characteristic and switching effect.** Early studies of iridates have also uncovered a distinct feature, namely, the non-ohmic behavior [4, 6]. The non-ohmic behavior exhibits current-controlled negative differential resistivity or NDR for both the  $a$ - and  $c$ -axis directions, as shown in figure 8. The  $I$ – $V$  curve near the voltage threshold  $V_{\text{th}}$  (onset of negative differential resistivity) for all temperatures shows a hysteresis effect. As the current  $I$  increases further (much higher than 100 mA in this case), the ohmic behavior is restored and gives rise to an  $I$ – $V$  curve characterized by an ‘S’ shape. The

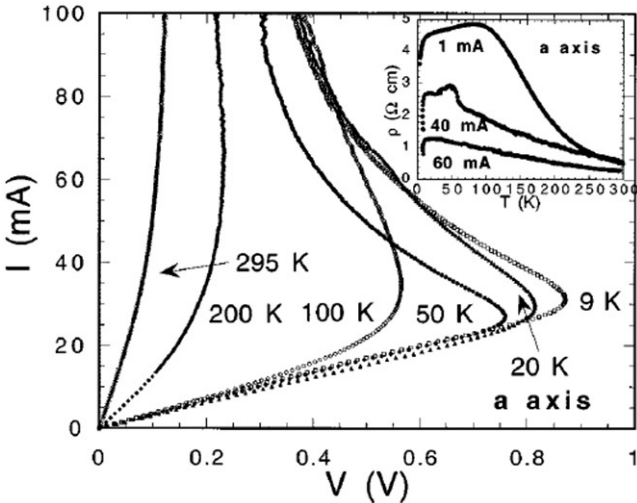


**Figure 8.**  $\text{Sr}_2\text{IrO}_4$ : current  $I$  versus voltage  $V$  for various temperatures. Inset:  $\rho$  along the  $a$ -axis versus temperature for various currents [4]. Reprinted figure with permission from [4], Copyright (1998) by the American Physical Society.

S-shaped effect is categorically different from the more commonly seen ‘N’-shaped effect or the Gunn effect, which is referred to as voltage-controlled NDR and attributed to electrons transferred between multienergy valleys [4, 6]. It has been reported previously that the S-shaped effect is observed in some materials with a metal-insulator transition such as  $\text{CuIr}_{2}\text{S}_{4-x}\text{Se}_x$ , and is attributed to an electro-thermal effect [102]. A similar  $I$ – $V$  characteristic has been found later in bulk single-crystal  $\text{BaIrO}_3$  [6] and  $\text{Ca}_3\text{Ru}_2\text{O}_7$  [6], and more recently in  $\text{VO}_2$  [103]. The S-shaped  $I$ – $V$  characteristic is restricted to the AFM insulating state. Its mechanism is still unclear, although it was suggested that the ‘S’ effect might be related to a small band gap associated with charge density waves (CDW) [4, 6]. In this case, the CDW is then pinned to the underlying lattice and slides relative to the lattice, giving rise to the NDR at  $V > V_{\text{th}}$ . Accordingly, one could assume a two-band model where the normal electrons and electrons in the CDW provide separate, independent channels for the conduction process [4, 6]. It is clear that  $\rho$  is current dependent and drastically decreases as  $I$  increases throughout the temperature range measured (see the inset of figure 8) [4]. A recent study using nanoscale contacts reports a continuous reduction of the resistivity of  $\text{Sr}_2\text{IrO}_4$  with increasing bias, which is characterized by a reduction in the transport activation energy by as much as 16% [89]. This behavior, which is qualitatively consistent with that reported earlier [4], is essentially attributed to changes in the  $\text{Ir}-\text{O}_2-\text{Ir}$  bond angle induced by the electric field [89].

**2.1.3.3. Thermal conductivity—pseudospin transport.** Pseudospin excitations give rise to significant thermal conductivity despite the insulating state (see figure 9) [104]. The analysis of the thermal conductivity reveals a relaxation of the pseudospin excitations at low temperatures. However, the relaxation rate dramatically increases as temperature rises due to thermally activated phonon scattering. The comparison of the results with those for the cuprates with  $S = 1/2$  spin excitations suggests a stronger coupling of the  $J_{\text{eff}} = 1/2$  pseudospin

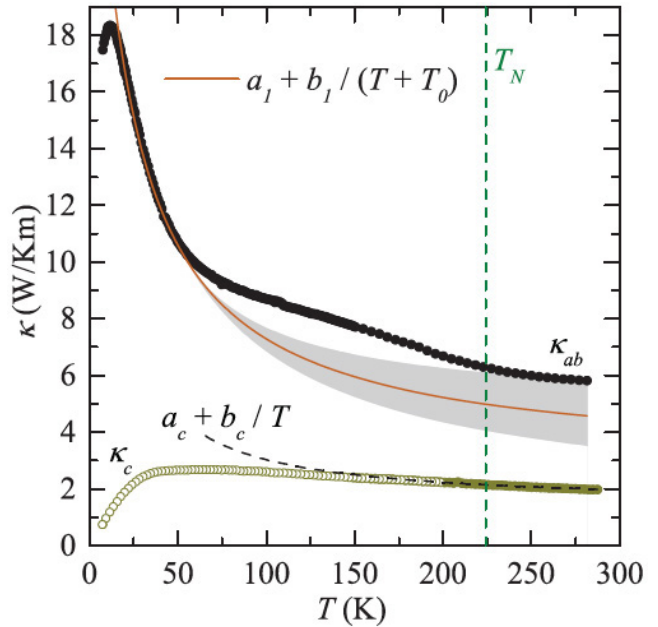


**Figure 9.**  $\text{Sr}_2\text{IrO}_4$ : heat conductivity  $\kappa$  for the  $ab$ -plane ( $\kappa_{ab}$ ) and along the  $c$ -direction ( $\kappa_c$ ). Phononic fits to  $\kappa$  are shown as solid line. The fit to the  $ab$ -direction is given by the values  $a_1 = 2.8 \text{ W Km}^{-1}$ ,  $b_1 = 530 \text{ W m}^{-1}$  and  $T_0 = 18 \text{ K}$ . Similarly, the fit to the  $c$ -direction (dashed line) with  $a_c = 1.43 \text{ W Km}^{-1}$ ,  $b_c = 160 \text{ W m}^{-1}$  [104]. Reproduced from [104]. © IOP Publishing Ltd. All rights reserved.

excitations to the lattice [104]. This is consistent with the other experimental observations and the underlying characteristic of the iridates that physical properties are intimately associated with the lattice owing to the strong SOI. It is noteworthy that the anomaly near  $T_N$  is weak in  $\kappa_{ab}$  and absent in  $\kappa_c$  (figure 9).

**2.1.4. Effects of high pressure.** A rare avoidance of metallization at high pressures in all known iridates further highlights the novelty of these materials [47, 94, 105–109]. It is commonly anticipated that an insulating state collapses and a metallic state emerges at high pressures as the unit cell shrinks and the bandwidth broadens (e.g. [110, 111] and references therein). In sharp contrast,  $\text{Sr}_2\text{IrO}_4$  [94, 108], along with other iridates (such as  $\text{Sr}_3\text{Ir}_2\text{O}_7$  [47, 107, 108]),  $\text{BaIrO}_3$  [105, 106],  $\text{SrIrO}_3$ ,  $\text{Na}_2\text{IrO}_3$ ,  $(\text{Na}_{0.10}\text{Li}_{0.90})_2\text{IrO}_3$  [112]), does not metallize at pressure up to 40 GPa (figure 10). In fact, pressure also destabilizes the ambient metallic state, resulting in an insulating state in iridates such as  $\text{SrIrO}_3$  and Gd-doped  $\text{BaIrO}_3$  [114]. A broad ‘U-shaped’ curve often characterizes the pressure dependence of the electrical resistance of these materials—the resistance drops initially, reaches a minimum (~20 GPa for  $\text{Sr}_2\text{IrO}_4$ ) and then rises again as pressure increases (figure 10(b)). This distinct behavior defines a signature characteristic of the iridates. Moreover, an x-ray magnetic circular dichroism (XMCD) study at high pressures suggests a loss of the long-range magnetic order near 20 GPa (figure 11) but the insulating state remains (figure 10(a)) [94]. The nature of the insulating state above 20 GPa generates speculations that spin liquids may form in square lattices [113]. This behavior further emboldens that transport properties of  $\text{Sr}_2\text{IrO}_4$  exhibit no discernible anomaly corresponding to the

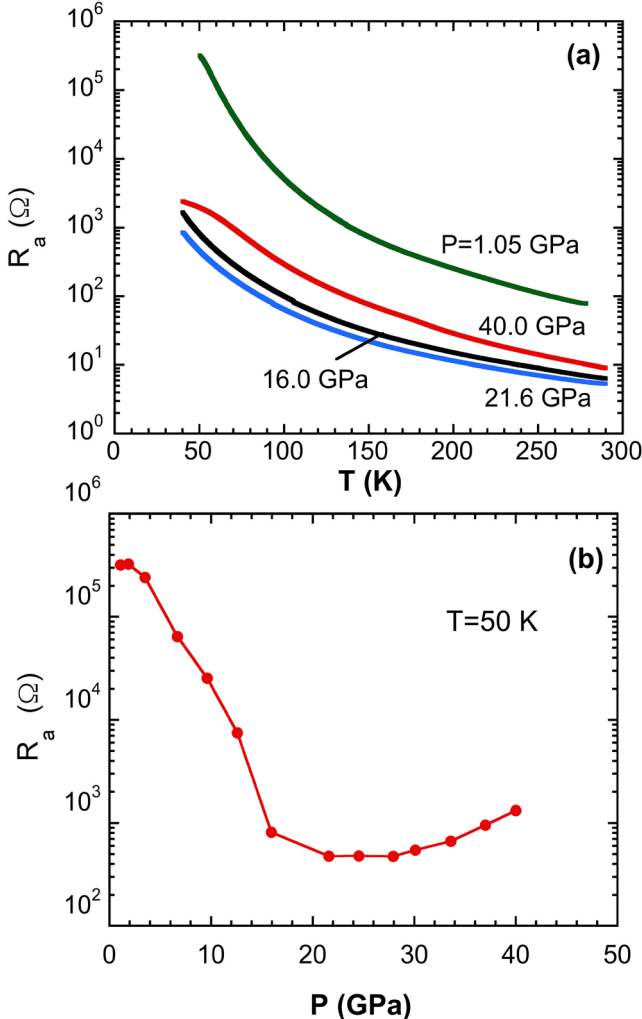


**Figure 10.**  $\text{Sr}_2\text{IrO}_4$ : (a) the temperature dependence of electrical resistance for the  $a$ -axis  $R_a$  at a few representative pressures. (b) The pressure dependence of  $R_a$  at a representative temperature of 50 K [94]. Reprinted figure with permission from [94], Copyright (2012) by the American Physical Society.

AFM transition at  $T_N$  (=240 K), indicating an unconventional correlation between the magnetic state and insulating gap. However, it is clear that structural distortions (such as directional bonding) play a role in the formation of an insulating gap that is much more critical than traditionally recognized. This is illustrated in many studies in which the electronic ground state of the iridates critically hinges on the bond angle Ir1–O2–Ir1 of  $\text{IrO}_6$  octahedra [50, 55, 57, 114–116], which in turn dictates the low-energy Hamiltonian [13], thus the ground state. Indeed, the conspicuous absence of bulk superconductivity widely predicted in  $\text{Sr}_2\text{IrO}_4$  is another testament to such an unconventional correlation despite structural, electronic and magnetic similarities between  $\text{Sr}_2\text{IrO}_4$  and  $\text{La}_2\text{CuO}_4$ . This unusual character has helped revitalize discussions of Mott, Mott–Hubbard and Slater insulators, in particular, the dependence of the charge gap formation on magnetic interactions in  $\text{Sr}_2\text{IrO}_4$  [52, 117, 118]. Remarkably, a time-resolved optical study indicates that  $\text{Sr}_2\text{IrO}_4$  is a unique system in which Slater- and Mott–Hubbard-type behaviors coexist [117], which might help explain the

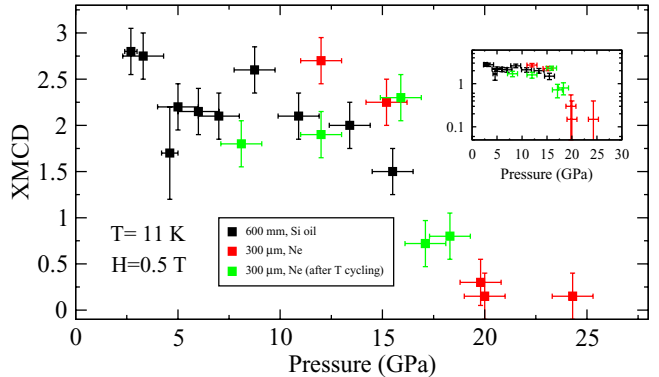


**Figure 11.**  $\text{Sr}_2\text{IrO}_4$ : the pressure dependence of XMCD at 11 K and 0.5 T. Note that the vanishing XMCD signal near 20 GPa where the electrical resistance exhibits a minimum in figure 10(b) [94]. XMCD involves two x-ray absorption spectra taken at a magnetic field, one taken with right circularly polarized light, and another with left circularly polarized light. Reprinted figure with permission from [94], Copyright (2012) by the American Physical Society.

absence of anomalies at  $T_N$  in transport and thermodynamic measurements discussed above. Clearly, a better understanding of the  $J_{\text{eff}} = 1/2$  state and its correlation with the AFM state in  $\text{Sr}_2\text{IrO}_4$  needs to be established. The unconventional correlation may ultimately change the notion of localization promoting Hund's rule magnetic moment formation versus spin liquids or spin dimers.

**2.1.5. Effects of chemical substitution.** In stark contrast, a growing body of experimental evidence has shown that a metallic state can be readily realized via slight chemical doping, either electron (e.g. La doping [50, 119]) or hole doping (e.g. K [50] or Rh [55] or Ru [53, 54] doping, for either Sr or Ir or oxygen [114]) despite the sizable energy gap ( $\sim 0.62$  eV shown in figure 2). Electron doping adds extra electrons to the partially filled  $J_{\text{eff}} = 1/2$  states, which is energetically favorable. Hole doping also adds additional charge carriers, resulting in a metallic state. However, because of the multi-orbital nature of the iridate, the mechanism of electron and hole doping in  $\text{Sr}_2\text{IrO}_4$  may not be symmetrical [18]. An important distinction lies in the energy gap to the nearest  $5d$  states [18, 52, 117, 118]. However, the same effect of both electron and hole doping, as suggested by some experimental evidence, is to reduce the structural distortions or relax the buckling of  $\text{IrO}_6$  octahedra, independent of the ionic radius of the dopant. As illustrated in figure 12(a), a dilute doping of either  $\text{La}^{3+}$  (electron doping) or  $\text{K}^+$  (hole doping) ions for  $\text{Sr}^{2+}$  ions leads to a larger  $\text{Ir1–O2–Ir1}$  bond angle  $\theta$ , despite the considerable differences between the ionic radii of Sr, La, and K, which are 1.18 Å, 1.03 Å and 1.38 Å, respectively. Empirical observations suggest that the reduced distortions, along with extra charge carriers, can effectively destabilize the  $J_{\text{eff}} = 1/2$  state, leading to a metallic state, since hopping between active  $t_{2g}$  orbitals is critically linked to  $\theta$ . Indeed,  $\rho_a$  ( $\rho_c$ ) is reduced by a factor of  $10^8$  ( $10^{10}$ ) at low temperatures for mere  $x = 0.04$  and 0.02 for La and K doping, respectively (figures 12(b)–(d)) [50]. Another possible contribution to the reduction in the resistivity is the formation of an impurity band due to doping. Furthermore, for La doping of  $x = 0.04$ , there is a sharp downturn near 10 K, indicative of a

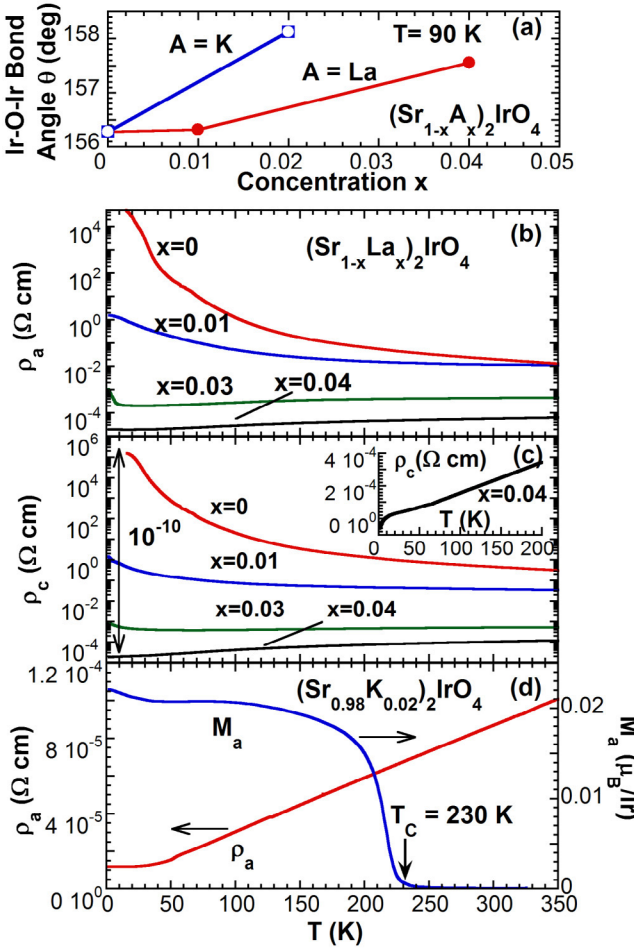


**Figure 12. K or La doped  $\text{Sr}_2\text{IrO}_4$ :** (a) the  $\text{Ir}_1\text{--O}_2\text{--Ir}_1$  bond angle  $\theta$  as a function of La and K doping concentration  $x$ . The temperature dependences of (b) the  $\alpha$ -axis resistivity  $\rho_a$ , and (c) the  $c$ -axis resistivity  $\rho_c$  for  $(\text{Sr}_{1-x}\text{La}_x)_2\text{IrO}_4$  with  $0 \leq x \leq 0.04$ . Inset in (c): enlarged  $\rho_c(T)$  at low  $T$ . (d) The temperature dependence of  $\rho_a$  and the  $\alpha$ -axis magnetization  $M_a$  at applied field  $\mu_0 H = 0.1$  T (right scale) for  $(\text{Sr}_{0.98}\text{K}_{0.02})_2\text{IrO}_4$  [50]. Reprinted figure with permission from [50], Copyright (2011) by the American Physical Society.

rapid decrease in inelastic scattering (figure 12(c) Inset), which is similar to an anomaly observed in oxygen-depleted or effectively electron-doped  $\text{Sr}_2\text{IrO}_{4-\delta}$  with  $\delta = 0.04$  [114]. Other studies of La-doped  $\text{Sr}_2\text{IrO}_4$  show similar effects of La doping on physical properties although behavior varies in detail [119].

It is noteworthy that  $T_N$  decreases with La doping in  $(\text{Sr}_{1-x}\text{La}_x)_2\text{IrO}_4$ , and vanishes at  $x = 0.04$ , where the metallic state is fully established. In contrast, magnetic order coexists with a fully metallic state in  $(\text{Sr}_{0.98}\text{K}_{0.02})_2\text{IrO}_4$ , as shown in figure 12(d). This comparison stresses that the occurrence of a metallic state does not necessarily demand any radical changes in the magnetic state of the iridate [50]. This observation is in accord with the absence of a resistivity anomaly near  $T_N$  discussed above.

For Ru- [53, 54] or Rh- [55] doped  $\text{Sr}_2\text{IrO}_4$ , effects of doping on magnetic and electronic properties are different in detail, but in essence Ru or Rh doping results in a metallic state that coexists with the AFM excitations. For example, for  $\text{Sr}_2\text{Ir}_{1-x}\text{Ru}_x\text{O}_4$ , the AFM excitations persist up to at least  $x = 0.77$  and the maximum energy scale of the magnetic

excitations at high dopings is comparable to that in undoped  $\text{Sr}_2\text{IrO}_4$  [118].

Remarkably, mere 3%  $\text{Tb}^{4+}$  substitution for Ir effectively suppresses  $T_N$  to zero but retains the insulating state, that is, the disappearance of the AFM state accompanies no emergence of a metallic state [57]. A recent theoretical study suggests that the interaction between the magnetic moments on the impurity  $\text{Tb}^{4+}$  ion and its surrounding  $\text{Ir}^{4+}$  ions can be described by a ‘compass’ model, i.e. an Ising-like interaction that favors the magnetic moments across each bond to align along the bond direction. This interaction quenches magnetic vortices near the impurities and drives a reentrant transition out of the AFM phase, leading to a complete suppression of the Néel temperature [57].

All this further highlights an unconventional correlation between the AFM and insulating states in which the magnetic transition plays a nonessential role in the formation of the charge gap in the iridate. There is experimental evidence that suggests that isoelectronic doping such as  $\text{Ca}^{2+}$  doping for  $\text{Sr}^{2+}$ , which adds no additional charge carriers to the  $J_{\text{eff}} = 1/2$  state, reduces electrical resistivity in Ca doped  $\text{Sr}_2\text{IrO}_4$  [51]. More recent studies on Ca and Ba doped  $\text{Sr}_2\text{IrO}_4$  and  $\text{Sr}_3\text{Ir}_2\text{O}_7$  single crystals show an insulator-metal transition, which is attributed to reduced structural distortions [119]. In short, a central empirical trend points to an unusually critical role of the  $\text{Ir}_1\text{--O}_2\text{--Ir}_1$  bond angle that mostly dictates the ground state of the iridates.

**2.1.6. Elusive superconductivity and odd-parity hidden order.**  $\text{Sr}_2\text{IrO}_4$  bears key structural, electronic and magnetic features similar to those of  $\text{La}_2\text{CuO}_4$  [1–4, 7, 9, 13, 16, 23–25], as pointed out in the beginning of this section. In particular, the magnon dispersion in  $\text{Sr}_2\text{IrO}_4$  is well-described by an AFM Heisenberg model with an effective spin one-half on a square lattice, which is similar to that in the cuprate. The magnon bandwidth in  $\text{Sr}_2\text{IrO}_4$  is of 200 meV, as compared to ~300 meV in  $\text{La}_2\text{CuO}_4$  [1–4, 7, 9, 24]. This smaller bandwidth is consistent with other energy scales, such as hopping  $t$  and  $U$ , which are uniformly smaller by approximately 50% in  $\text{Sr}_2\text{IrO}_4$  than in the cuprate [22]. Largely because of these apparent similarities, a pseudo-spin-singlet d-wave superconducting phase with a critical temperature,  $T_C$ , approximately half of that in the superconducting cuprate is anticipated in electron-doped  $\text{Sr}_2\text{IrO}_4$  whereas pseudo-spin triplet pairing may emerge in the hole-doped iridate so long as the Hund’s rule coupling is not strong enough to drive the ground state to a ferromagnetic state [18, 22–28]. A growing list of theoretical proposals has motivated extensive investigations both theoretically and experimentally in search of superconductivity in the iridates in recent years. Indeed, there is some experimental evidence signaling behavior parallel to that of the cuprates. Besides results of resonant inelastic x-ray scattering (RIXS) that indicate the similar magnon dispersion in  $\text{Sr}_2\text{IrO}_4$  to that in  $\text{La}_2\text{CuO}_4$  [24, 120], Raman studies also reveal excitations at 0.7 eV in  $\text{Sr}_2\text{IrO}_4$ , about 50% smaller than 1.5 eV observed in  $\text{La}_2\text{CuO}_4$  [121]. Studies of angle-resolved photoemission spectroscopy (ARPES) reveal an evolution of Fermi surface with doping (e.g. pseudogaps, Fermi arcs) that is strikingly similar

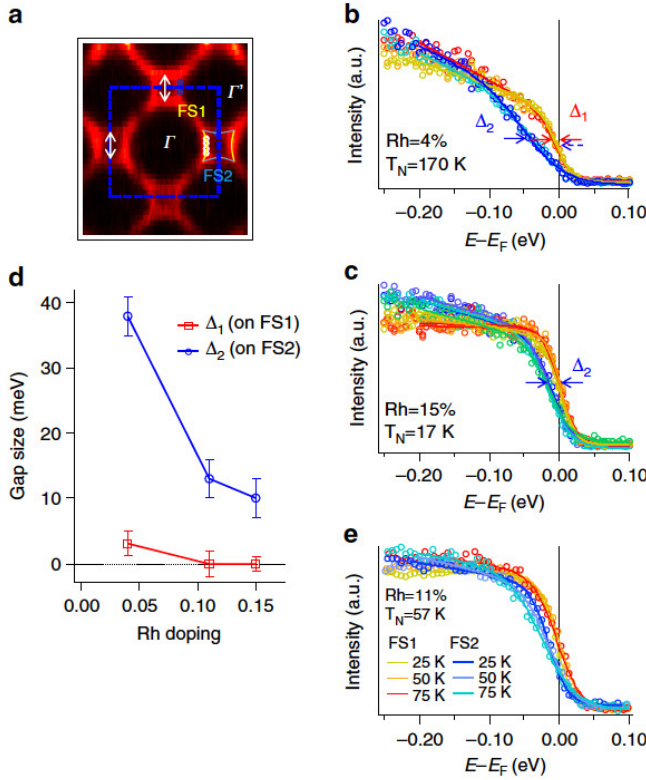


**Figure 13.** Fermi surface (FS) segments and pseudogaps in  $\text{Sr}_2\text{Ir}_{1-x}\text{Rh}_x\text{O}_4$  according to the ARPES results: (a) The FS spectral weight for  $x = 15\%$ , with a hole-like Fermi pocket centered around the  $(\pi, 0)$  point of the unfolded (blue dashed) Brillouin zone. The FS pocket is separated into segments FS1 (yellow) and FS2 (blue), with FS1 facing  $\Gamma$  and FS2 facing  $\Gamma'$ .  $Q$  vectors (white arrows) are possible density wave nesting vectors. (b) and (c) Energy distribution curves (EDCs) from multiple locations along the FS1 and FS2 segments (yellow and blue, respectively) taken from  $x = 4\%$  and  $x = 15\%$ . The leading edges of most EDCs do not reach  $E_F$ , suggesting an occurrence of pseudogaps. Gap sizes are shown in (b) and (c) and compiled in (d), with  $\Delta_1$  labelling the gaps from FS1 and  $\Delta_2$  the gaps from FS2. (e) EDCs from FS1 (dashed) and FS2 (solid) showing minimal temperature dependence across the magnetic phase transition for  $x = 11\%$  [118]. Reprinted by permission from Macmillan Publishers Ltd: Nature Communication [118], Copyright (2016).

to that in the cuprates and is observed in  $\text{Sr}_2\text{IrO}_4$  with either electron-doping (e.g. La doping) or hole-doping (e.g. Rh doping) [118, 120]. For example, the Fermi surface segments and pseudogaps for Rh doped  $\text{Sr}_2\text{IrO}_4$  (hole doping) are illustrated in figure 13. It is particularly interesting that a temperature and doping dependence of Fermi arcs at low temperatures is observed with in-situ K doping in the cleaved crystal surface of  $\text{Sr}_2\text{IrO}_4$ . This phenomenology is strikingly similar to that of the cuprates. The similarities to the cuprates are further signified in a more recent RIXS study of La-doped  $\text{Sr}_2\text{IrO}_4$  [122]. This study uncovers well-defined dispersive magnetic excitations. The dispersion is almost intact along the anti-nodal direction but exhibits significant softening along the nodal direction, similar to those in hole-doped cuprates [122].

However, superconductivity, which is characterized by zero-resistivity and diamagnetism, remains markedly elusive, although a metallic state is a common occurrence in doped  $\text{Sr}_2\text{IrO}_4$ . The absence of superconductivity may be a

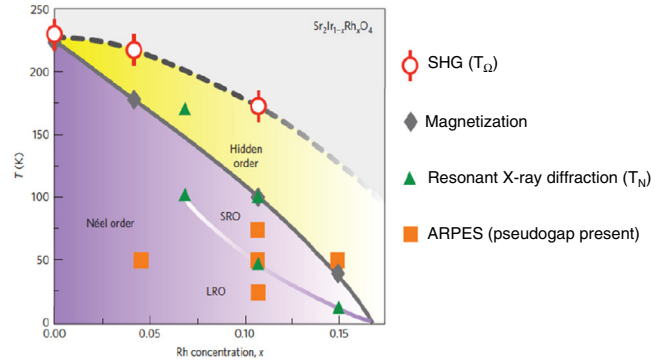


**Figure 14.** The phase diagram of temperature versus Rh doping for  $\text{Sr}_2\text{Ir}_{1-x}\text{Rh}_x\text{O}_4$ . Note the boundaries of the hidden order and the long-range (LRO) and short-range (SRO) in the AFM regions [88]. Reprinted by permission from Macmillan Publishers Ltd: Nature Physics [88], Copyright (2016).

manifestation of the particular importance of lattice properties which separates the iridates from the cuprates, in spite of all the similarities between these two classes of materials described herein and in literature. Indeed, the lattice-dependence of physical properties is much weaker in the cuprates, where the SOI is generally negligible. The spin and orbits are separated in the cuprates whereas they are strongly coupled by the SOI in the iridates. The Cooper pairs in the iridates would then be formed within pseudospin space, rather than with ordinary spins.

Interestingly, an optical second-harmonic generation (SHG) study of single-crystal  $\text{Sr}_2\text{Ir}_{1-x}\text{Rh}_x\text{O}_4$  has recently revealed an odd-parity hidden order that sets in at a temperature  $T_\Omega$ , emerging prior to the formation of the AFM state, as shown in figure 14 [88] (a recent, detailed study confirms the existence of this odd-parity hidden order [123]). This order breaks both the spatial inversion and rotational symmetries of the underlying tetragonal lattice, which is expected from an electronic phase that has the symmetries of a magneto-electric loop-current order [124, 125]. The onset temperature of this phase is monotonically suppressed with hole doping, although much more weakly than is the Néel temperature, revealing an extended region of the phase diagram with purely hidden order (figure 14). Driving this hidden phase to its quantum critical point might open a new avenue toward realizing the widely anticipated superconducting state in  $\text{Sr}_2\text{IrO}_4$  [88].

## 2.2. $\text{Sr}_3\text{Ir}_2\text{O}_7$ ( $n = 2$ )

The splitting between the  $J_{\text{eff}} = 1/2$  and  $J_{\text{eff}} = 3/2$  bands narrows as the effective dimensionality (i.e.  $n$ ) increases in  $\text{Sr}_{n+1}\text{Ir}_n\text{O}_{3n+1}$ , and the two bands progressively broaden and contribute a finite density of states near the Fermi surface. In particular, the bandwidth  $W$  of the  $J_{\text{eff}} = 1/2$  band increases from 0.48 eV for  $n = 1$ , to 0.56 eV for  $n = 2$ , and 1.01 eV for  $n = \infty$  [8, 84]. The ground state evolves with decreasing charge gap  $\Delta$  as  $n$  increases, from a robust insulating state for  $\text{Sr}_2\text{IrO}_4$  ( $n = 1$ ) to a metallic state for  $\text{SrIrO}_3$  ( $n = \infty$ ). A well-defined, yet weak, insulating state exists in the case of  $\text{Sr}_3\text{Ir}_2\text{O}_7$  ( $n = 2$ ) [5]. Given the delicate balance between relevant interactions,  $\text{Sr}_3\text{Ir}_2\text{O}_7$  is theoretically predicted to be at

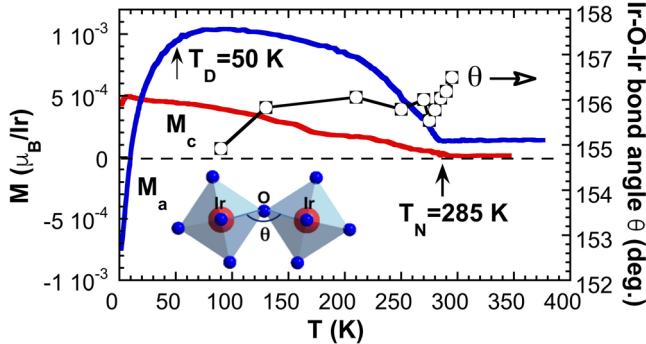


**Figure 15.**  $\text{Sr}_3\text{Ir}_2\text{O}_7$ : temperature dependence of the magnetization for the  $a$ - and  $c$ -axis  $M_a$ ,  $M_c$ , and the Ir–O–Ir bond angle  $\theta$  (right scale). Note that  $M$  is measured via a field-cooled sequence; no magnetic order can be discerned in a zero-field-cooled sequence [5]. Reprinted figure with permission from [5], Copyright (2002) by the American Physical Society.

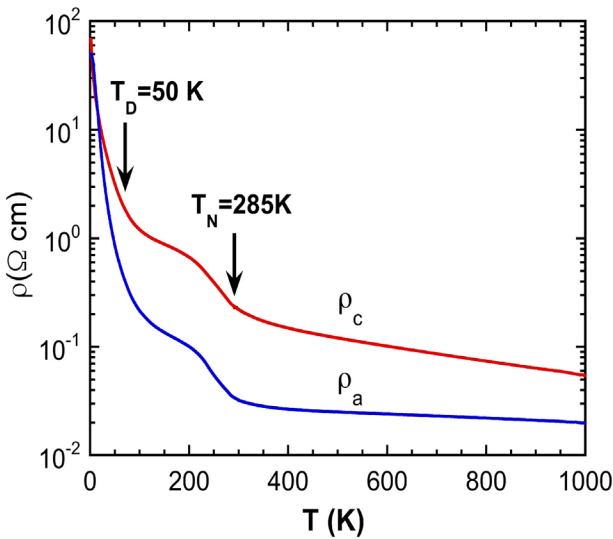


**Figure 16.**  $\text{Sr}_3\text{Ir}_2\text{O}_7$ : temperature dependence of the  $a$ -axis resistivity  $\rho_a$  and the  $c$ -axis  $\rho_c$  for  $1.7 < T \leq 1000$  K [5]. Reprinted figure with permission from [5], Copyright (2002) by the American Physical Society.

the border between a collinear AFM insulator and a spin-orbit Mott insulator [18, 126]. Early experimental observations indicated an insulating state and a long-range magnetic order at  $T_N = 285$  K with an unusual magnetization reversal below 50 K (figures 15 and 16) [5]. The value of the charge gap (180 meV) [84], much smaller than that (0.62 eV) of  $\text{Sr}_2\text{IrO}_4$ , but the magnetic gap is unusually large at 92 meV [127]. The borderline nature of the weak insulating state of  $\text{Sr}_3\text{Ir}_2\text{O}_7$  is apparent in an ARPES study of the near-surface electronic structure, which exhibits weak metallicity evidenced by finite electronic spectral weight at the Fermi level [128].

**2.2.1. Critical structural features.**  $\text{Sr}_3\text{Ir}_2\text{O}_7$  has strongly-coupled, double Ir–O layers separated from adjacent double layers along the  $c$ -axis by Sr–O interlayers, as shown in figure 3. The crystal structure features an orthorhombic cell with  $a = 5.5221$  Å,  $b = 5.5214$  Å,  $c = 20.9174$  Å and Bbca symmetry [5] (although a recent study suggests a space group  $C2/c$  [129]). The  $\text{IrO}_6$  octahedra are elongated along

the crystallographic  $c$ -axis. The average Ir–O apical bond distances along the  $c$ -axis are 2.035 Å and 1.989 Å in the  $\text{IrO}_6$  octahedra in the double layers. Like those in  $\text{Sr}_2\text{IrO}_4$ , the  $\text{IrO}_6$  octahedra are rotated about the  $c$ -axis by 11° at room temperature. It is found that within a layer the rotations of the  $\text{IrO}_6$  octahedra alternate in sign, forming a staggered structure, with the two layers comprising a double-layer being out of phase with one another [5].

**2.2.2. Magnetic properties.** The onset of magnetic order is observed at  $T_N = 285$  K in  $\text{Sr}_3\text{Ir}_2\text{O}_7$  (figure 15) [5]. It is generally recognized that the magnetic ground state is AFM and closely associated with the rotation of the  $\text{IrO}_6$  octahedra about the  $c$ -axis, which characterizes the crystal structure of both  $\text{Sr}_2\text{IrO}_4$  and  $\text{Sr}_3\text{Ir}_2\text{O}_7$  [1–5, 129]. Indeed, the temperature dependence of the magnetization  $M(T)$  closely tracks the rotation of the octahedra, as reflected in the Ir–O–Ir bond angle  $\theta$  (figure 15). Unlike  $\text{Sr}_2\text{IrO}_4$ ,  $\text{Sr}_3\text{Ir}_2\text{O}_7$  exhibits an intriguing magnetization reversal in the  $a$ -axis magnetization  $M_a(T)$  below  $T_D = 50$  K, which marks the turning point where  $M(T)$  starts to decrease with temperature; both  $T_N$  and  $T_D$  can be observed only when the system is field-cooled (FC) from above  $T_N$ . This magnetic behavior is robust but not observed in the zero-field cooled (ZFC) magnetization, which instead remains positive and displays no anomalies that are seen in the FC magnetization [5]. It is also noteworthy that the signature of magnetic order is much weaker and not so well defined in the  $c$ -axis magnetization  $M_c(T)$  (figure 15). It is unusual that all magnetic anomalies are absent in the case of ZFC measurements, implying that magnetostriction may occur near  $T_N$  and ‘lock’ up a certain magnetic configuration.

This magnetic behavior of  $\text{Sr}_3\text{Ir}_2\text{O}_7$  is distinctively different from that of  $\text{Sr}_2\text{IrO}_4$ . A number of experimental and theoretical studies indicate that magnetic moments are aligned along the  $c$ -axis [130, 131] but there may exist a nearly degenerate magnetic state with canted spins in the basal plane [132]. A transition to a collinear antiferromagnet via multiorbital Hubbard interactions is predicted within the mean-field approximation [18, 132]. Indeed, a resonant x-ray diffraction study reveals an easy collinear antiferromagnetic structure along the  $c$ -axis in  $\text{Sr}_3\text{Ir}_2\text{O}_7$ , rather than within the basal plane, as observed in  $\text{Sr}_2\text{IrO}_4$ . This study further suggests a spin-flop transition as a function of the number of  $\text{IrO}_2$  layers, due to strong competition among intra- and inter-layer bond-directional, pseudodipolar interactions [131].

The magnetic configuration of  $\text{Sr}_3\text{Ir}_2\text{O}_7$  is highly sensitive to the lattice structure. In particular, the staggered rotation of  $\text{IrO}_6$  octahedra between adjacent layers plays a crucial role in both insulating and magnetic states [18, 132].  $\text{Sr}_3\text{Ir}_2\text{O}_7$  is a unique magnetic insulator, given its tiny magnetic moment [5] and is more prone to undergo a transition [18, 132]. It is not surprising that any slight perturbation such as magnetic field could induce a canted spin structure, as indicated in a magnetic x-ray scattering study [133]. In addition, a more recent RIXS study reveals that the magnon dispersion is comprised of two branches well separated in energy and gapped across the entire Brillouin zone, rather than a single dominant branch. It suggests dimerization induced by the Heisenberg

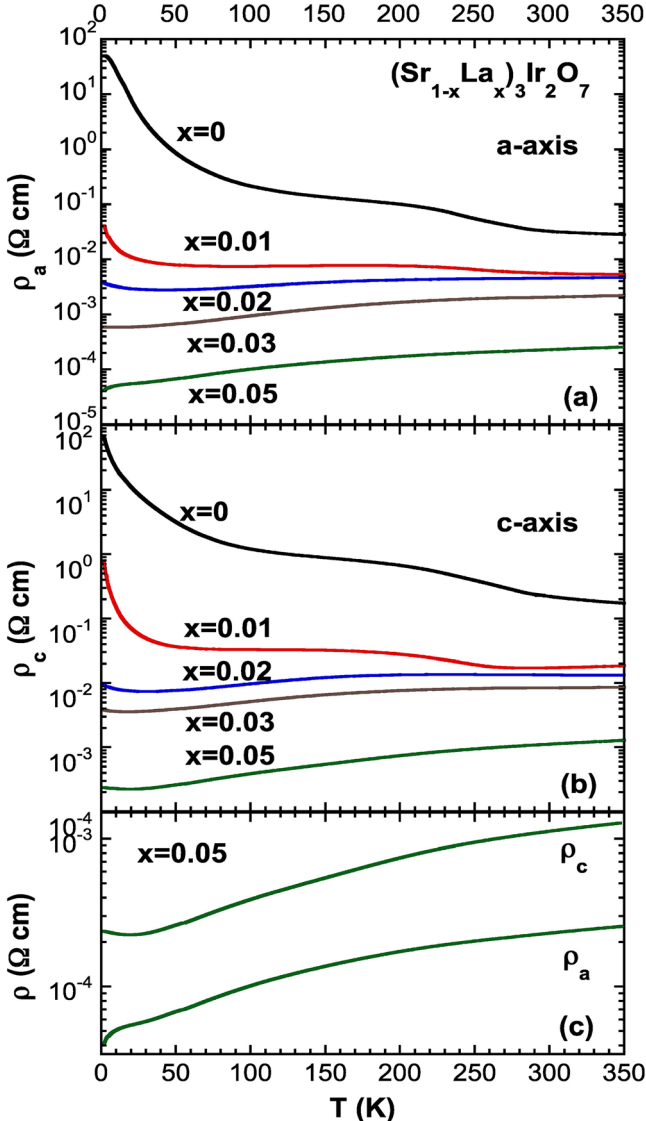


**Figure 17.**  $(\text{Sr}_{1-x}\text{La}_x)_3\text{Ir}_2\text{O}_7$ : temperature dependence of (a) the  $a$ -axis resistivity  $\rho_a$ ; and (b) the  $c$ -axis resistivity  $\rho_c$ . (c)  $\rho_a$  and  $\rho_c$  for  $x = 0.05$  [136]. Reprinted figure with permission from [136], Copyright (2013) by the American Physical Society.

exchange that couples Ir ions in adjacent planes of the bilayer [134]. A better understanding of the magnetic behavior has yet to be established.

**2.2.3. Transport properties.** An insulating state is illustrated in the electrical resistivity  $\rho(T)$  over the range  $1.7 < T < 1000$  K, as shown in figure 16. The insulating behavior persists up to 1000 K in  $\text{Sr}_3\text{Ir}_2\text{O}_7$  [5]; however,  $\rho$  is at least four orders of magnitude smaller than that of  $\text{Sr}_2\text{IrO}_4$  (figure 5(b)). Both  $\rho_a$  and  $\rho_c$  increase slowly with temperature decreasing from 1000 to 300 K, but then rise rapidly in the vicinity of  $T_N$  and  $T_D$ , demonstrating a coupling between magnetic and transport properties (although the magnetoresistivity is negligible at high temperatures and becomes sizable only below 50 K [5]). Nevertheless, the transport behavior of  $\text{Sr}_3\text{Ir}_2\text{O}_7$  contrasts with that of  $\text{Sr}_2\text{IrO}_4$ , where such a correlation is absent. The differing behavior may be due in part to the difference in the

charge gap  $\Delta$  between  $\text{Sr}_3\text{Ir}_2\text{O}_7$  ( $\Delta \sim 0.18$  eV) and  $\text{Sr}_2\text{IrO}_4$  ( $\Delta \sim 0.62$  eV) and, thus, the relative effect of the AFM excitation energy on the charge gap. A Raman study also suggests different influence of frustrating exchange interactions on  $\text{Sr}_2\text{IrO}_4$  and  $\text{Sr}_3\text{Ir}_2\text{O}_7$  [99]. Finally, like those of  $\text{Sr}_2\text{IrO}_4$ , transport properties of  $\text{Sr}_3\text{Ir}_2\text{O}_7$  can be tuned electrically [135].

**2.2.4. Effects of chemical substitution.** The effects of chemical doping in  $\text{Sr}_3\text{Ir}_2\text{O}_7$  are similar to those in  $\text{Sr}_2\text{IrO}_4$  discussed in section 2.1.5. For example, 5% La doping readily precipitates a metallic state reflected in the electrical resistivity  $\rho$  of single-crystal  $(\text{Sr}_{1-x}\text{La}_x)_3\text{Ir}_2\text{O}_7$ , as shown in figure 17 [136]. The  $a$ -axis resistivity  $\rho_a$  (the  $c$ -axis resistivity  $\rho_c$ ) is reduced by as much as a factor of  $10^6$  ( $10^5$ ) at low temperatures as  $x$  evolves from 0 to 0.05, (see figures 17(a) and (b)). For  $x = 0.05$ , there is a sharp downturn in  $\rho_a$  near 10 K, indicative of a rapid decrease in inelastic scattering (figure 17(c)). Such low-temperature behavior is observed in oxygen-depleted  $\text{Sr}_2\text{IrO}_{4-\delta}$  with  $\delta = 0.04$ , and La-doped  $\text{Sr}_2\text{IrO}_4$ , as discussed in section 2.1.5. La doping not only adds electrons to states but also significantly increases the Ir–O–Ir bond angle  $\theta$ , which is more energetically favorable for electron hopping and superexchange interactions.

It should be stressed that the occurrence of the metallic state in this system is not accompanied by a complete disappearance of the magnetic order, although it is significantly weakened. A study of  $(\text{Sr}_{1-x}\text{La}_x)_3\text{Ir}_2\text{O}_7$  utilizing resonant elastic and inelastic x-ray scattering at the Ir-L<sub>3</sub> edge reveals that with increasing doping  $x$ , the three-dimensional long-range AFM order is gradually suppressed and evolves into a three-dimensional short-range order across the insulator-to-metal transition from  $x = 0$  to  $x = 0.05$ , which is then followed by a transition to two-dimensional short range order between  $x = 0.05$  and  $x = 0.065$ . Because of the interactions between the  $J_{\text{eff}} = 1/2$  pseudospins and the emergent itinerant electrons, magnetic excitations undergo damping, anisotropic softening, and gap collapse, accompanied by spin-orbit excitons that are weakly dependent on doping (figure 18) [137]. It is also suggested that electron doping suppresses the magnetic anisotropy and interlayer couplings and drives  $(\text{Sr}_{1-x}\text{La}_x)_3\text{Ir}_2\text{O}_7$  into a correlated metallic state with two-dimensional short-range AFM order. Strong AFM fluctuations of the  $J_{\text{eff}} = 1/2$  moments persist deep in this correlated metallic state, with the magnetic gap strongly suppressed [137]. More intriguing, a subtle charge-density-wave-like Fermi surface instability is observed in the metallic region of  $(\text{Sr}_{1-x}\text{La}_x)_3\text{Ir}_2\text{O}_7$  near 200 K which shows resemblance to that observed in cuprates [138]. The absence of any signatures of a new spatial periodicity below 200 K seems to suggest an unconventional and possibly short-ranged density wave order [138].

**2.2.5. Effects of high pressure.**  $\text{Sr}_3\text{Ir}_2\text{O}_7$  responds to pressure in a fashion similar to that of  $\text{Sr}_2\text{IrO}_4$  at lower pressures as discussed above. An early pressure study reveals an abrupt change in electrical resistivity along with an apparent second-order structural change near 13 GPa [107]. A more recent study using both RIXS and electrical resistivity indicates that

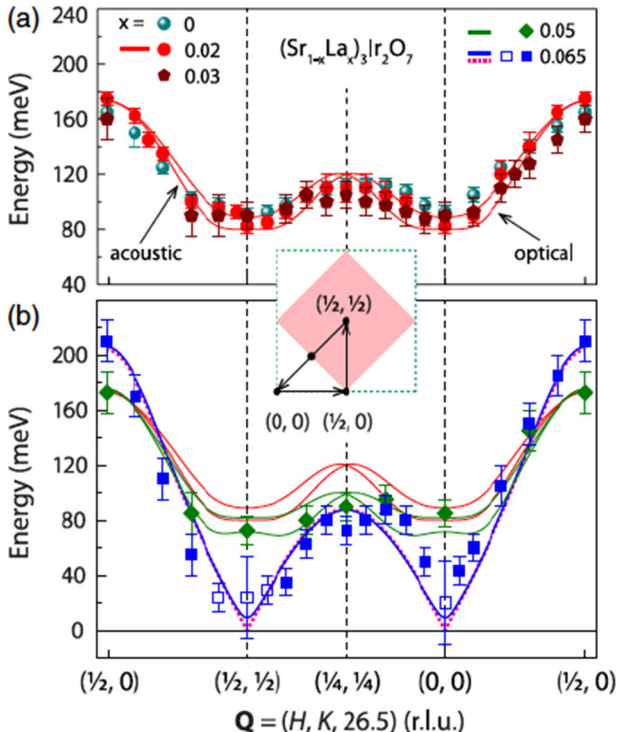


**Figure 18.**  $(\text{Sr}_{1-x}\text{La}_x)_3\text{Ir}_2\text{O}_7$ : doping-dependent magnon dispersions for: (a)  $x = 0, 0.02$ , and  $0.03$  and (b)  $x = 0.05$  and  $0.065$ . The dispersions for  $x \leq 0.05$  and the blue solid squares of  $x = 0.065$  are obtained by selecting the peak positions of the magnetic excitations. The blue open squares of  $x = 0.065$  are extracted from fitting of the magnetic excitations. The solid curves are fits to the dispersions for  $x = 0.02, 0.05$ , and  $0.065$  using the bilayer model, which includes an acoustic and an optical branch. The pink dashed curve is the fitting of the dispersion for  $x = 0.065$  [137]. Reprinted figure with permission from [137], Copyright (2017) by the American Physical Society.

$\text{Sr}_3\text{Ir}_2\text{O}_7$  becomes a confined metal at 59.5 GPa, featuring a metallic state in the basal plane but an insulating behavior along the  $c$ -axis (figure 19) [47]. This novel insulator-metal transition is attributed to a possible first-order structural change at nearby pressures [47]. The study further suggests that the structural transition above 54 GPa is likely triggered by a saturated  $\text{IrO}_6$  octahedron rotation, which inevitably leads to changes in the band structure in  $\text{Sr}_3\text{Ir}_2\text{O}_7$  [47]. As recognized now, the pressure-induced metallic state does not commonly occur, but when it does, it has an extraordinary nature, such as in this case.

### 2.3. $\text{SrIrO}_3$ and its derivative ( $n = \infty$ )

The effects of the SOI and  $U$  are largely local and remain essentially unchanged throughout the entire series  $\text{Sr}_{n+1}\text{Ir}_n\text{O}_{3n+1}$ , and it is now known that the ground state evolves with increasing dimensionality (i.e.  $n$ ), from a robust AFM insulating state for  $\text{Sr}_2\text{IrO}_4$  ( $n = 1$ ) to a paramagnetic, semimetallic state for  $\text{SrIrO}_3$  ( $n = \infty$ ) [8, 45, 48]. The semimetallic state of  $\text{SrIrO}_3$  has been of great interest both theoretically and experimentally, despite the presence of strong SOI [8, 45, 139–149]. Initial work indicated that a strong SOI reduces the threshold

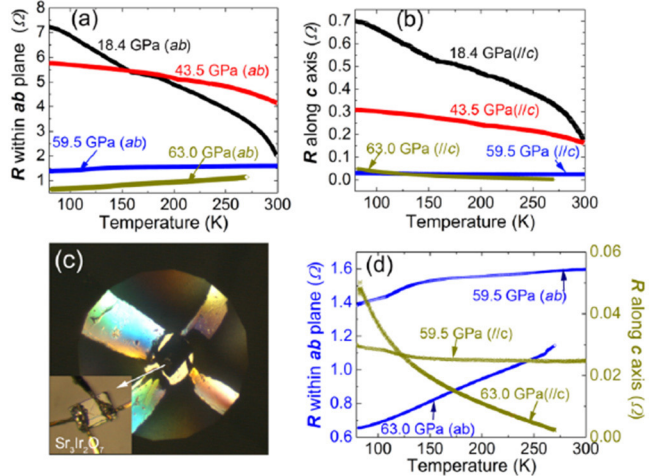


**Figure 19.**  $\text{Sr}_3\text{Ir}_2\text{O}_7$ : electrical resistance at high pressure as a function of temperature for (a) the basal plane and (b) the  $c$ -axis. (c) Four gold electric leads and the sample loaded into a symmetric diamond anvil cell. The inset shows two of the leads attached to the top of the single crystal, and the other two attached to the bottom. (d) Temperature dependence of the electrical resistances at 59.5 and 63.0 GPa. Note the metallic behavior in the basal plane, and the insulating behavior along the  $c$ -axis [47]. Reprinted figure with permission from [47], Copyright (2016) by the American Physical Society.

of  $U$  for a metal-insulator transition [139, 140]. A more recent theoretical study finds that an even larger critical  $U$  is required for a metal-insulator transition to occur in  $\text{SrIrO}_3$ , due to a combined effect of the lattice structure, strong SOI and the protected line of Dirac nodes in the  $J_{\text{eff}} = 1/2$  bands near the Fermi level [141]. In essence, small hole and electron pockets with low densities of states, which are present in  $\text{SrIrO}_3$ , render  $U$  less effective in driving a magnetic insulating state because of protected line node [141]. We stress that tuning the relative strength of the SOI and  $U$  is highly effective in changing the nature of the ground state in the iridates. The rare occurrence of a semimetallic state in  $\text{SrIrO}_3$  therefore provides a unique opportunity to closely examine the intricate interplay of the SOI,  $U$  and lattice degrees of freedom, as well as the correlation between the AFM state and the metal-insulator transition in iridates. Indeed, tuning the relative strength of the SOI and  $U$  effectively changes the ground state in the iridates.

A large number of experimental studies of the orthorhombic perovskite  $\text{SrIrO}_3$  have been conducted in recent years [8, 45, 139–149]. However, the bulk single-crystal  $\text{SrIrO}_3$  forms only at high pressures and high temperatures [48], and almost all studies of this system are limited to samples in thin-film or polycrystalline form; little work on bulk single-crystal samples of this system has been done; critical information concerning magnetic properties and their correlation with the electronic state, corresponding anisotropies, etc., is still lacking. However, a recent study on bulk single-crystals of Ir-deficient, orthorhombic perovskite  $\text{Sr}_{0.94}\text{Ir}_{0.77}\text{O}_{2.68}$  offers some insights [150]. In essence,  $\text{Sr}_{0.94}\text{Ir}_{0.77}\text{O}_{2.68}$  retains the very same crystal structure as stoichiometric  $\text{SrIrO}_3$ , albeit with a rotation of  $\text{IrO}_6$  octahedra within the basal plane by about  $9.54^\circ$  [150], which is a structural signature for all layered perovskite iridates [1–5, 87, 129].

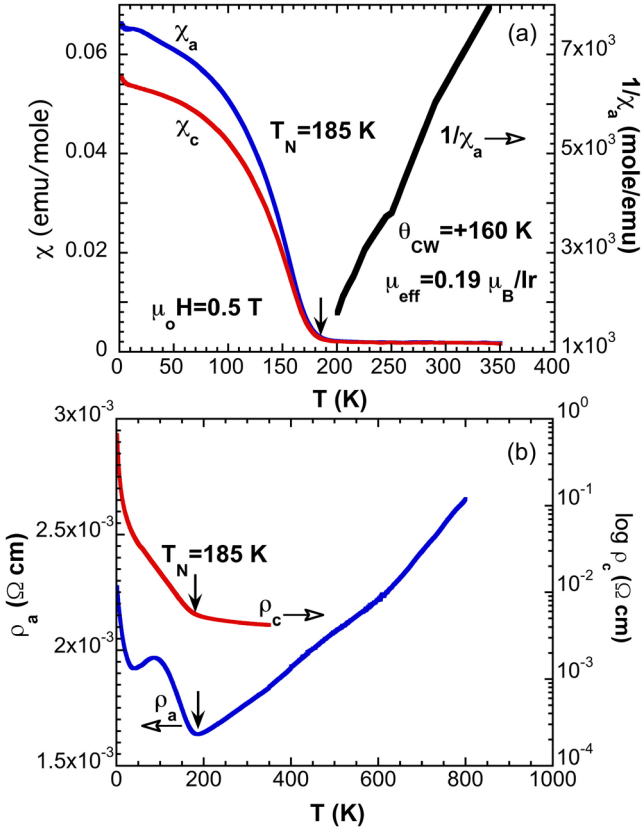


**Figure 20.**  $\text{Sr}_{0.94}\text{Ir}_{0.77}\text{O}_{2.68}$ : the temperature dependence of the magnetic susceptibility  $\chi$  for  $a$ -axis  $\chi_a$  and  $c$ -axis  $\chi_c$ , and  $\chi_a^{-1}$  (right scale) at  $\mu_0 H = 0.5$  T, and (b) the  $a$ -axis resistivity  $\rho_a$  up to 800 K, and the  $c$ -axis resistivity  $\rho_c$  (right scale) [150]. Reprinted figure with permission from [150], Copyright (2016) by the American Physical Society.

$\text{Sr}_{0.94}\text{Ir}_{0.77}\text{O}_{2.68}$  exhibits sharp, simultaneous AFM and metal-insulator transitions at  $T_N = 185$  K with a charge gap of 0.027 eV, sharply contrasting stoichiometric  $\text{SrIrO}_3$ , which is paramagnetic and semimetallic (figure 20). Recalling the rotation of  $\text{IrO}_6$  octahedra in  $\text{Sr}_2\text{IrO}_4$  and  $\text{Sr}_3\text{Ir}_2\text{O}_7$  [1–5] is critical in determining the AFM ground state [13], one suspects that the emerging AFM state in  $\text{Sr}_{0.94}\text{Ir}_{0.77}\text{O}_{2.68}$  might be in part a result of the increased in-plane rotation of  $\text{IrO}_6$  octahedra,  $9.54^\circ$  (compared to  $8.75^\circ$  for  $\text{SrIrO}_3$  [48]). Alternatively, the absence of proper glide symmetry in  $\text{Sr}_{0.94}\text{Ir}_{0.77}\text{O}_{2.68}$  weakens the nodal line protection, thus  $U$  becomes more effective, leading to the AFM state [142]. The transport properties feature an extended regime of linear-temperature basal-plane resistivity between 185 K and 800 K, and an abrupt sign change in the Hall resistivity below 40 K (rather than  $T_N = 185$  K) that signals a transition from hole-like to electron-like behavior with decreasing temperature [150]. These studies of  $\text{SrIrO}_3$  underscore the delicacy of a metallic state that is in close proximity to an AFM insulating state, and a ground state highly sensitive to slight lattice defects. The simultaneous AFM and metal-insulator transitions illustrate a direct correlation between the AFM transition and charge gap in  $\text{SrIrO}_3$ , which is notably absent in  $\text{Sr}_2\text{IrO}_4$ .

The contrasting ground states observed in isostructural  $\text{Sr}_{0.94}\text{Ir}_{0.77}\text{O}_{2.68}$  and  $\text{SrIrO}_3$  with space group  $\text{Pbnm}$  highlight the ultra-high sensitivity of SOI-coupled iridates to the lattice

which, along with the delicate interplay of the SOI and  $U$ , need to be adequately addressed both experimentally and theoretically.

### 3. Magnetism of Honeycomb lattices and other geometrically frustrated iridates

The interest in frustrated iridates received a major boost when a theoretical analysis [13] showed that the oxygen-mediated superexchange processes between the  $\text{Ir}^{4+}$  moments in the honeycomb iridates  $\text{Na}_2\text{IrO}_3$  and  $\text{Li}_2\text{IrO}_3$  can relate to the celebrated Kitaev model applied to the  $J_{\text{eff}} = 1/2$  degrees of freedom. The Kitaev model can be solved exactly, and its ground state is an exotic magnetically disordered quantum ‘spin liquid’ [151]. However, the long-sought spin-liquid state has remained elusive. That both honeycomb lattices  $\text{Na}_2\text{IrO}_3$  and  $\text{Li}_2\text{IrO}_3$  (including  $\beta$  and  $\gamma$  phases) are magnetically ordered suggests that the Heisenberg interaction is still sizable. In addition, trigonal crystal fields also compete with the Kitaev interaction.

#### 3.1. Two-dimensional honeycomb lattices

**3.1.1.  $\text{Na}_2\text{IrO}_3$  and  $\text{Li}_2\text{IrO}_3$ .** The honeycomb lattices feature  $\text{IrO}_6$  octahedra that are edge-sharing with  $90^\circ$  Ir–O–Ir bonds. The magnetic exchange is anisotropically bond-dependent. Such a bond-dependent interaction gives rise to strong frustration when Ir ions are placed on a honeycomb lattice, and would seem to favor a Kitaev spin liquid [13, 151]. Theoretical treatments of the honeycomb lattices  $\text{Na}_2\text{IrO}_3$  and  $\text{Li}_2\text{IrO}_3$  have inspired a large body of experimental work that anticipates Kitaev physics [13, 15, 31–34, 38, 65, 67, 152–157]. If individual spins at the sites of a honeycomb lattice are restricted to align along any one of the 3 bond directions (six degrees of freedom for ‘up’ and ‘down’ spins), the Kitaev model predicts a quantum spin-liquid ground state [151]. This novel state features short-range correlations, and the spin degrees of freedom fractionalize into Majorana fermions and a  $Z_2$  gauge field. The honeycomb iridates are often described in terms of competing Heisenberg and Kitaev interactions; the former favors an AFM state, and the latter a spin liquid state. However, no experimental confirmation of the spin liquid state has been reported, and it is experimentally established that all known honeycomb iridates order magnetically [31–33, 65, 67, 152–159].

$\text{Na}_2\text{IrO}_3$  exhibits a peculiar ‘zig-zag’ magnetic order at  $T_N = 15$  K with a Mott gap of  $\sim 0.42$  eV [159]. The magnetic order was first reported in [30, 31] and later confirmed by neutron diffraction and other studies that indicate that  $\text{Na}_2\text{IrO}_3$  orders magnetically below  $18.1(2)$  K with  $\text{Ir}^{4+}$  ions forming zig-zag spin chains within the layered honeycomb network with an ordered moment of  $0.22(1)\mu_B/\text{Ir}$  (figure 21) [33]. Inelastic neutron scattering on polycrystalline samples offers some insights into the magnetic state [32], whereas RIXS studies characterize a branch of magnetic excitations at high-energies near 30 meV [158]. The magnetic state of  $\alpha\text{-Li}_2\text{IrO}_3$  is not as well-characterized as that of  $\text{Na}_2\text{IrO}_3$ , partly due to the lack of large single-crystal samples needed for more

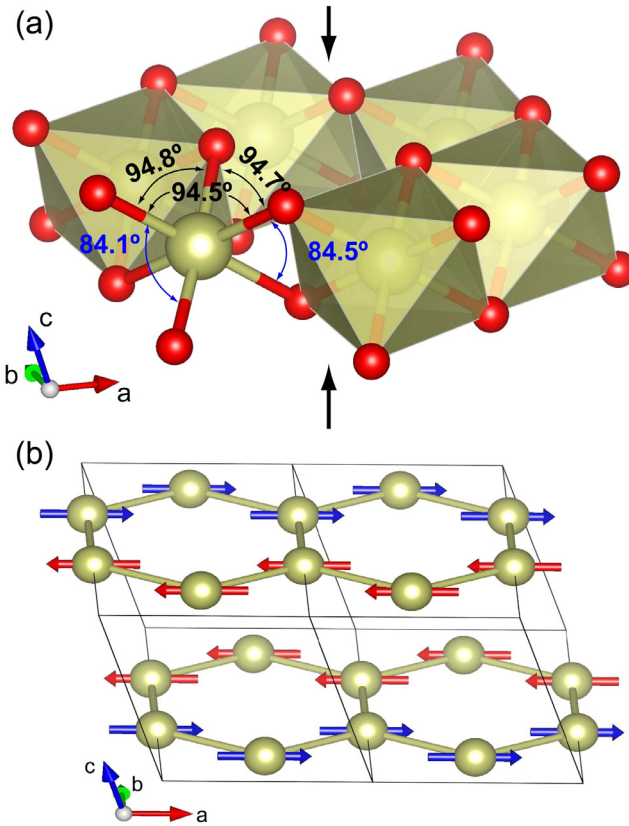


**Figure 21.**  $\text{Na}_2\text{IrO}_3$ : (a) local structure within the basal plane. The compression of  $\text{IrO}_6$  octahedron along the stacking marked by the black arrows leads to the decrease of O–Ir–O bond angles across the shared edges. (b) The zigzag order that is consistent with the symmetry associated with observed magnetic reflections. The Ir moments between honeycomb layers are antiferromagnetically coupled [33]. Reprinted figure with permission from [33], Copyright (2012) by the American Physical Society.

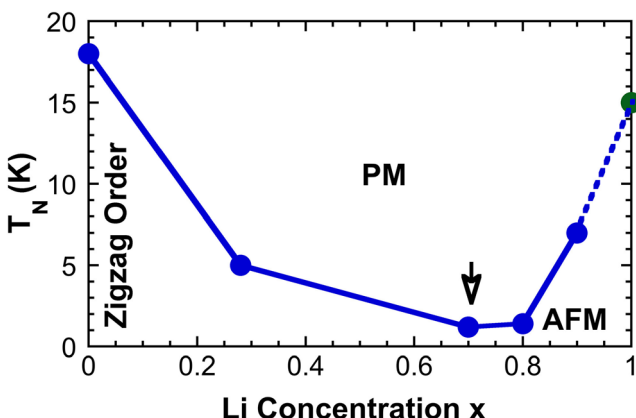


**Figure 22.** Phase diagram of  $(\text{Na}_{1-x}\text{Li}_x)_2\text{IrO}_3$ ; the Néel temperature  $T_N$  a function of  $x$ . Note that the lowest  $T_N$  is 1.2 K at  $x = 0.7$  [153]. Reprinted figure with permission from [153], Copyright (2013) by the American Physical Society.

definitive magnetic studies.  $\alpha\text{-Li}_2\text{IrO}_3$  was initially reported to feature a paramagnetic phase [160], and then AFM order at  $T_N = 15$  K [152]; more recently, an incommensurate magnetic order with Ir magnetic moments counter-rotating on nearest-neighbor sites was reported [63].

Indeed, the magnetic ground state of  $\text{Na}_2\text{IrO}_3$  and  $\alpha\text{-Li}_2\text{IrO}_3$  appear not to be related. Studies of single-crystal  $(\text{Na}_{1-x}\text{Li}_x)_2\text{IrO}_3$  indicate that, as  $x$  is tuned, the lattice parameters evolve monotonically from Na to Li, and retain the honeycomb structure of the  $\text{Ir}^{4+}$  planes and Mott insulating state for all  $x$ . However, there is a non-monotonic, dramatic change in  $T_N$  with  $x$ , in which  $T_N$  initially decreases from 18 K at  $x = 0$  to 1.2 K at  $x = 0.70$ , before it rises to 7 K at  $x = 0.90$  (see figure 22) [153]. Indeed, the corresponding frustration parameter  $\theta_{\text{CW}}/T_N$  ( $\theta_{\text{CW}}$  is the Curie–Weiss temperature) peaks at  $x = 0.70$  at a value of 31.6, which suggests strongly enhanced frustration. The complicated evolution of the magnetic behavior clearly demonstrates that the magnetic ground states attained at  $x = 0$  and 1 are indeed not related linearly [153] as had been previously suggested [36]. X-ray structure data also show that the  $\text{Ir}^{4+}$  honeycomb lattice is minimally distorted at  $x \approx 0.7$ , where the lowest  $T_N$  and highest frustration parameter are observed. In addition, the high-temperature anisotropy in the magnetic susceptibility is simultaneously reversed and enhanced upon Li doping. Another study of  $(\text{Na}_{1-x}\text{Li}_x)_2\text{IrO}_3$  suggests a phase separation in the range  $0.25 < x < 0.6$  [161], which calls for more investigations. Nevertheless, the evolution of structural, thermodynamic, and magnetic properties of  $(\text{Na}_{1-x}\text{Li}_x)_2\text{IrO}_3$  with  $x$  suggests two possible tuning parameters for the phase transition: The crystal field splitting and the anisotropy of the distortion of the honeycomb layers, both of which change sign from the Na to Li compounds, likely compete in such a manner that explains the magnetic ordering. A relevant study of Ti-doped honeycomb lattices reveals the Curie–Weiss temperature decreases with increasing  $x$  in  $\text{Na}_2(\text{Ir}_{1-x}\text{Ti}_x)\text{O}_3$ , but remains essentially unchanged in  $\text{Li}_2(\text{Ir}_{1-x}\text{Ti}_x)\text{O}_3$  [162], which further highlights the distinct differences between the magnetic ground states of  $\text{Na}_2\text{IrO}_3$  and  $\text{Li}_2\text{IrO}_3$ .

There are many theoretical proposals for interactions supplementary to the Kitaev model which would cause magnetic ordering, including additional exchange processes, strong trigonal fields, or weak coupling instabilities. A consensus is yet to be reached. It is recently suggested that the Kitaev spin liquid on the honeycomb lattice is extremely fragile against the second-nearest-neighbor Kitaev coupling, which is a dominant perturbation beyond the nearest-neighbor model in  $\text{Na}_2\text{IrO}_3$  [157]. It is thought that this coupling accounts for the zig-zag ordering observed in  $\text{Na}_2\text{IrO}_3$  [157].

Finally, it is worth mentioning that chemical doping cannot induce a metallic state in the honeycomb iridates, despite extensive experimental efforts [61]. This behavior contrasts with that in the perovskite iridates, in which chemical doping can readily prompt a metallic state, as discussed in section 2, may be due to the multi-orbital nature of the honeycomb lattices (It is noted that Na or Li ions are out of plane in the unit cell, thus chemical substitution for Na or Li might only lead to a small impurity potential.). On the other hand, like the perovskite iridates, the honeycomb iridates do not metallize up to 40 GPa [163].

### 3.1.2. Ru-based Honeycomb lattices $\text{Na}_2\text{RuO}_3$ , $\text{Li}_2\text{RuO}_3$ , and $\alpha\text{-RuCl}_3$

The investigations of the honeycomb iridates have also spread to their ruthenate counterparts,  $\text{Na}_2\text{RuO}_3$

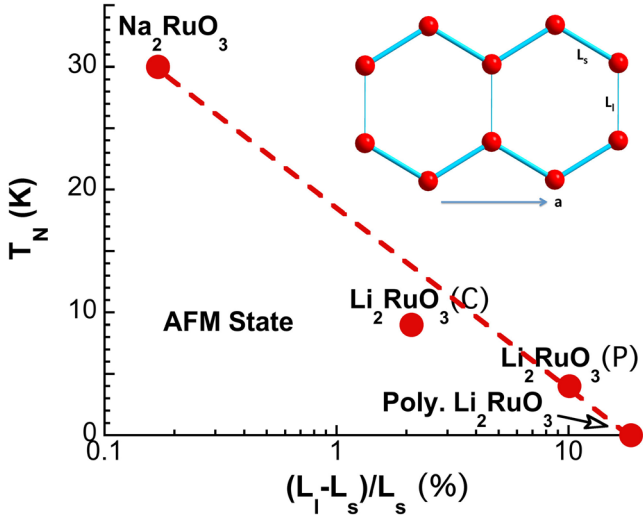


**Figure 23.** A phase diagram for honeycomb ruthenates: The Néel temperature  $T_N$  as a function of the bond distance ratio  $(L_l - L_s)/L_s$  (%) for all honeycomb ruthenates. Inset: a schematic of the honeycomb lattice featuring long bond  $L_l$  and short bond  $L_s$  [168]. Note that single-crystal  $\text{Li}_2\text{RuO}_3$  (C) and  $\text{Li}_2\text{RuO}_3$  (P) stand for the structural phases with  $C2/m$  and  $P2_1/m$  space group, respectively, and Poly  $\text{Li}_2\text{RuO}_3$  for polycrystalline  $\text{Li}_2\text{RuO}_3$  (also see text). Reprinted figure with permission from [168], Copyright (2014) by the American Physical Society.

and  $\text{Li}_2\text{RuO}_3$ , and, more recently, Ru based  $\alpha\text{-RuCl}_3$  (with  $\text{Ru}^{3+}(4d^5)$ ). Both of the ruthenates feature  $\text{Ru}^{4+}(4d^4)$  ions and a weaker or ‘intermediate strength’ SOI ( $\sim 0.16$  eV, compared to  $\sim 0.4$  eV for Ir ions) (see table 2). The different d-shell filling and contrasting hierarchy of energy scales between the ruthenates and iridates provide a unique opportunity to gain a deeper understanding of the fundamental problem of interacting electrons on the honeycomb lattices. The magnetism of  $\text{Ru}^{4+}$  ions as well as other ‘heavy  $d^4$  ions’ (such as  $\text{Rh}^{5+}(4d^4)$ ,  $\text{Re}^{3+}(5d^4)$ ,  $\text{Os}^{4+}(5d^4)$  and  $\text{Ir}^{5+}(5d^4)$ ) is interesting in their own right, as emphasized recently [164–169]. Materials with heavy  $d^4$  ions tend to adopt a low-spin state because larger crystal fields often overpower the Hund’s rule coupling. On the other hand, SOI with the intermediate strength may still be strong enough to impose a competing singlet ground state or a total angular momentum  $J_{\text{eff}} = 0$  state. Novel magnetic states may thus emerge when the singlet-triplet splitting (0.05–0.20 eV) becomes comparable to exchange interactions (0.05–0.10 eV) and/or non-cubic crystal fields [164].

Both  $\text{Na}_2\text{RuO}_3$  and  $\text{Li}_2\text{RuO}_3$  adopt a honeycomb structure.  $\text{Na}_2\text{RuO}_3$  features a nearly ideal honeycomb lattice with space group  $C2/m$ , and orders antiferromagnetically below 30 K [168]. On the other hand, **single-crystal  $\text{Li}_2\text{RuO}_3$**  adopts a less ideal honeycomb lattice with either  $C2/m$  or more distorted  $P2_1/m$  space group below 300 K; these two phases are denoted as  $\text{Li}_2\text{RuO}_3$  (C) and  $\text{Li}_2\text{RuO}_3$  (P) for  $C2/m$   $P2_1/m$  space group, respectively. Both phases exhibit a well-defined, though different, magnetic state. It is interesting that the magnetic state in single-crystal  $\text{Li}_2\text{RuO}_3$  contrasts with the nonmagnetic state or singlet ground state due to dimerization observed in **polycrystalline  $\text{Li}_2\text{RuO}_3$**  (denoted as Poly  $\text{Li}_2\text{RuO}_3$  in figure 23) [170]. Careful examinations of structural details reveal that

these honeycomb lattices feature two bond distances (long and short,  $L_l$  and  $L_s$ , respectively), which, to a large extent, dictate the ground state of the honeycomb lattice  $\text{Na}_2\text{RuO}_3$  and  $\text{Li}_2\text{RuO}_3$  (see figure 23), as discussed below.

A study of these materials [168] show that the magnetic ordering temperature systematically decreases with increasing  $(L_l - L_s)/L_s$  and eventually vanishes at a critical value where dimerization emerges, which leads to the singlet ground state observed in polycrystalline  $\text{Li}_2\text{RuO}_3$ . A phase diagram generated in this study uncovers a direct correlation between the ground state and basal-plane distortions (lattice-tuned magnetism) in the honeycomb ruthenates, as shown in figure 23 [168]. In addition, a few other observations are remarkable: (1) Both  $\text{Li}_2\text{RuO}_3$  and  $\text{Li}_2\text{IrO}_3$  are more structurally distorted and behave with more complexities than their Na counterparts. (2) Although the SOI is expected to impose a singlet  $J_{\text{eff}} = 0$  state for  $\text{Ru}^{4+}(4d^4)$  ions (and a  $J_{\text{eff}} = 1/2$  state for  $\text{Ir}^{4+}(5d^5)$  ions), the observed magnetic states in the honeycomb ruthenates as in many other ruthenates [19] indicate that the SOI is not sufficient to induce a  $J_{\text{eff}} = 0$  state. (3) All honeycomb ruthenates and iridates magnetically order in a similar temperature range despite the different role of the SOI in them [168].

A Ru-based honeycomb lattice,  $\alpha\text{-RuCl}_3$ , with  $\text{Ru}^{3+}(4d^5)$  (rather than the commonplace  $\text{Ru}^{4+}$  state for ruthenates) [171, 172] has recently drawn a great deal of attention as a candidate for the spin liquid state [173–177].  $\alpha\text{-RuCl}_3$ , with space group  $P3_112$  ( $C2/m$  was also reported), supports a Mott state with an AFM order below  $T_N = 7$  K [177] ( $T_N$  is sample dependent in early reports; it is now recognized that  $T_N = 7$  K is intrinsic). The magnetic structure is determined to be zig-zag, similar to that of  $\text{Na}_2\text{IrO}_3$  [177]; but  $\alpha\text{-RuCl}_3$  adopts a more ideal honeycomb lattice without the distortions found in  $\text{Na}_2\text{IrO}_3$ . This simplified structure, combined with the weaker neutron absorption cross-section of Ru compared to Ir, favors  $\alpha\text{-RuCl}_3$  for further experimental studies of Kitaev physics. On the other hand, the weaker SOI in the  $4d$  shell might result in a large overlap between the  $J_{\text{eff}} = 1/2$  and  $J_{\text{eff}} = 3/2$  bands, thereby reducing the signature of the  $J_{\text{eff}}$  states in experimental data. This issue is addressed in recent studies [18, 175, 177].

### 3.2. $\beta\text{-Li}_2\text{IrO}_3$ and $\gamma\text{-Li}_2\text{IrO}_3$

Two derivatives of the two-dimensional honeycomb lattices discussed above are the hyper-honeycomb  $\text{Li}_2\text{IrO}_3$  and stripy-honeycomb  $\text{Li}_2\text{IrO}_3$ , formally termed,  $\beta\text{-Li}_2\text{IrO}_3$  and  $\gamma\text{-Li}_2\text{IrO}_3$ , respectively. They are a result of strong, mainly trigonal and monoclinic distortions of networks of edge-shared octahedra similar to those found in  $\text{Na}_2\text{IrO}_3$  and  $\alpha\text{-Li}_2\text{IrO}_3$ . With a  $J_{\text{eff}} = 1/2$  state, both  $\beta\text{-Li}_2\text{IrO}_3$  and  $\gamma\text{-Li}_2\text{IrO}_3$  antiferromagnetically order at 38 K into incommensurate, counter-rotating spirals. But unlike the in-plane moments in  $\alpha\text{-Li}_2\text{IrO}_3$ , the  $\beta$ - and  $\gamma$ -phase moments are non-coplanar, forming three-dimensional honeycomb lattices [65, 67]. There are some subtle differences in magnetic moments, but the two distorted honeycomb lattices are strikingly similar in terms of incommensurate propagation vectors ([0.57, 0, 0]) [64, 66], which implies a possible common mechanism drives the ground state. A burgeoning list of theoretical proposals emphasize a

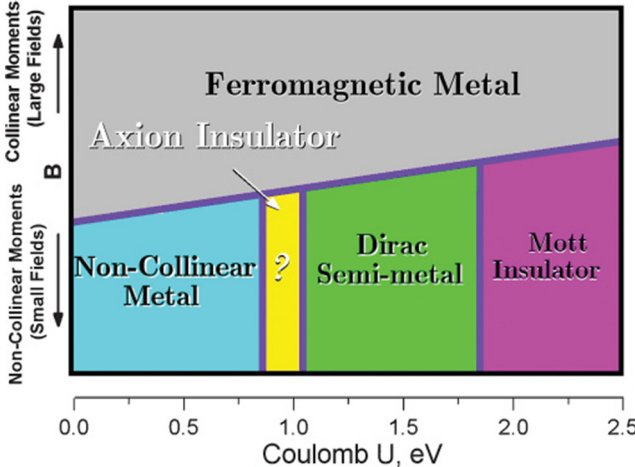


**Figure 24.** The predicted phase diagram for pyrochlore iridates: the horizontal axis corresponds to  $U$  whereas the vertical axis represents external magnetic field, which can trigger a transition out of the noncollinear ‘all-in/all-out’ ground state that includes several electronic phases [29]. Reprinted figure with permission from [29], Copyright (2011) by the American Physical Society.

combined effect of the ferromagnetic Kitaev limit, structural distortions and exchange interactions between nearest neighbors (or even next-nearest neighbors), which may account for the stability of the incommensurate order on the three-dimensional honeycomb lattice [157, 178–182].

### 3.3. Hyperkagome $\text{Na}_4\text{Ir}_3\text{O}_8$ and pyrochlore iridates

A large number of theoretical and experimental studies on other frustrated iridates, such as the hyper-kagome  $\text{Na}_4\text{Ir}_3\text{O}_8$  [20, 183, 184] and the pyrochlore iridates [17, 71, 72, 185], have been conducted [17].

$\text{Na}_4\text{Ir}_3\text{O}_8$  with a frustrated hyperkagome lattice was first reported in 2007 [20]. It features magnetic and thermal properties appropriate for a spin-liquid state (e.g. no long-range magnetic order above 2 K and no magnetic field dependence of the magnetization and heat capacity) [20]. More recent studies confirmed the absence of long-range magnetic order down to  $T = 75$  mK [183]. This work [20] has helped generate a great deal of interest in geometrically frustrated iridates.

The pyrochlore iridates,  $\text{R}_2\text{Ir}_2\text{O}_7$  ( $\text{R} = \text{Y}$ , rare earth ion or  $\text{Bi}$  or  $\text{Pb}$ ), are mostly magnetic insulators, except for  $\text{Pr}_2\text{Ir}_2\text{O}_{7-\delta}$ , which exhibits correlated metallic behavior [186–189],  $\text{Bi}_2\text{Ir}_2\text{O}_7$  and  $\text{Pb}_2\text{Ir}_2\text{O}_7$  [68–70], which also present a metallic ground state. Many of these iridates have been intensively studied as potential platforms for exotic states such as spin liquids, Weyl semimetals, axion insulators, topological insulators, etc [17, 29]. A recent study using scanning microwave imaging reveals one-dimensional metallic channels along all-in-all-out (AIAO)/all-out-all-in magnetic domain walls [185]. A rich phase diagram has been predicated for the pyrochlore iridates (see figure 24) [29]. It is established that the ground state of these materials sensitively depends on the relative strengths of competing SOI and  $U$ , and a hybridization interaction that is controlled by the Ir–O–Ir bond angle [17, 29, 189, 190]; and therefore,

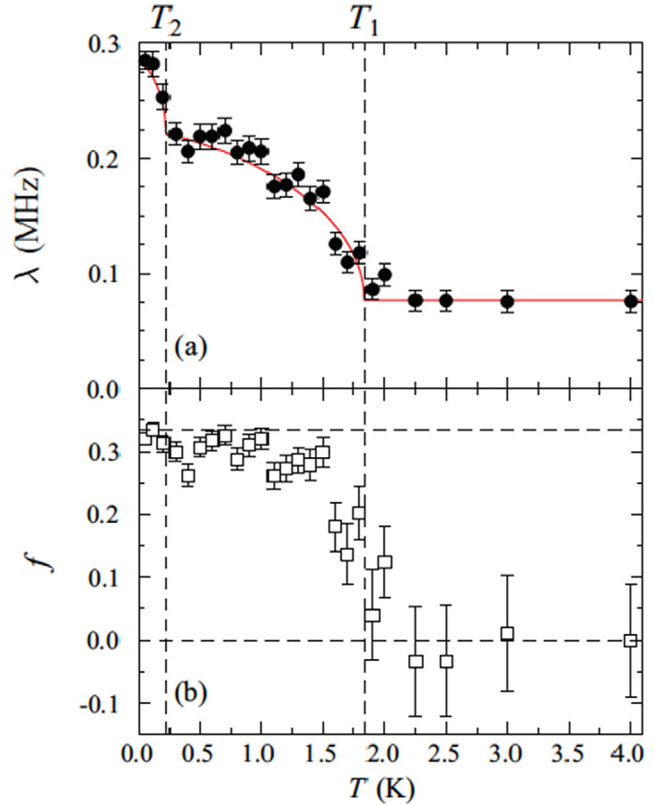


**Figure 25.**  $\text{Bi}_2\text{Ir}_2\text{O}_7$ : (a)  $\mu$ -spin relaxation rate  $\lambda$ . The solid line is a guide to the eye. (b) Fractional amplitude of the nonrelaxing asymmetry,  $f$ . Dashed lines show transition temperatures and limiting values of  $f$  [70]. Reprinted figure with permission from [70], Copyright (2013) by the American Physical Society.

small perturbations can easily tip the balance between the competing energies and ground states [17, 189]. This is perfectly illustrated in a phase diagram presented in [189], in which the ground state of  $\text{R}_2\text{Ir}_2\text{O}_7$  ( $\text{R}$  = rare earth ion) sensitively depends on the ionic radius of the rare earth ion [17, 189]. However, the nature of the magnetic state is yet to be conclusively determined, in part due to experimental challenge of synthesizing large, high-quality single crystals of the pyrochlore iridates.

A relevant, but less studied pyrochlore iridate is  $\text{Bi}_2\text{Ir}_2\text{O}_7$  (where the  $\text{Bi}^{3+}$  ion substitutes for a rare-earth ion) [68]. Investigations of single-crystal  $\text{Bi}_2\text{Ir}_2\text{O}_7$  indicate a significantly enhanced hybridization between the Bi-6s/6p and Ir-5d electrons, which overpowers the SOI and  $U$ , and drives the material into a metallic state with the Fermi energy residing near a sharp peak in the density of states, despite the large  $Z$  (thus SOI) for both Bi and Ir [69, 70, 191]. Muon spin relaxation ( $\mu$ SR) measurements show that  $\text{Bi}_2\text{Ir}_2\text{O}_7$  undergoes a bulk magnetic transition at  $1.84(3)$  K (figure 25(a)) [70]. This is accompanied by increases in the muon spin relaxation rate and the amplitude of the nonrelaxing part of the signal (figure 25(b)). The magnetic field experienced by muons is estimated to be 0.7 mT at low temperature, around two orders of magnitude smaller than that observed in other pyrochlore iridates [70]. These results suggest that the low-temperature state involves exceptionally small static magnetic moments, 0.01

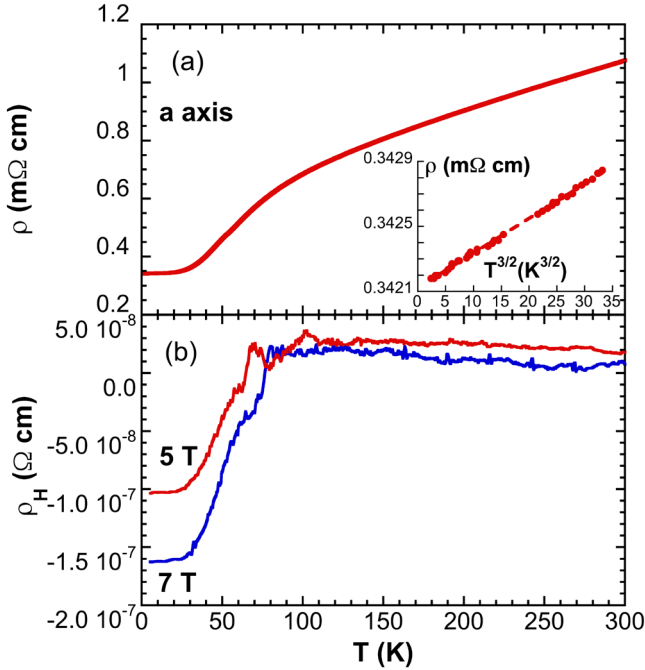


**Figure 26.**  $\text{Bi}_2\text{Ir}_2\text{O}_7$ : the temperature dependence of (a) the  $a$ -axis electrical resistivity  $\rho$ , and (b) the Hall resistivity at 3 T and 5 T. Inset: the  $a$ -axis  $\rho$  versus  $T^{3/2}$  for  $1.7 \text{ K} < T < 10 \text{ K}$  [69]. Reproduced from [69]. © IOP Publishing Ltd. All rights reserved.

$\mu_B/\text{Ir}$ . The relaxation rate increases further below 0.23(4) K, consistent with an upturn in the specific heat, suggesting the existence of a second low-temperature magnetic transition. Indeed, the coefficients ( $\gamma$  and  $\beta$ ) of the low-temperature  $T$  and  $T^3$  terms of the specific heat  $C(T)$  are strongly field-dependent. The state also has a conspicuously large Wilson ratio  $R_W \approx 53.5$  and an unusual Hall resistivity that abruptly changes below 80 K without any correlation with the magnetic behavior (figure 26(b)) [69]. These unconventional properties, along with the novel behavior observed in metallic hexagonal  $\text{SrIrO}_3$  [58], define an exotic class of SOI metals (figure 26(a)) in which strongly competing interactions induce non-Fermi liquid states that generate magnetic instabilities.

#### 4. Double-perovskite iridates with $\text{Ir}^{5+}(5d^4)$ ions: nonmagnetic singlet $J_{\text{eff}} = 0$ state?

The strong SOI limit is expected to lead to a nonmagnetic singlet ground state, which can be simply understood as a  $J_{\text{eff}} = 0$  state arising from four electrons filling the lower  $J_{\text{eff}} = 3/2$  quadruplet in materials with  $d^4$  ions, such as  $\text{Ru}^{4+}(4d^4)$ ,  $\text{Rh}^{5+}(4d^4)$ ,  $\text{Re}^{3+}(5d^4)$ ,  $\text{Os}^{4+}(5d^4)$ , as well as  $\text{Ir}^{5+}(5d^4)$  (see the schematic in figure 1(d), and 27(c)) [17, 73–75, 79, 164–169, 192]. Indeed, the  $J_{\text{eff}} = 0$  state has been used to explain the absence of magnetic ordering in the pentavalent post perovskite  $\text{NaIrO}_3$  [80], although it has also been attributed to structural distortions [167]. On the other hand, a low-spin  $S = 1$  state is expected large crystalline fields when  $U$  and the Hund's rule coupling  $J_H$  are much greater than the SOI  $\lambda$ , which is a condition commonly seen in ruthenates (figure 27(a)) [19]. In this case only the  $t_{2g}$ -orbitals are

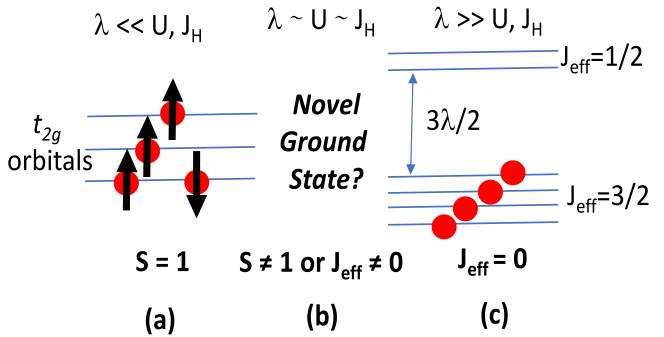


**Figure 27.** The ground state of  $4d^4$  or  $5d^4$  ions: (a) the low spin state  $S = 1$ , and (c) the singlet  $J_{\text{eff}} = 0$  state and (b) an intermediate state between  $S = 1$  and  $J_{\text{eff}} = 0$  states.

relevant, which are all singly occupied except for the one with lowest energy, yielding an effective  $S = 1$ .

Nevertheless, theoretical and experimental studies suggest that novel states in these materials can emerge when exchange interactions (0.05–0.10 eV),  $J_H$ , singlet-triplet splitting (0.050–0.20 eV) and the SOI are comparable, and therefore compete. Exotic states are expected in  $d^4$ -Mott insulators that support ‘intermediate-strength’ SOI and  $U$  [165–169, 193].

Pentavalent iridates attracted attention when experimental and theoretical studies showed evidence that contradicted the anticipated  $J_{\text{eff}} = 0$  state [75, 164–167]. One surprising experiment addressed a distorted double-perovskite  $\text{Sr}_2\text{YIrO}_6$  that exhibits an exotic magnetic state below 1.3 K rather than an expected  $J_{\text{eff}} = 0$  state or a  $S = 1$  state (figure 27(b)) [73].  $\text{Sr}_2\text{YIrO}_6$  adopts a monoclinic structure essentially derived from the  $\text{SrIrO}_3$  perovskite by replacing every other Ir by non-magnetic Y; the remaining magnetic  $\text{Ir}^{5+}$  ions form a network of edge-sharing tetrahedra or a face centered cubic (FCC) structure with lattice parameters elongated compared to the parent cubic structure, as shown in figure 28. Because of the differences in valence state and ionic radius between  $\text{Y}^{3+}$  and  $\text{Ir}^{5+}$  ions, no significant intersite disorder is expected. This and other related double perovskite iridates have two strongly unfavorable conditions for magnetic order, namely, pentavalent  $\text{Ir}^{5+}(5d^4)$  ions which are anticipated to have  $J_{\text{eff}} = 0$  singlet ground states in the strong SOI limit, and geometric frustration in a FCC structure formed by the  $\text{Ir}^{5+}$  ions (figure 28).

The emergence of the unexpected magnetic ground state was initially attributed to effects of non-cubic crystal fields on the  $J_{\text{eff}} = 1/2$  and  $J_{\text{eff}} = 3/2$  states because such effects were not included in the original model [7, 8]. However, there are other possible origins for a magnetic moment in pentavalent Ir systems: As the hopping of the  $t_{2g}$  electrons increases, the width of the bands increases and the  $J_{\text{eff}} = 1/2$  and  $J_{\text{eff}} = 3/2$  bands may overlap so that the  $J_{\text{eff}} = 1/2$  state is partially filled and the  $J_{\text{eff}} = 3/2$  state has a corresponding number of holes. This may result in a magnetic moment. Interactions, in particular, the Hund's rule exchange,  $J_H$ , and  $U$  couple the different orbitals. Recent theoretical studies [165–167, 169, 193] predict a quantum phase transition with increasing hopping of the electrons from the expected  $J_{\text{eff}} = 0$  state to a novel magnetic state with local  $5d^4$  moments. Furthermore, a band

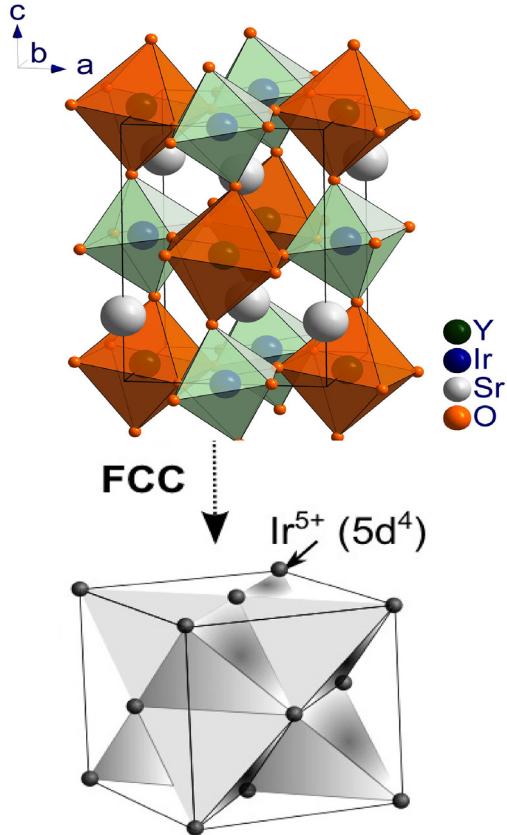


**Figure 28. Double-perovskite  $\text{Sr}_2\text{YIrO}_6$ :** upper panel: the double perovskite crystal structure of  $\text{Sr}_2\text{YIrO}_6$ ; lower panel: the ordered replacement of nonmagnetic Y ions for magnetic Ir ions leading to a FCC lattice with geometrically frustrated edge-sharing tetrahedra formed by the pentavalent Ir<sup>5+</sup> ions [73]. Reprinted figure with permission from [73], Copyright (2014) by the American Physical Society.

structure study of a series of double-perovskite iridates with Ir<sup>5+</sup>(5d<sup>4</sup>) ions shows that the e<sub>g</sub> orbitals play no role in determining the ground state. It confirms the observed magnetic state in distorted  $\text{Sr}_2\text{YIrO}_6$  [167] and also predicts a breakdown of the  $J_{\text{eff}} = 0$  state in undistorted, cubic  $\text{Ba}_2\text{YIrO}_6$  as well because the magnetic order is a result of band structure, rather than of non-cubic crystal fields in these double-perovskites.

Indeed, a low-temperature magnetic ground state is recently observed in the entire series of  $(\text{Ba}_{1-x}\text{Sr}_x)_2\text{YIrO}_6$  [194]. This observed magnetic state, which is similar to that in  $\text{Sr}_2\text{YIrO}_6$ , evolves gradually with changes of the lattice parameters while retaining the underlying AMF characteristics (see figure 29). However, the small value of the ordered magnetic moment and small magnetic entropy removal associated with heat capacity anomalies imply that this magnetic state is weak and barely stable compared to either the  $S = 1$  state that is commonly observed among heavy  $d^4$  transition element ions, or the  $J_{\text{eff}} = 0$  state driven by strong SOI [194]. These circumstances make this magnetic state unique and intriguing. Indeed, a recent resonant inelastic x-ray scattering (RIXS) reveals that the Hund's rule coupling  $J_H = 0.25$  eV for Ir<sup>5+</sup> in the double perovskite iridates, suggesting that  $J_H$  should be treated on equal footing with the SOI in these materials [195]. A more

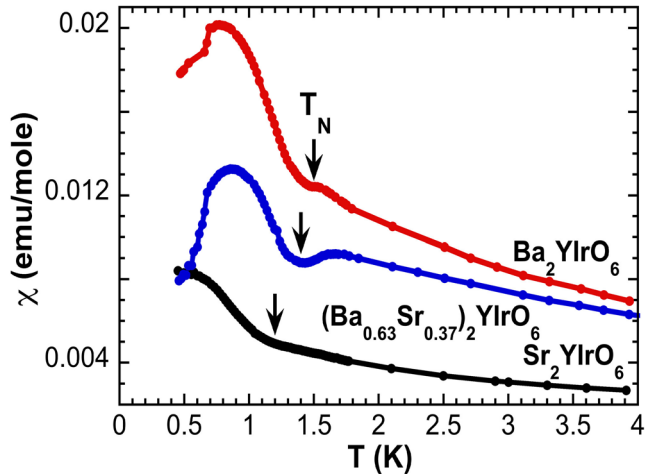


**Figure 29. Double perovskite  $(\text{Ba}_{1-x}\text{Sr}_x)_2\text{YIrO}_6$ :** the temperature dependence of magnetic susceptibility  $\chi(T)$  at low temperatures [194]. Reprinted figure with permission from [194], Copyright (2017) by the American Physical Society.

commonly accepted argument is that the SOI competes with a comparable exchange interaction  $J_H$  and a generically large electron hopping (because of the extended nature of 5d-orbitals) that suppresses the singlet  $J_{\text{eff}} = 0$  ground state. At the same time, the SOI breaks down the low-spin  $S = 1$  state. This ‘simultaneous’ destabilization of the  $S = 1$  and  $J_{\text{eff}} = 0$  states leads to a magnetic state that resides somewhere between the other two. The above picture is not without controversy. There are also theoretical and experimental studies that suggest a non-magnetic state in the double-perovskite iridates [74, 75, 192, 196].

While the  $J_{\text{eff}} = 1/2$  insulating state model successfully captures the new physics observed in many iridates, recent studies suggest that it may not be adequate to describe new phenomena when the relative strength of the SOI critically competes with the strength of electron hopping and exchange interactions. It is worth mentioning once again that the  $J_{\text{eff}} = 1/2$  model is a single-particle approach that assumes that SOI is greater than Hund’s rule interactions among the electrons. Its validity needs to be closely examined when the Hund’s rule interactions among the electrons are comparable to SOI in  $d^4$ -electron systems [195]. Nevertheless, the anticipated magnetic ground state [165–167, 169, 193] may indicate that the SOI may not be as dominating as initially anticipated, thus leading to magnetic order rather than a singlet ground state in the double perovskite iridates. This magnetic state could be extraordinarily fragile as evidenced in the varied magnetic behavior reported in both experimental and theoretical studies [74, 75, 192, 194]. It is clear that the stability limits of the spin-orbit-coupled  $J_{\text{eff}}$  states in heavy transition metal materials must be investigated.

## 5. Future challenges and outlook

The SOI is a strong competitor with  $U$  and other interactions, and creates an entirely new hierarchy of energy scales in iridates (table 2), which provides fertile ground for the discovery

of novel physics. Indeed, a burgeoning list of theoretical proposals and predictions of exotic states, such as the spin liquid state, superconductivity, Weyl semimetals, correlated topological insulators, etc is truly remarkable and stimulating. It is perhaps even more intriguing that these predictions have met only limited experimental confirmation thus far. The physics of iridates clearly presents urgent intellectual challenges both theoretically and experimentally, and this field is still in its infancy.

Iridates tend to be magnetic insulators, chiefly because of the combined effect of SOI and U; and they also display a number of interesting empirical trends that defy conventional wisdom. In particular, iridates rarely metallize at high pressures, regardless of their crystal structures; however, when they do, the induced metallic state is extraordinary, such as that in  $\text{Sr}_3\text{Ir}_2\text{O}_7$  near 60 GPa. On the other hand, a metallic state can be readily induced via slight chemical doping in layered perovskite and hexagonal iridates, but remarkably not in honeycomb iridates. The charge gap and the magnetic state do not necessarily track each other. There are seldom first-order phase transitions in iridates, if any at all: all known transitions induced by temperature, magnetic field, pressure, or chemical doping are gradual and continuous (the sharp transitions in the ‘S’-shaped IV curves may be a rare exception). Moreover, non-linear Ohmic behavior and/or switching effects are also commonplace in iridates. While all these curious properties pose tantalizing prospects for unique functional materials and devices, they also pose a series of intriguing questions that may provide the impetus for advancing our understanding of this class of materials:

- Is the  $J_{\text{eff}} = 1/2$  insulating state ubiquitous in other 5d-materials (even in non-cubic crystal fields and/or with non-negligible Hund’s rule interactions between the electrons)?
- Why do iridates seldom metallize at high pressures?
- In contrast, why can even small chemical doping readily induce a metallic state in most insulating iridates (except for honeycomb iridates)?
- Why does superconductivity remain elusive in  $\text{Sr}_2\text{IrO}_4$  despite its similarities to the cuprates, and extensive theoretical and experimental efforts addressing superconductivity in this model material?
- Will driving the hidden non-dipolar magnetic order to its quantum critical point provide a path toward generating the elusive superconducting state in  $\text{Sr}_2\text{IrO}_4$ ?
- Why do all honeycomb iridates and ruthenates magnetically order in a similar temperature range, despite their different SOI?
- Can we go beyond discussions of Mott, Mott-Hubbard and Slater insulators to better understand the role of the magnetic transition in the formation of an insulating state in iridates?
- A metallic state is rare in iridates, but when it does happen it has extraordinary properties. How do we describe it?
- How do we explain current-sensitive transport properties or non-linear Ohmic behavior, in particular, the S-shaped  $I$ - $V$  characteristic?

- Does the nonmagnetic singlet  $J_{\text{eff}} = 0$  state exist in iridates with  $\text{Ir}^{5+}(5d^4)$  ions?
- More generally, how do we describe the Mott insulating state with ‘intermediate-strength’ or strong SOI in materials with  $d^4$  ions, such as  $\text{Ru}^{4+}(4d^4)$ ,  $\text{Rh}^{5+}(4d^4)$ ,  $\text{Re}^{3+}(5d^4)$ ,  $\text{Os}^{4+}(5d^4)$  and  $\text{Ir}^{5+}(5d^4)$ ?

It needs to be reiterated that one defining characteristic of iridates is that the strong SOI renders a strong coupling of physical properties to the lattice degrees of freedom, which is seldom seen in other materials. The wide range of novel phenomena and the limited experimental confirmation for many predicted ground states imply a critical role of subtle, local lattice properties that control ground states, and needs to be more adequately addressed both experimentally and theoretically.

Because of the unique distortions of the Ir–O–Ir bond in iridates, the lattice properties, and therefore physical properties, can be readily tuned via perturbations such as magnetic field, electric field, pressure, epitaxial strain or chemical doping. That transport properties sensitively change with electrical current or electric field (e.g. the S-shaped IV curves) is particularly promising in terms of fundamental research and development of potential functional devices, since the application of an electric field is much more convenient than the application of a magnetic field or pressure.

Of course, the nature of the extraordinary structural sensitivity of iridates also calls for extraordinarily high-quality single crystals and epitaxial thin-films. Moreover, the strong neutron absorption caused by the high atomic number of iridium, 77, requires not only high-quality but also large and preferably plate-like, bulk single crystals for more definitive magnetic studies such as inelastic neutron scattering. This is particularly urgent for a number of iridates such as pyrochlore iridates,  $\text{Li}_2\text{IrO}_3$ ,  $\text{Sr}_3\text{Ir}_2\text{O}_7$  and double perovskites with  $\text{Ir}^{5+}$  ions, whose magnetic structures are yet to be conclusively determined. This is a daunting experimental challenge because iridates tend to have both high melting points and high vapor pressure, which require sophisticated techniques for single-crystal synthesis.

Finally, we would like to reiterate that it is impossible to review such a broad and rapidly evolving field in a single article. We can only provide a basic introduction, some general remarks and observations, and a number of hopefully instructive examples.

## Acknowledgments

This work is supported by the US National Science Foundation via grants DMR-1265162 and DMR-1712101. PS is supported by the US Department of Energy (Basic Energy Sciences) under grant No. DE-FG02-98ER45707. GC is deeply indebted to Drs. Lance De Long, Feng Ye, Daniel Haskel, Hae Young Kee and David Hsieh for their insightful comments and suggestions, which significantly improve this *Review*.

**ORCID iDs**Gang Cao  <https://orcid.org/0000-0001-9779-430X>**References**

- [1] Huang Q, Soubeyroux J L, Chmaissem O, Natalisora I, Santoro A, Cava R J, Krajewski J J and Peck W F Jr 1994 Neutron powder diffraction study of the crystal structures of  $\text{Sr}_2\text{RuO}_4$  and  $\text{Sr}_2\text{IrO}_4$  at room temperature and at 10 K *J. Solid State Chem.* **112** 355
- [2] Cava R J, Batlogg B, Kiyono K, Takagi H, Krajewski J J, Peck W F Jr, Rupp L W and Chen C H 1994 Localized-to-itinerant electron transition in  $\text{Sr}_2\text{Ir}_{1-x}\text{Ru}_x\text{O}_4$  *Phys. Rev. B* **49** 11890
- [3] Crawford M K, Subramanian M A, Harlow R L, Fernandez-Baca J A, Wang Z R and Johnston D C 1994 Structural and magnetic studies of  $\text{Sr}_2\text{IrO}_4$  *Phys. Rev. B* **49** 9198
- [4] Cao G, Bolivar J, McCall S, Crow J E and Guertin R P 1998 Weak ferromagnetism, metal-to-nonmetal transition, and negative differential resistivity in single-crystal  $\text{Sr}_2\text{IrO}_4$  *Phys. Rev. B* **57** R11039
- [5] Cao G, Xin Y, Alexander C S, Crow J E, Schlottmann P, Crawford M K, Harlow R L and Marshall W 2002 Anomalous magnetic and transport behavior in the magnetic insulator  $\text{Sr}_3\text{Ir}_2\text{O}_7$  *Phys. Rev. B* **66** 214412
- [6] Cao G, Crow J E, Guertin R P, Henning P F, Homes C C, Strongin M, Basov D N and Lochner E 2000 Charge density wave formation accompanying ferromagnetic ordering in quasi-one-dimensional  $\text{BaIrO}_3$  *Solid State Commun.* **113** 657
- [7] Kim B J *et al* 2008 Novel  $J_{\text{eff}} = 1/2$  Mott state induced by relativistic spin-orbit coupling in  $\text{Sr}_2\text{IrO}_4$  *Phys. Rev. Lett.* **101** 076402
- [8] Moon S J *et al* 2008 Dimensionality-controlled insulator-metal transition and correlated metallic state in 5d transition metal oxides  $\text{Sr}_{n+1}\text{Ir}_n\text{O}_{3n+1}$  ( $n = 1, 2$ , and  $\infty$ ) *Phys. Rev. Lett.* **101** 226402
- [9] Kim B J, Ohsumi H, Komesu T, Sakai S, Morita T, Takagi H and Arima T 2009 Phase-sensitive observation of a spin-orbital Mott state in  $\text{Sr}_2\text{IrO}_4$  *Science* **323** 1329
- [10] Landau L D and Lifshitz E M 1977 *Quantum Mechanics* 3rd edn (New York: Pergamon) p 268
- [11] Shanavas K V, Popović Z S and Satpathy S 2014 Theoretical model for Rashba spin-orbit interaction in d electrons *Phys. Rev. B* **90** 165108
- [12] Liu X *et al* 2012 Testing the validity of the strong spin-orbit coupling limit for octahedrally coordinated iridate compounds in a model system  $\text{Sr}_3\text{CuIrO}_6$  *Phys. Rev. Lett.* **109** 157401
- [13] Jackeli G and Khaliullin G 2009 Mott insulators in the strong spin-orbit coupling limit: from Heisenberg to a quantum compass and Kitaev models *Phys. Rev. Lett.* **102** 017205
- [14] Chern G W and Perkins N 2009 Large-J approach to strongly coupled spin-orbital systems *Phys. Rev. B* **80** 180409
- [15] Chaloupka J, Jackeli G and Khaliullin G 2010 Kitaev–Heisenberg model on a Honeycomb lattice: possible exotic phases in iridium oxides  $\text{A}_2\text{IrO}_3$  *Phys. Rev. Lett.* **105** 027204
- [16] Shitade A, Katsura H, Kunes J, Qi X L, Zhang S C and Nagaosa N 2009 Quantum spin Hall effect in a transition metal oxide  $\text{Na}_2\text{IrO}_3$  *Phys. Rev. Lett.* **102** 256403
- [17] Witczak-Krempa W, Chen G, Kim Y B and Balents L 2014 Correlated quantum phenomena in the strong spin-orbit regime *Annu. Rev. Condens. Matter Phys.* **5** 57
- [18] Rau J G, Lee E K H and Kee H Y 2016 Spin-orbit physics giving rise to novel phases in correlated systems: iridates and related materials *Annu. Rev. Condens. Matter Phys.* **7** 195
- [19] Cao G and DeLong L 2013 *Frontiers of 4d- and 5d-Transition Metal Oxides* (Singapore: World Scientific) 328 p
- [20] Okamoto Y, Nohara M, Aruga-Katori H and Takagi H 2007 Spin-liquid state in the  $S = 1/2$  hyperkagome antiferromagnet  $\text{Na}_4\text{Ir}_3\text{O}_8$  *Phys. Rev. Lett.* **99** 137207
- [21] Takayama T, Yaresko A, Matsumoto A, Nuss J, Ishii K, Yoshida M, Mizuki J and Takagi H 2014 Spin-orbit coupling induced semi-metallic state in the 1/3 hole-doped hyper-kagome  $\text{Na}_3\text{Ir}_3\text{O}_8$  *Sci. Rep.* **4** 6818
- [22] Wang F and Senthil T 2011 Twisted Hubbard model for  $\text{Sr}_2\text{IrO}_4$ : magnetism and possible high temperature superconductivity *Phys. Rev. Lett.* **106** 136402
- [23] Watanabe H, Shirakawa T and Yunoki S 2013 Monte Carlo study of an unconventional superconducting phase in iridium oxide  $J_{\text{eff}} = 1/2$  Mott insulators induced by carrier doping *Phys. Rev. Lett.* **110** 027002
- [24] Kim J *et al* 2012 Magnetic excitation spectra of  $\text{Sr}_2\text{IrO}_4$  probed by resonant inelastic x-ray scattering: establishing links to cuprate superconductors *Phys. Rev. Lett.* **108** 177003
- [25] Khaliullin G, Koshiba W and Maekawa S 2004 Low energy electronic states and triplet pairing in layered cobaltate *Phys. Rev. Lett.* **93** 176401
- [26] Yang Y, Wang W S, Liu J G, Chen H, Dai J H and Wang Q H 2014 Superconductivity in doped  $\text{Sr}_2\text{IrO}_4$ : a functional renormalization group study *Phys. Rev. B* **89** 094518
- [27] You Y Z, Kimchi I and Vishwanath A 2012 Doping a spin-orbit Mott insulator: topological superconductivity from the Kitaev–Heisenberg model and possible application to  $(\text{Na}_2/\text{Li}_2)\text{IrO}_3$  *Phys. Rev. B* **86** 085145
- [28] Meng Z Y, Kim Y B and Kee H Y 2014 Odd-parity triplet superconducting phase in multiorbital materials with a strong spin-orbit coupling: application to doped  $\text{Sr}_2\text{IrO}_4$  *Phys. Rev. Lett.* **113** 177003
- [29] Wan X G, Turner A M, Vishwanath A and Savrasov S Y 2011 Topological semimetal and Fermi-arc surface states in the electronic structure of pyrochlore iridates *Phys. Rev. B* **83** 205101
- [30] Singh Y and Gegenwart P 2010 Antiferromagnetic Mott insulating state in single crystals of the honeycomb lattice material  $\text{Na}_2\text{IrO}_3$  *Phys. Rev. B* **82** 064412
- [31] Liu X, Berlijn T, Yin W G, Ku W, Tsvelik A, Kim Y J, Gretarsson H, Singh Y, Gegenwart P and Hill J P 2011 Long-range magnetic ordering in  $\text{Na}_2\text{IrO}_3$  *Phys. Rev. B* **83** 220403
- [32] Choi S K *et al* 2012 Spin waves and revised crystal structure of honeycomb iridate  $\text{Na}_2\text{IrO}_3$  *Phys. Rev. Lett.* **108** 127204
- [33] Ye F, Chi S X, Cao H B, Chakoumakos B C, Fernandez-Baca J A, Custelcean R, Qi T F, Korneta O B and Cao G 2012 Direct evidence of a zigzag spin-chain structure in the honeycomb lattice: a neutron and x-ray diffraction investigation of single-crystal  $\text{Na}_2\text{IrO}_3$  *Phys. Rev. B* **85** 180403
- [34] Price C C and Perkins N B 2012 Critical properties of the Kitaev–Heisenberg model *Phys. Rev. Lett.* **109** 187201
- [35] Chaloupka J, Jackeli G and Khaliullin G 2013 Zigzag magnetic order in the iridium oxide  $\text{Na}_2\text{IrO}_3$  *Phys. Rev. Lett.* **110** 097204
- [36] Kim C H, Kim H S, Jeong H, Jin H and Yu J 2012 Topological quantum phase transition in 5d transition metal oxide  $\text{Na}_2\text{IrO}_3$  *Phys. Rev. Lett.* **108** 106401
- [37] Bhattacharjee S, Lee S S and Kim Y B 2012 Spin-orbital locking, emergent pseudo-spin and magnetic order in honeycomb lattice iridates *New J. Phys.* **14** 073015

- [38] Mazin I I, Jeschke H O, Foyevtsova K, Valenti R and Khomskii D I 2012  $\text{Na}_2\text{IrO}_3$  as a molecular orbital crystal *Phys. Rev. Lett.* **109** 197201
- [39] Serra C R *et al* 2013 Epitaxy-distorted spin-orbit Mott insulator in  $\text{Sr}_2\text{IrO}_4$  thin films *Phys. Rev. B* **87** 085121
- [40] Nichols J, Korneta O B, Terzic J, De Long L E, Cao G, Brill J W and Seo S S A 2013 Anisotropic electronic properties of a-axis-oriented  $\text{Sr}_2\text{IrO}_4$  epitaxial thin-films *Appl. Phys. Lett.* **103** 131910
- [41] Lupascu A *et al* 2014 Tuning magnetic coupling in  $\text{Sr}_2\text{IrO}_4$  thin films with epitaxial strain *Phys. Rev. Lett.* **112** 147201
- [42] Yang B J and Nagaosa N 2014 Emergent topological phenomena in thin films of pyrochlore iridates *Phys. Rev. Lett.* **112** 246402
- [43] Uchida M, Nie Y F, King P D C, Kim C H, Fennie C J, Schlom D G and Shen K M 2014 Correlated versus conventional insulating behavior in the  $J_{\text{eff}} = 1/2$  versus  $3/2$  bands in the layered iridate  $\text{Ba}_2\text{IrO}_4$  *Phys. Rev. B* **90** 075142
- [44] Nie Y F *et al* 2015 Interplay of spin-orbit interactions, dimensionality, and octahedral rotations in semimetallic  $\text{SrIrO}_3$  *Phys. Rev. Lett.* **114** 016401
- [45] Matsuno J, Ihara K, Yamamura S, Wadati H, Ishii K, Shankar V V, Kee H Y and Takagi H 2015 Engineering a spin-orbital magnetic insulator by tailoring superlattices *Phys. Rev. Lett.* **114** 247209
- [46] Liu J *et al* 2016 Strain-induced nonsymmorphic symmetry breaking and removal of Dirac semimetallic nodal line in an orthoperovskite iridate *Phys. Rev. B* **93** 085118
- [47] Ding Y *et al* 2016 Pressure-induced confined metal from the mott insulator  $\text{Sr}_3\text{Ir}_2\text{O}_7$  *Phys. Rev. Lett.* **116** 216402
- [48] Longo J M, Kafalas J A and Arnott R J 1971 Structure and properties of the high and low pressure forms of  $\text{SrIrO}_3$  *J. Solid State Chem.* **3** 174
- [49] Okabe H, Isobe M, Takayama-Muromachi E, Koda A, Takeshita S, Hiraishi M, Miyazaki M, Kadono R, Miyake Y and Akimitsu J 2011  $\text{Ba}_2\text{IrO}_4$ : a spin-orbit Mott insulating quasi-two-dimensional antiferromagnet *Phys. Rev. B* **83** 155118
- [50] Ge M, Qi T F, Korneta O B, De Long D E, Schlottmann P, Crummett W P and Cao G 2011 Lattice-driven magnetoresistivity and metal-insulator transition in single-layered iridates *Phys. Rev. B* **84** 100402
- [51] Chen X and Wilson S D 2016 Structural evolution and electronic properties of  $(\text{Sr}_{1-x}\text{Ca}_x)_{2-x}\text{IrO}_{4+z}$  spin-orbit-assisted insulators *Phys. Rev. B* **94** 195115
- [52] Li Q *et al* 2013 Atomically resolved spectroscopic study of  $\text{Sr}_2\text{IrO}_4$ : experiment and theory *Sci. Rep.* **3** 3073
- [53] Calder S *et al* 2015 Evolution of competing magnetic order in the  $J_{\text{eff}} = 1/2$  insulating state of  $\text{Sr}_2\text{Ir}_{1-x}\text{Ru}_x\text{O}_4$  *Phys. Rev. B* **92** 165128
- [54] Yuan S J, Aswartham S, Terzic J, Zheng H, Zhao H D, Schlottmann P and Cao G 2015 From  $J_{\text{eff}} = 1/2$  insulator to p-wave superconductor in single-crystal  $\text{Sr}_2\text{Ir}_{1-x}\text{Ru}_x\text{O}_4$  ( $0 \leq x \leq 1$ ) *Phys. Rev. B* **92** 245103
- [55] Qi T F, Korneta O B, Li L, Butrouna K, Cao V S, Wan X G, Schlottmann P, Kaul R K and Cao G 2012 Spin-orbit tuned metal-insulator transitions in single-crystal  $\text{Sr}_2\text{Ir}_{1-x}\text{Rh}_x\text{O}_4$  ( $0 \leq x \leq 1$ ) *Phys. Rev. B* **86** 125105
- [56] Gim Y, Sethi A, Zhao Q, Mitchell J F, Cao G and Cooper S L 2016 Isotropic and anisotropic regimes of the field-dependent spin dynamics in  $\text{Sr}_2\text{IrO}_4$ : Raman scattering studies *Phys. Rev. B* **93** 024405
- [57] Wang J C *et al* 2015 Decoupling of the antiferromagnetic and insulating states in Tb-doped  $\text{Sr}_2\text{IrO}_4$  *Phys. Rev. B* **92** 214411
- [58] Cao G, Durairaj V, Chikara S, DeLong L E, Parkin S and Schlottmann P 2007 Non-Fermi-liquid behavior in nearly ferromagnetic  $\text{SrIrO}_3$  single crystals *Phys. Rev. B* **76** 100402
- [59] Cao G, Durairaj V, Chikara S, Parkin S and Schlottmann P 2007 Partial antiferromagnetism in spin-chain  $\text{Sr}_5\text{Rh}_4\text{O}_{12}$ ,  $\text{Ca}_5\text{Ir}_3\text{O}_{12}$ , and  $\text{Ca}_4\text{IrO}_6$  single crystals *Phys. Rev. B* **75** 134402
- [60] Dey T, Mahajan A V, Khuntia P, Baenitz M, Koteswararao B and Chou F C 2012 Spin-liquid behavior in  $J_{\text{eff}} = 12$  triangular lattice compound  $\text{Ba}_3\text{IrTi}_2\text{O}_9$  *Phys. Rev. B* **86** 140405
- [61] Cao G unpublished
- [62] Kim S J, Smith M D, Darriet J and zur Loye H C 2004 Crystal growth of new perovskite and perovskite related iridates:  $\text{Ba}_3\text{LiIr}_2\text{O}_9$ ,  $\text{Ba}_3\text{NaIr}_2\text{O}_9$ , and  $\text{Ba}_{3.44}\text{K}_{1.56}\text{Ir}_2\text{O}_{10}$  *J. Solid State Chem.* **177** 1493
- [63] Williams S C *et al* 2016 Incommensurate counterrotating magnetic order stabilized by Kitaev interactions in the layered honeycomb  $\alpha\text{-Li}_2\text{IrO}_3$  *Phys. Rev. B* **93** 195158
- [64] Biffin A, Johnson R D, Choi S, Freund F, Manni S, Bombardi A, Manuel P, Gegenwart P and Coldea R 2014 Unconventional magnetic order on the hyperhoneycomb Kitaev lattice in  $\beta\text{-Li}_2\text{IrO}_3$ : full solution via magnetic resonant x-ray diffraction *Phys. Rev. B* **90** 205116
- [65] Takayama T, Kato A, Dinnebier R, Nuss J, Kono H, Veiga L S I, Fabbris G, Haskel D and Takagi H 2015 Hyperhoneycomb iridate  $\beta\text{-Li}_2\text{IrO}_3$  as a platform for Kitaev magnetism *Phys. Rev. Lett.* **114** 077202
- [66] Biffin A, Johnson R D, Kimchi I, Morris R, Bombardi A, Analytis J G, Vishwanath A and Coldea R 2014 Noncoplanar and counterrotating incommensurate magnetic order stabilized by Kitaev interactions in  $\gamma\text{-Li}_2\text{IrO}_3$  *Phys. Rev. Lett.* **113** 197201
- [67] Modic K A *et al* 2014 Realization of a three-dimensional spin-anisotropic harmonic honeycomb iridate *Nat. Commun.* **5** 4203
- [68] Kennedy B J 1996 Oxygen vacancies in pyrochlore oxides: powder neutron diffraction study of  $\text{Pb}_2\text{Ir}_2\text{O}_{6.5}$  and  $\text{Bi}_2\text{Ir}_2\text{O}_{7-y}$  *J. Solid State Chem.* **123** 14
- [69] Qi T F, Korneta O B, Wan X G, DeLong L E, Schlottmann P and Cao G 2012 Strong magnetic instability in correlated metallic  $\text{Bi}_2\text{Ir}_2\text{O}_7$  *J. Phys.: Condens. Matter* **24** 345601
- [70] Baker P J, Moller J S, Pratt F L, Hayes W, Blundell S J, Lancaster T, Qi T F and Cao G 2013 Weak magnetic transitions in pyrochlore  $\text{Bi}_2\text{Ir}_2\text{O}_7$  *Phys. Rev. B* **87** 180409
- [71] Canals B and Lacroix C 1998 Pyrochlore antiferromagnet: a three-dimensional quantum spin liquid *Phys. Rev. Lett.* **80** 2933
- [72] Gingras M J P and McClarty P A 2014 Quantum spin ice: a search for gapless quantum spin liquids in pyrochlore magnets *Rep. Prog. Phys.* **77** 056501
- [73] Cao G, Qi T F, Li L, Terzic J, Yuan S J, DeLong L E, Murthy G and Kaul R K 2014 Novel magnetism of  $\text{Ir}^{5+}(5d^4)$  ions in the double perovskite  $\text{Sr}_2\text{YIrO}_6$  *Phys. Rev. Lett.* **112** 056402
- [74] Phelan B F, Seibel E M, Badoe D, Xie W W and Cava R J 2016 Influence of structural distortions on the Ir magnetism in  $\text{Ba}_{2-x}\text{Sr}_x\text{YIrO}_6$  double perovskites *Solid State Commun.* **236** 37
- [75] Dey T *et al* 2016  $\text{Ba}_2\text{YIrO}_6$ : a cubic double perovskite material with  $\text{Ir}^{5+}$  ions *Phys. Rev. B* **93** 014434
- [76] Cao G, Terzic J, Zhao H and Ye F 2016 unpublished
- [77] Cao G *et al* 2013 Magnetism and electronic structure of  $\text{La}_2\text{ZnIrO}_6$  and  $\text{La}_2\text{MgIrO}_6$ : candidate  $J_{\text{eff}} = 1/2$  Mott insulators *Phys. Rev. B* **87** 155136
- [78] Ferreira T, Morrison G, Yeon J and zur Loye H C 2016 Design and crystal growth of magnetic double perovskite iridates:  $\text{Ln}_2\text{MIrO}_6$  ( $\text{Ln} = \text{La}, \text{Pr}, \text{Nd}, \text{Sm-Gd}; \text{M} = \text{Mg}, \text{Ni}$ ) *Cryst. Growth Des.* **16** 2795

- [79] Bremholm M, Dutton S E, Stephens P W and Cava R J 2011  $\text{NaIrO}_3$ —a pentavalent post-perovskite *J. Solid State Chem.* **184** 601
- [80] Ohgushi K, Gotou H, Yagi T, Kiuchi Y, Sakai F and Ueda Y 2006 Metal-insulator transition in  $\text{Ca}_{1-x}\text{NaxIrO}_3$  with post-perovskite structure *Phys. Rev. B* **74** 241104
- [81] Bogdanov N A, Katukuri V M, Stoll H, van den Brink J and Hozoi L 2012 Post-perovskite  $\text{CaIrO}_3$ : A  $j = 1/2$  quasi-one-dimensional antiferromagnet *Phys. Rev. B* **85** 235147
- [82] Terzic J, Wang J C, Ye F, Song W H, Yuan S J, Aswartham S, DeLong L E, Streltsov S V, Khomskii D I and Cao G 2015 Coexisting charge and magnetic orders in the dimer-chain iridate  $\text{Ba}_5\text{AlIr}_2\text{O}_{11}$  *Phys. Rev. B* **91** 235147
- [83] Singleton J *et al* 2016 Magnetic properties of  $\text{Sr}_3\text{NiIrO}_6$  and  $\text{Sr}_3\text{CoIrO}_6$ : magnetic hysteresis with coercive fields of up to 55 T *Phys. Rev. B* **94** 224408
- [84] Wang Q, Cao Y, Waugh J A, Park S R, Qi T F, Korneta O B, Cao G and Dessau D S 2013 Dimensionality-controlled Mott transition and correlation effects in single-layer and bilayer perovskite iridates *Phys. Rev. B* **87** 245109
- [85] Fujiyama S, Ohsumi H, Komesu T, Matsuno J, Kim B J, Takata M, Arima T and Takagi H 2012 Two-dimensional Heisenberg behavior of  $J_{\text{eff}} = 1/2$  isospins in the paramagnetic state of the spin-orbital Mott insulator  $\text{Sr}_2\text{IrO}_4$  *Phys. Rev. Lett.* **108** 247212
- [86] Dai J X, Calleja E, Cao G and McElroy K 2014 Local density of states study of a spin-orbit-coupling induced Mott insulator  $\text{Sr}_2\text{IrO}_4$  *Phys. Rev. B* **90** 041102
- [87] Ye F, Chi S X, Chakoumakos B C, Fernandez-Baca J A, Qi T F and Cao G 2013 Magnetic and crystal structures of  $\text{Sr}_2\text{IrO}_4$ : a neutron diffraction study *Phys. Rev. B* **87** 140406
- [88] Zhao L, Torchinsky D H, Chu H, Ivanov V, Lifshitz R, Flint R, Qi T, Cao G and Hsieh D 2016 Evidence of an odd-parity hidden order in a spin-orbit coupled correlated iridate *Nat. Phys.* **12** 32
- [89] Wang C, Seinige H, Cao G, Zhou J S, Goodenough J B and Tsoi M 2015 Electrically tunable transport in the antiferromagnetic Mott insulator  $\text{Sr}_2\text{IrO}_4$  *Phys. Rev. B* **92** 115136
- [90] Mott N 1990 *Metal-Insulator Transitions* (London: Taylor and Francis)
- [91] Imada M, Fujimori A and Tokura Y 1998 Metal-insulator transitions *Rev. Mod. Phys.* **70** 1039
- [92] Boseggia S, Walker H C, Vale J, Springell R, Feng Z, Perry R S, Moretti Sala M, Rønnow H M, Collins S P and McMorrow D F 2013 Locking of iridium magnetic moments to the correlated rotation of oxygen octahedra in  $\text{Sr}_2\text{IrO}_4$  revealed by x-ray resonant scattering *J. Phys.: Condens. Matter* **25** 422202
- [93] Torchinsky D H, Chu H, Zhao L, Perkins N B, Sizyuk Y, Qi T, Cao G and Hsieh D 2015 Structural distortion-induced magnetoelectric locking in  $\text{Sr}_2\text{IrO}_4$  revealed through nonlinear optical harmonic generation *Phys. Rev. Lett.* **114** 096404
- [94] Haskel D, Fabbri G, Zhernenkov M, Kong P P, Jin C Q, Cao G and van Veenendaal M 2012 Pressure tuning of the spin-orbit coupled ground state in  $\text{Sr}_2\text{IrO}_4$  *Phys. Rev. Lett.* **109** 027204
- [95] Lobanov M V, Greenblatt M, Caspi E N, Jorgensen J D, Sheptyakov D V, Toby B H, Botez C E and Stephens P W 2004 Crystal and magnetic structure of the  $\text{Ca}_3\text{Mn}_2\text{O}_7$  Ruddlesden-Popper phase: neutron and synchrotron x-ray diffraction study *J. Phys.: Condens. Matter* **16** 5339
- [96] Chikara S, Korneta O, Crummett W P, DeLong L E, Schlottmann P and Cao G 2009 Giant magnetoelectric effect in the  $J_{\text{eff}} = 1/2$  Mott insulator  $\text{Sr}_2\text{IrO}_4$  *Phys. Rev. B* **80** 140407
- [97] Franke I, Baker P J, Blundell S J, Lancaster T, Hayes W, Pratt F L and Cao G 2011 Measurement of the internal magnetic field in the correlated iridates  $\text{Ca}_4\text{IrO}_6$ ,  $\text{Ca}_5\text{Ir}_3\text{O}_{12}$ ,  $\text{Sr}_3\text{Ir}_2\text{O}_7$  and  $\text{Sr}_2\text{IrO}_4$  *Phys. Rev. B* **83** 094416
- [98] Bahr S, Alfonsov A, Jackeli G, Khaliullin G, Matsumoto A, Takayama T, Takagi H, Buchner B and Kataev V 2014 Low-energy magnetic excitations in the spin-orbital Mott insulator  $\text{Sr}_2\text{IrO}_4$  *Phys. Rev. B* **89** 180401
- [99] Gretarsson H, Sung N H, Hoppner M, Kim B J, Keimer B and Le Tacon M 2016 Two-magnon Raman scattering and pseudospin-lattice interactions in  $\text{Sr}_2\text{IrO}_4$  and  $\text{Sr}_3\text{Ir}_2\text{O}_7$  *Phys. Rev. Lett.* **116** 136401
- [100] Kim D J, Xia J and Fisk Z 2014 Topological surface state in the Kondo insulator samarium hexaboride *Nat. Mater.* **13** 466
- [101] Wang C, Seinige H, Cao G, Zhou J S, Goodenough J B and Tsoi M 2014 Anisotropic magnetoresistance in antiferromagnetic  $\text{Sr}_2\text{IrO}_4$  *Phys. Rev. X* **4** 041034
- [102] Chudnovskii F A, Odynets L L, Pergament A L and Stefanovich G B 1996 Electroforming and switching in oxides of transition metals: the role of metal-insulator transition in the switching mechanism *J. Solid State Chem.* **122** 95
- [103] Okimura K, Ezrenea N, Sasakawa Y and Sakai J 2009 Electric-field-induced multistep resistance switching in planar  $\text{VO}_2/\text{c-Al}_2\text{O}_3$  structure *Japan. J. Appl. Phys.* **48** 065003
- [104] Steckel F, Matsumoto A, Takayama T, Takagi H, Buchner B and Hess C 2016 Pseudospin transport in the  $J_{\text{eff}} = 1/2$  antiferromagnet  $\text{Sr}_2\text{IrO}_4$  *Europhys. Lett.* **114** 57007
- [105] Korneta O B, Chikara S, Parkin S, DeLong L E, Schlottmann P and Cao G 2010 Pressure-induced insulating state in  $\text{Ba}_{1-x}\text{R}_x\text{IrO}_3$  ( $R = \text{Gd}, \text{Eu}$ ) single crystals *Phys. Rev. B* **81** 045101
- [106] Laguna-Marco M A, Fabbri G, Souza-Neto N M, Chikara S, Schilling J S, Cao G and Haskel D 2014 Different response of transport and magnetic properties of  $\text{BaIrO}_3$  to chemical and physical pressure *Phys. Rev. B* **90** 014419
- [107] Zhao Z *et al* 2014 Pressure induced second-order structural transition in  $\text{Sr}_3\text{Ir}_2\text{O}_7$  *J. Phys.: Condens. Matter* **26** 215402
- [108] Zocco D A, Hamlin J J, White B D, Kim B J, Jeffries J R, Weir S T, Vohra Y K, Allen J W and Maple M B 2014 Persistent non-metallic behavior in  $\text{Sr}_2\text{IrO}_4$  and  $\text{Sr}_3\text{Ir}_2\text{O}_7$  at high pressures *J. Phys.: Condens. Matter* **26** 255603
- [109] Donnerer C *et al* 2016 Pressure dependence of the structure and electronic properties of  $\text{Sr}_3\text{Ir}_2\text{O}_7$  *Phys. Rev. B* **93** 174118
- [110] Hanfland M, Syassen K, Christensen N E and Novikov D L 2000 New high-pressure phases of lithium *Nature* **408** 174
- [111] Snow C S, Cooper S L, Cao G, Crow J E, Fukazawa H, Nakatsuji S and Maeno Y 2002 Pressure-tuned collapse of the Mott-like state in  $\text{Ca}_{n+1}\text{Ru}_n\text{O}_{3n+1}$  ( $n = 1, 2$ ): Raman spectroscopic studies *Phys. Rev. Lett.* **89** 226401
- [112] Jin C Q and Cao G unpublished
- [113] Yang X and Wang F 2016 Schwinger boson spin-liquid states on square lattice *Phys. Rev. B* **94** 035160
- [114] Korneta O B, Qi T F, Chikara S, Parkin S, De Long L E, Schlottmann P and Cao G 2010 Electron-doped  $\text{Sr}_2\text{IrO}_{4-\delta}$  ( $0 \leq \delta \leq 0.04$ ): evolution of a disordered  $J_{\text{eff}} = 1/2$  Mott insulator into an exotic metallic state *Phys. Rev. B* **82** 115117
- [115] Cao G, Lin X N, Chikara S, Durairaj V and Elhami E 2004 High-temperature weak ferromagnetism on the verge of a metallic state: impact of dilute Sr doping on  $\text{BaIrO}_3$  *Phys. Rev. B* **69** 174418

- [116] Moon S J, Jin H, Choi W S, Lee J S, Seo S S A, Yu J, Cao G, Noh T W and Lee Y S 2009 Temperature dependence of the electronic structure of the  $J_{\text{eff}} = 1/2$  Mott insulator  $\text{Sr}_2\text{IrO}_4$  studied by optical spectroscopy *Phys. Rev. B* **80** 195110
- [117] Hsieh D, Mahmood F, Torchinsky D H, Cao G and Gedik N 2012 Observation of a metal-to-insulator transition with both Mott–Hubbard and Slater characteristics in  $\text{Sr}_2\text{IrO}_4$  from time-resolved photocarrier dynamics *Phys. Rev. B* **86** 035128
- [118] Cao Y *et al* 2016 Hallmarks of the Mott–metal crossover in the hole-doped pseudospin-1/2 Mott insulator  $\text{Sr}_2\text{IrO}_4$  *Nat. Commun.* **7** 11367
- [119] Chen X *et al* 2015 Influence of electron doping on the ground state of  $(\text{Sr}_{1-x}\text{La}_x)_2\text{IrO}_4$  *Phys. Rev. B* **92** 075125
- [120] Clancy J P, Lupascu A, Gretarsson H, Islam Z, Hu Y F, Casa D, Nelson C S, LaMarra S C, Cao G and Kim Y J 2014 Dilute magnetism and spin-orbital percolation effects in  $\text{Sr}_2\text{Ir}_{1-x}\text{Rh}_x\text{O}_4$  *Phys. Rev. B* **89** 054409
- [121] Yang J A, Huang Y P, Hermele M, Qi T F, Cao G and Reznik D 2015 High-energy electronic excitations in  $\text{Sr}_2\text{IrO}_4$  observed by Raman scattering *Phys. Rev. B* **91** 195140
- [122] Liu X *et al* 2016 Anisotropic softening of magnetic excitations in lightly electron-doped  $\text{Sr}_2\text{IrO}_4$  *Phys. Rev. B* **93** 241102
- [123] Jeong J, Sidis Y, Louat A, Brouet V and Bourges P 2017 Time-reversal symmetry breaking hidden order in  $\text{Sr}_2(\text{Ir},\text{Rh})\text{O}_4$  *Nat. Commun.* **8** 15119
- [124] Varma C M 1997 Non-Fermi-liquid states and pairing instability of a general model of copper oxide metals *Phys. Rev. B* **55** 14554
- [125] Fauque B, Sidis Y, Hinkov V, Pailhes S, Lin C T, Chaud X and Bourges P 2006 Magnetic order in the pseudogap phase of high- $T_C$  superconductors *Phys. Rev. Lett.* **96** 197001
- [126] Carter J M, Shankar V V, Zeb M A and Kee H Y 2012 Semimetal and topological insulator in perovskite iridates *Phys. Rev. B* **85** 115105
- [127] Kim J, Said A H, Casa D, Upton M H, Gog T, Daghofer M, Jackeli G, van den Brink J, Khaliullin G and Kim B J 2012 Large spin-wave energy gap in the bilayer iridate  $\text{Sr}_3\text{Ir}_2\text{O}_7$ : evidence for enhanced dipolar interactions near the mott metal-insulator transition *Phys. Rev. Lett.* **109** 157402
- [128] Liu C *et al* 2014 Spin-correlated electronic state on the surface of a spin-orbit Mott system *Phys. Rev. B* **90** 045127
- [129] Hogan T, Bjaalie L, Zhao L Y, Belvin C, Wang X P, Van de Walle C G, Hsieh D and Wilson S D 2016 Probing the spin-orbit Mott state in  $\text{Sr}_3\text{Ir}_2\text{O}_7$  by electron doping *Phys. Rev. B* **93** 134110
- [130] Lovesey S W, Khalyavin D D, Manuel P, Chapon L C, Cao G and Qi F T 2012 Magnetic symmetries in neutron and resonant x-ray Bragg diffraction patterns of four iridium oxides *J. Phys.: Condens. Matter* **24** 496003
- [131] Kim J W, Choi Y, Kim J, Mitchell J F, Jackeli G, Daghofer M, van den Brink J, Khaliullin G and Kim B J 2012 Dimensionality Driven spin-flop transition in layered iridates *Phys. Rev. Lett.* **109** 037204
- [132] Carter J M and Kee H Y 2013 Microscopic theory of magnetism in  $\text{Sr}_3\text{Ir}_2\text{O}_7$  *Phys. Rev. B* **87** 014433
- [133] Clancy J P, Plumb K W, Nelson C S, Islam Z, Cao G, Qi T and Kim Y-J 2012 Field-induced magnetic behavior of the bilayer iridate  $\text{Sr}_3\text{Ir}_2\text{O}_7$  arXiv:1207.0960
- [134] Sala M M *et al* 2015 Evidence of quantum dimer excitations in  $\text{Sr}_3\text{Ir}_2\text{O}_7$  *Phys. Rev. B* **92** 024405
- [135] Seinige H, Williamson M, Shen S D, Wang C, Cao G, Zhou J S, Goodenough J B and Tsai M 2017 unpublished
- [136] Li L, Kong P P, Qi T F, Jin C Q, Yuan S J, DeLong L E, Schlottmann P and Cao G 2013 Tuning  $J_{\text{eff}} = 1/2$  insulating state via electron doping and pressure in double-layered iridate  $\text{Sr}_3\text{Ir}_2\text{O}_7$  *Phys. Rev. B* **87** 235127
- [137] Lu X Y, McNally D E, Sala M M, Terzic J, Upton M H, Casa D, Ingold G, Cao G and Schmitt T 2017 Doping evolution of magnetic order and magnetic excitations in  $(\text{Sr}_{1-x}\text{La}_x)_3\text{Ir}_2\text{O}_7$  *Phys. Rev. Lett.* **118** 027202
- [138] Chu H, Zhao L, de la Torre A, Hogan T, Wilson S D and Hsieh D 2017 A charge density wave-like instability in a doped spin-orbit-assisted weak Mott insulator *Nat. Mater.* **16** 200
- [139] Pesin D and Balents L 2010 Mott physics and band topology in materials with strong spin-orbit interaction *Nat. Phys.* **6** 376
- [140] Watanabe H, Shirakawa T and Yunoki S 2010 Microscopic study of a spin-orbit-induced Mott insulator in Ir oxides *Phys. Rev. Lett.* **105** 216410
- [141] Zeb M A and Kee H Y 2012 Interplay between spin-orbit coupling and Hubbard interaction in  $\text{SrIrO}_3$  and related Pbnm perovskite oxides *Phys. Rev. B* **86** 085149
- [142] Chen Y G, Lu Y M and Kee H Y 2015 Topological crystalline metal in orthorhombic perovskite iridates *Nat. Commun.* **6** 6593
- [143] Zhao J G, Yang L X, Yu Y, Li F Y, Yu R C, Fang Z, Chen L C and Jin C Q 2008 High-pressure synthesis of orthorhombic  $\text{SrIrO}_3$  perovskite and its positive magnetoresistance *J. Appl. Phys.* **103** 074301
- [144] Bremholm M, Yim C K, Hirai D, Climent-Pascual E, Xu Q, Zandbergen H W, Ali M N and Cava R J 2012 Destabilization of the 6H- $\text{SrIrO}_3$  polymorph through partial substitution of zinc and lithium *J. Mater. Chem.* **22** 16431
- [145] Qasim I, Kennedy B J and Avdeev M 2013 Stabilizing the orthorhombic perovskite structure in  $\text{SrIrO}_3$  through chemical doping. Synthesis, structure and magnetic properties of  $\text{SrIr}_{1-x}\text{Mg}_x\text{O}_3$  ( $0.20 \leq x \leq 0.33$ ) *J. Mater. Chem. A* **1** 13357
- [146] Qasim I, Kennedy B J and Avdeev M 2013 Synthesis, structures and properties of transition metal doped  $\text{SrIrO}_3$  *J. Mater. Chem. A* **1** 3127
- [147] Blanchard P E R, Reynolds E, Kennedy B J, Kimpton J A, Avdeev M and Belik A A 2014 Anomalous thermal expansion in orthorhombic perovskite  $\text{SrIrO}_3$ : interplay between spin-orbit coupling and the crystal lattice *Phys. Rev. B* **89** 214106
- [148] Gruenewald J H, Nichols J, Terzic J, Cao G, Brill J W and Seo S S A 2014 Compressive strain-induced metal–insulator transition in orthorhombic  $\text{SrIrO}_3$  thin films *J. Mater. Res.* **29** 2491
- [149] Nie Y F, Di Sante D, Chatterjee S, King P D C, Uchida M, Ciuchi S, Schlom D G and Shen K M 2015 Formation and observation of a quasi-two-dimensional  $d_{xy}$  electron liquid in epitaxially stabilized  $\text{Sr}_{2-x}\text{La}_x\text{TiO}_4$  thin films *Phys. Rev. Lett.* **115** 096405
- [150] Zheng H, Terzic J, Ye F, Wan X G, Wang D, Wang J C, Wang X P, Schlottmann P, Yuan S J and Cao G 2016 Simultaneous metal-insulator and antiferromagnetic transitions in orthorhombic perovskite iridate  $\text{Sr}_{0.94}\text{Ir}_{0.78}\text{O}_{2.68}$  single crystals *Phys. Rev. B* **93** 235157
- [151] Kitaev A 2006 Anyons in an exactly solved model and beyond *Ann. Phys.* **321** 2
- [152] Singh Y, Manni S, Reuther J, Berlijn T, Thomale R, Ku W, Trebst S and Gegenwart P 2012 Relevance of the Heisenberg–Kitaev model for the honeycomb lattice iridates  $\text{A}_2\text{IrO}_3$  *Phys. Rev. Lett.* **108** 127203
- [153] Cao G, Qi T F, Li L, Terzic J, Cao V S, Yuan S J, Tovar M, Murthy G and Kaul R K 2013 Evolution of magnetism

- in the single-crystal honeycomb iridates  $(\text{Na}_{1-x}\text{Li}_x)_2\text{IrO}_3$  *Phys. Rev. B* **88** 220414
- [154] Chun S H *et al* 2015 Direct evidence for dominant bond-directional interactions in a honeycomb lattice iridate  $\text{Na}_2\text{IrO}_3$  *Nat. Phys.* **11** 462
- [155] Pratt F L, Baker P J, Blundell S J, Lancaster T, Ohira-Kawamura S, Baines C, Shimizu Y, Kanoda K, Watanabe I and Saito G 2011 Magnetic and non-magnetic phases of a quantum spin liquid *Nature* **471** 612
- [156] Gegenwart P and Trebst S 2015 Spin-orbit physics: Kitaev matter *Nat. Phys.* **11** 444
- [157] Rousoschatzakis I, Reuther J, Thomale R, Rachel S and Perkins N B 2015 Phase diagram and quantum order by disorder in the Kitaev  $\mathbf{K}_1 - \mathbf{K}_2$  honeycomb magnet *Phys. Rev. X* **5** 041035
- [158] Gretarsson H *et al* 2013 Magnetic excitation spectrum of  $\text{Na}_2\text{IrO}_3$  probed with resonant inelastic x-ray scattering *Phys. Rev. B* **87** 220407
- [159] Comin R *et al* 2012  $\text{Na}_2\text{IrO}_3$  as a novel relativistic Mott insulator with a 340 meV gap *Phys. Rev. Lett.* **109** 266406
- [160] Felner I and Bradaric I M 2002 The magnetic behavior of  $\text{Li}_2\text{MO}_3$  ( $\text{M} = \text{Mn}$ , Ru and Ir) and  $\text{Li}_2(\text{Mn}_{1-x}\text{Ru}_x)\text{O}_3$  *Physica B* **311** 195
- [161] Manni S, Choi S, Mazin I I, Coldea R, Altmeyer M, Jeschke H O, Valenti R and Gegenwart P 2014 Effect of isoelectronic doping on the honeycomb-lattice iridate  $\text{A}_2\text{IrO}_3$  *Phys. Rev. B* **89** 245113
- [162] Manni S, Tokiwa Y and Gegenwart P 2014 Effect of nonmagnetic dilution in the honeycomb-lattice iridates  $\text{Na}_2\text{IrO}_3$  and  $\text{Li}_2\text{IrO}_3$  *Phys. Rev. B* **89** 241102
- [163] Jin C Q and Cao G unpublished
- [164] Khaliullin G 2013 Excitonic magnetism in Van Vleck-type  $d^4$  Mott insulators *Phys. Rev. Lett.* **111** 197201
- [165] Chen G, Balents L and Schnyder A P 2009 Spin-orbital singlet and quantum critical point on the diamond lattice:  $\text{FeSc}_2\text{S}_4$  *Phys. Rev. Lett.* **102** 096406
- [166] Meetei O N, Cole W S, Randeria M and Trivedi N 2015 Novel magnetic state in  $d^4$  Mott insulators *Phys. Rev. B* **91** 054412
- [167] Bhosal S, Baidya S, Dasgupta I and Saha-Dasgupta T 2015 Breakdown of  $\mathbf{J} = \vec{0}$  nonmagnetic state in  $d^4$  iridate double perovskites: a first-principles study *Phys. Rev. B* **92** 121113
- [168] Wang J C, Terzic J, Qi T F, Ye F, Yuan S J, Aswartham S, Streltsov S V, Khomskii D I, Kaul R K and Cao G 2014 Lattice-tuned magnetism of  $\text{Ru}^{4+}(4d^4)$  ions in single crystals of the layered honeycomb ruthenates  $\text{Li}_2\text{RuO}_3$  and  $\text{Na}_2\text{RuO}_3$  *Phys. Rev. B* **90** 161110
- [169] Kim A J, Jeschke H O, Werner P and Valenti R 2017 Freezing and Hund's rules in spin-orbit-coupled multiorbital Hubbard models *J. Phys. Rev. Lett.* **118** 086401
- [170] Miura Y, Yasui Y, Sato M, Igawa N and Kakurai K 2007 New-type phase transition of  $\text{Li}_2\text{RuO}_3$  with Honeycomb structure *J. Phys. Soc. Japan* **76** 033705
- [171] Binotto L, Pollini I and Spinolo G 1971 Optical and transport properties of the magnetic semiconductor  $\alpha\text{-RuCl}_3$  *Phys. Status Solidi b* **44** 245
- [172] Kobayashi Y, Okada T, Asai K, Katada M, Sano H and Ambe Mössbauer F 1992 Spectroscopy and magnetization studies of  $\alpha$ - and  $\beta$ - $\text{RuCl}_3$  *Inorg. Chem.* **31** 4570
- [173] Sears J A, Songvilay M, Plumb K W, Clancy J P, Qiu Y, Zhao Y, Parshall D and Kim Y J 2015 Magnetic order in  $\alpha\text{-RuCl}_3$ : a honeycomb-lattice quantum magnet with strong spin-orbit coupling *Phys. Rev. B* **91** 144420
- [174] Plumb K W, Clancy J P, Sandilands L J, Shankar V V, Hu Y F, Burch K S, Kee H Y and Kim Y J 2014  $\alpha\text{-RuCl}_3$ : a spin-orbit assisted Mott insulator on a honeycomb lattice *Phys. Rev. B* **90** 041112
- [175] Kubota Y, Tanaka H, Ono T, Narumi Y and Kindo K 2015 Successive magnetic phase transitions in  $\alpha\text{-RuCl}_3$ : XY-like frustrated magnet on the honeycomb lattice *Phys. Rev. B* **91** 094422
- [176] Majumder M, Schmidt M, Rosner H, Tsirlin A A, Yasuoka H and Baenitz M 2015 Anisotropic  $\text{Ru}^{3+} 4d^5$  magnetism in the  $\alpha\text{-RuCl}_3$  honeycomb system: susceptibility, specific heat, and zero-field NMR *Phys. Rev. B* **91** 180401
- [177] Banerjee A *et al* 2016 Proximate Kitaev quantum spin liquid behaviour in a honeycomb magnet *Nat. Mater.* **15** 733
- [178] Lee E K H, Schaffer R, Bhattacharjee S and Kim Y B 2014 Heisenberg–Kitaev model on the hyperhoneycomb lattice *Phys. Rev. B* **89** 045117
- [179] Kimchi I, Analytis J G and Vishwanath A 2014 Three-dimensional quantum spin liquids in models of harmonic-honeycomb iridates and phase diagram in an infinite-D approximation *Phys. Rev. B* **90** 205126
- [180] Lee E K H, Bhattacharjee S, Hwang K, Kim H S, Jin H and Kim Y B 2014 Topological and magnetic phases with strong spin-orbit coupling on the hyperhoneycomb lattice *Phys. Rev. B* **89** 205132
- [181] Lee S, Lee E K H, Paramentri A and Kim Y B 2014 Order-by-disorder and magnetic field response in the Heisenberg–Kitaev model on a hyperhoneycomb lattice *Phys. Rev. B* **89** 014424
- [182] Lee E K H and Kim Y B 2015 Theory of magnetic phase diagrams in hyperhoneycomb and harmonic-honeycomb iridates *Phys. Rev. B* **91** 064407
- [183] Singh Y, Tokiwa Y, Dong J and Gegenwart P 2013 Spin liquid close to a quantum critical point in  $\text{Na}_4\text{Ir}_3\text{O}_8$  *Phys. Rev. B* **88** 220413
- [184] Podolsky D and Kim Y B 2011 Spin-orbit coupling in the metallic and spin-liquid phases of  $\text{Na}_4\text{Ir}_3\text{O}_8$  *Phys. Rev. B* **83** 054401
- [185] Ma E Y, Cui Y-T, Ueda K, Tang S, Chen K, Tamura N, Wu P M, Fujioka J, Tokura Y and Z-X Shen 2015 Mobile metallic domain walls in an all-in-all-out magnetic insulator *Science* **350** 538
- [186] Nakatsuji S, Machida Y, Maeno Y, Tayama T, Sakakibara T, van Duijn J, Balicas L, Millican J N, Macaluso R T and Chan J Y 2006 Metallic spin-liquid behavior of the geometrically frustrated Kondo lattice  $\text{Pr}_2\text{Ir}_2\text{O}_7$  *Phys. Rev. Lett.* **96** 087204
- [187] Machida Y, Nakatsuji S, Onoda S, Tayama T and Sakakibara T 2010 Time-reversal symmetry breaking and spontaneous Hall effect without magnetic dipole order *Nature* **463** 210
- [188] Yanagishima D and Maeno Y 2001 Metal-nonmetal changeover in pyrochlore iridates *J. Phys. Soc. Japan* **70** 2880
- [189] Matsuhira K, Wakushima M, Nakanishi R, Yamada T, Nakamura A, Kawano W, Takagi S and Hinatsu Y 2007 Metal-insulator transition in pyrochlore iridates  $\text{Ln}_2\text{Ir}_2\text{O}_7$  ( $\text{Ln} = \text{Nd}$ , Sm, and Eu) *J. Phys. Soc. Japan.* **76** 043706
- [190] Yang B J and Kim Y B 2010 Topological insulators and metal-insulator transition in the pyrochlore iridates *Phys. Rev. B* **82** 085111
- [191] Wang Q, Cao Y, Wan X G, Denlinger J D, Qi T F, Korneta O B, Cao G and Dessau D S 2015 Experimental electronic structure of the metallic pyrochlore iridate  $\text{Bi}_2\text{Ir}_2\text{O}_7$  *J. Phys.: Condens. Matter* **27** 015502
- [192] Pajskr K, Novak P, Pokorný V, Kolorenc J, Arita R and Kunes J 2016 On the possibility of excitonic magnetism in Ir double perovskites *Phys. Rev. B* **93** 035129

- [193] Svoboda C, Randeria M and Trivedi N 2017 Effective magnetic interactions in spin-orbit coupled  $d^4$  Mott insulators *Phys. Rev. B* **95** 014409
- [194] Terzic J, Zheng H, Feng Ye, Schlottmann P, Zhao H D, DeLong L, Yuan S J and Cao G 2017 New evidence for a magnetic state in double-perovskite iridates with  $\text{Ir}^{5+}(5d^4)$  ions *Phys. Rev. B* **96** 064436
- [195] Yuan B *et al* 2017 Determination of Hund's coupling in 5d oxides using resonant inelastic x-ray scattering *Phys. Rev. B* **95** 235114
- [196] Ranjbar B, Reynolds E, Kayser P, Kennedy B J, Hester J R and Kimpton J A 2015 Structural and magnetic properties of the iridium double perovskites  $\text{Ba}_{2-x}\text{Sr}_x\text{YIrO}_6$  *Inorg. Chem.* **54** 10468



**Gang Cao** is Professor of Physics at the University of Colorado at Boulder in USA. He is a Fellow of the American Physical Society. Dr Cao's research encompasses a methodical search for novel quantum materials in the single-crystal form, and a systematic effort to elucidate the underlying physics of these materials. Visit his homepage for details: <https://www.colorado.edu/lab/cao/>.



**Dr Pedro Schlottmann** Pedro Schlottmann received his PhD from the Technical University of Munich (Germany) in 1973. After postdoctoral appointments at the Max-Planck Institute in Munich, the Freie Universitaet Berlin and U. C. Berkeley, he became Assistant Professor at the Freie Universitaet Berlin and a Heisenberg Fellow of the German National Science Foundation. He was a research scientist at the Kernforschungsanlage Juelich (1982–1985) and joined Physics Department of Temple University in Philadelphia in 1985. From 1990 to 2017 he was Professor of Physics at Florida State University and is Emeritus Professor since 2017.